

**Single cell transcriptomics reveal regulators of
progenitor cell fate and postmitotic maturation
during brain development.**

Dissertation

zur Erlangung des akademischen Grades

doctor rerum naturalium (Dr. rer. nat)

**vorgelegt dem Rat der Medizinischen Fakultät
der Friedrich-Schiller-Universität Jena**

von Dipl. Biologe Daniel Pensold

geboren am 17.06.1986 in Magdeburg

Gutachter:

1. Dr. rer. nat. Geraldine Zimmer, Universitätsklinikum Jena
2. Prof. Dr. rer. nat. Aria Baniahmad, Universitätsklinikum Jena
3. Prof. Dr. rer. nat. Tomas Pieler, Georg-August-Universität Göttingen

Tag der öffentlichen Verteidigung: 31.01.2017

Table of Content

List of abbreviations	I
1 Summary	1
2 Zusammenfassung	3
3 Introduction	5
3.1 Development of the neocortex	5
3.1.1 Development of cortical excitatory projection neurons	6
3.1.2 Development of cortical interneurons	8
3.1.2.1 Transcriptional code of interneuron subtypes	11
3.1.2.2 Complex postmitotic phase of cortical interneuron maturation	12
3.1.2.3 What defines interneuron subtype identity? Extrinsic versus intrinsic determination.	14
3.2 Multifunctional molecules involved in brain development	15
3.2.1 The role of ephrins during brain development	15
3.2.2 Epigenetic regulation of gene expression	18
3.3 Single cell analysis is required to reveal subtype specific developmental mechanisms	19
3.4 Aims	21
4 Methods	23
4.1 Animals	23
4.2 General considerations for working in sterile and in ribonuclease- (RNase)-free conditions	23
4.3 Brain and tissue preparation	24
4.4 Primary Cell culture	24
4.4.1 Preparation of dissociated single cells	24
4.4.2 Pair-cell assay	25
4.4.3 Cultivation of thalamic explants	25
4.4.4 Co-culture of thalamic explants with cortical single cells	26
4.4.5 Pak6 siRNA transfections in primary neuronal culture and verification of siRNA treatment in cell culture.	26
4.4.6 FACS enrichment of tdTomato cells	27
4.5 Molecular biology methods	27
4.5.1 RNA isolation of tissue and FAC-sorted cells	27
4.5.2 Amplification protocols	28
4.5.2.1 Genotyping and Standard PCR	28
4.5.2.2 Quantitative reverse transcription PCR (qRT-PCR)	29
4.5.2.3 cDNA synthesis from single cells, thalamic fibers and tissue-RNA dilution	30
4.5.2.4 Qualitative evaluation of amplified cDNAs from single-cells and thalamic axons	31
4.5.3 Next Generation Sequencing	32
4.5.3.1 Library preparation and data processing of tissue RNA	33
4.5.3.2 Library preparation and data processing of 3' limited cDNA	33
4.6 NanoString Codeset design	34
4.7 NanoString hybridization, data processing and analysis	35
4.8 Validation using NanoString	36
4.9 Immunohistochemistry and immunocytochemistry	38
4.10 <i>In situ</i> hybridization	39
4.11 Microscopy and image analysis	39
4.12 Statistical analysis	40
5 Results	41
5.1 Validation of the single cell amplification protocol	41
5.1.1 Correlation of native tissue RNA with amplicates from diluted templates	42
5.1.2 Transcript representation was preserved after additional amplification	45

Table of content

5.2	Regulation of cortical progenitor division by thalamic fibers expressing <i>EfnA5</i>	46
5.2.1	EFNA5 affects the division mode of cortical progenitors	46
5.2.2	<i>EfnA5</i> transcripts were not detected in cortical cells by single cell-based expression analysis while <i>Epha4</i> was confirmed in progenitors	47
5.2.3	<i>EfnA5</i> transcripts were detected in axonal compartments of the thalamus.....	49
5.2.4	Ephrin A-ligand expressing thalamocortical axons affected cortical progenitor division	51
5.3	DNMT1 is required for the migration of POA-derived cortical interneurons	52
5.3.1	Approaching the diversity of neurons generated in the embryonic subpallium with NanoString-based single cell analysis	52
5.3.1.1	Discriminating MGE and POA subtypes by single cell-based principal component analysis	53
5.3.1.2	The profiling strategy confirmed known cellular subtypes of the basal telencephalon	56
5.3.1.3	Cluster IV embraced pallial excitatory neurons invading the POA	59
5.3.1.4	Postmitotic POA derived GABAergic cells segregated into two main clusters	60
5.3.2	PAK6 promoted neurite outgrowth and negatively correlated with the expression of the epigenetic modifier <i>Dnmt1</i>	61
5.3.3	Expression of <i>Dnmt1</i> correlated with cell motion associated genes and was detected in migrating POA-derived GABAergic interneurons	63
5.3.4	Postmitotic <i>Dnmt1</i> deletion in the mouse model system led to reduced numbers of cortical interneurons.....	65
5.3.5	<i>Dnmt1</i> -deficiency led to a reduction of migrating cells during embryonic development	68
5.3.6	DNMT1 promotes migration by suppression of post-migratory processes.....	70
5.3.7	<i>Pak6</i> expression levels are elevated in <i>Dnmt1</i> deficient cells	71
6	Discussion	73
6.1	Advantages and limitations of the single cell analysis strategy	73
6.1.1	The relevance of low abundant transcript detection	74
6.1.2	Comparison to other single cell approaches	75
6.1.3	Manual isolation – old fashioned or still required?.....	77
6.2	EFNA5/EPHA4 interaction influence cortical projection neurogenesis	78
6.2.1	Eph-receptor/Ephrin-ligand interactions are involved in neuronal proliferation and differentiation	78
6.2.2	EPHA4 mediates the effect on progenitor division in <i>EfnA5</i> knockout mice.....	79
6.2.3	<i>EfnA5</i> imported by thalamic fibers into the developing cortex has an impact on cortical progenitor division	79
6.3	Exploring interneuron diversity and the factors driving their developmental maturation	81
6.3.1	Principal component analysis results in biological reasonable cluster affiliations	83
6.3.2	Epigenetic regulation of cell migration by DNMT1.....	86
6.3.3	DNMT1 regulates gene expression of maturational processes like neurite outgrowth, which is promoted by PAK6	88
6.4	Conclusion and further perspectives	90
7	References	II
8	Appendix	XX
8.1	Appendix Tables.....	XX
8.2	Index of Figures.....	XXIV
8.3	Index of Table.....	XXV
8.4	Ehrenwörtliche Erklärung	XXVI
8.5	Danksagung.....	XXVII

List of abbreviations

bp	Base pair
CGE	Caudal ganglionic eminence
CB	Calbindin
CCK	Cholecystokinin
CP	Cortical plate
CR	Calretinin
CS	Codeset
DAVID	Database for Annotation, Visualization and Integrated Discovery
DEPC	Diethylpyrocarbonat
DMEM	Dulbecco's Modified Eagle Medium
DNA	Deoxyribonucleic acid
E	Ependymal
E1 – E20	Embryonic day 1-20
EDTA	Ethylenediaminetetraacetic acid
FACS	Fluorescence-activated cell sorting
FBS	Fetal bovine serum
FCS/SSC	Forward scatter/ Side scatter
FISH	Fluorescence in situ hybridization
FDR	False discovery rate
GABA	Gamma-Aminobutyric acid (γ -Aminobutyric acid)
GO	Gene ontology
GPI	Glycosylphosphatidylinositol
HBSS	Hank's balanced salt solution
IMZ	Intermediate zone
IPC	Intermediate progenitor cells
kb	Kilo base
KO	Knockout
LAPi	Intermediate stratum of the lateropallial amygdalopiriform area
LGE	Lateral ganglionic eminence
LTS	Low threshold spike
MGE	Medial ganglionic eminence
MZ	Marginal zone
neg. Ctl.	Negative control
NGF	Nerve growth factor
NGS	Next Generation Sequencing
NOS	Nitric oxide synthase
OLM	Oriens/lacunosum moleculare
PBS	Phosphate-buffered saline
PC	Principle component
PCA	Principal component analysis
PCR	Polymerase chain reaction
PFA	Paraformaldehyde
POA	Preoptic area
pos. Ctl.	Positive control
PP	Preplate
qRT-PCR	Quantitative realtime PCR
RGC	Radial glia cell
RNA	Ribonucleic acid
RT-PCR	Reverse transcription PCR
SAM	Sterile α -motif
scRNA-seq	Single cell RNA-sequencing
scRT-PCR	Single cell reverse transcription PCR
SDS	Sodium dodecyl sulfate
SP	Subplate
Str	Striatum
Strs	Superficial stratum of the striatum
SVZ	Subventricular zone
TUNEL	Terminal deoxynucleotidyl transferase dUTP nick end labeling
UMI	Unique molecular identifiers
VIP	Vasointestinal peptide
VZ	Ventricular zone
WM	White matter
WT	Wild-type

1 Summary

Transcriptome analysis of cellular diversity within a given tissue presupposes the availability of robust, quantitative methods, combining the suitability for analysis of even low copy number transcripts in individual cells with the processing of large numbers of samples in a short time. In this thesis the direct and sensitive NanoString nCounter technology was applied to validate an improved PCR-based strategy for quantitative and qualitative global single cell transcriptome analysis, enabling multiple analytical runs. RNA isolates from whole tissue were quantitatively compared with cDNA amplicates prepared from single cell equivalent dilutions of the same RNA. A significant correlation was obtained between the values measured for RNA and cDNA amplicates for transcript copy numbers from 10 to several thousand. This method was then used to investigate two distinct neurodevelopmental issues.

The first neuroscientific question dealt with the generation of cortical projection neurons, whose fate is specified at the progenitor level and depends on the mode of division, orchestrated by various intrinsic and extrinsic factors. With the help of the high resolution of the single cell amplification method, it was possible to reveal a mechanism of extracortical regulation of neurogenesis. Thalamic afferents invading the developing cortex import membrane bound *EfnA5* ligands, that interact with the membranous *EphA4*-receptor expressed by radial glia cells (RGCs) influencing their mode of division. As a consequence, the loss of *EfnA5* results in altered output of progenitor subtypes causing the changes in adult cortical layering (Gerstmann et al. 2015). In accordance with this, recombinant EFNA5-Fc, as well as ephrin A ligand-expressing thalamic axons affect the output of cortical progenitor division *in vitro*. In conclusion, the data presented here provide evidence for an extra-cortical fine-tuning of cortical progenitor output via the Eph-receptor/ephrin-ligand system.

The single cell transcriptomics approach was further applied to investigate the topic of interneuron development, especially to their post-mitotic phase of tangential migration. Disrupted inhibitory circuits are suggested to contribute to the pathophysiology of psychiatric disorders and defective development seemed to be linked to the etiology of such symptoms. The migration from their sites of origin within the basal telencephalon to the distinct targets, requires tight regulation to ensure correct interneuron numbers and distribution necessary for proper information processing. To identify factors orchestrating the migration of cortical interneurons, we analyzed single cell

transcriptomes of cells derived from distinct proliferative niches of interneurons in the basal telencephalon. Differential gene expression revealed particular subtypes of progenitors and post-mitotic neurons. Interestingly, we observed *DNA methyltransferase 1 (Dnmt1)* expression in a fraction of post-mitotic POA-derived interneurons fating for the cortex. Deletion of *Dnmt1* in this interneuron lineage caused defective migration, resulting in drastically reduced numbers of cortical interneurons in adults. Comparative next generation sequencing analysis of FAC-sorted *Dnmt1* wild-type and *Dnmt1* knockout mice revealed DNMT1-dependent repression of genes involved in late maturational processes like neurite outgrowth. In this context, further experiments provide evidence that DNMT1 preserves the migratory shape of post-mitotic GABAergic interneurons in part through negative regulation of *Pak6*, which stimulates neuritogenesis at post-migratory stages.

In conclusion, the NanoString-based analysis of representative single cell cDNA libraries generated by exponential amplification is reliably applicable for transcriptome analyses at single-cell resolution. We have established a valid analysis strategy for profiling of particular neuronal subtypes, which highlights distinct gene expression and lead to the discovery of two novel mechanisms during embryonic brain development. This approach will be also generally applicable to the analysis of particular cell fates in other complex tissues, including diagnostic screening of individual cells in disease-relevant tissue preparations.

2 Zusammenfassung

Die Einzelzell-Transkriptom-Analyse zur Ergründung zellulärer Diversität in komplexen Geweben setzt robuste und quantitative Methoden voraus. Idealerweise sollten solche Techniken zusätzlich die Detektion von sehr gering abundanten Transkripten ermöglichen und einen hohen Probendurchsatz aufweisen. In der vorliegenden Arbeit wurde ein direktes und hoch sensitives Messverfahren, die NanoString nCounter Plattform, verwendet, um ein PCR-basiertes Amplifikationsprotokoll zur Erstellung von globalen Einzelzell-Transkriptomen zu validieren. Dazu wurden cDNA-Amplifikate aus Einzelzell-äquivalenten Verdünnungen einer Gewebe-RNA erstellt und mit der Ausgangs-RNA hinsichtlich der quantitativen und qualitativen Übereinstimmung verglichen. Für Transkripte, welche mit mehr als zehn Kopien vor der Amplifikation vorlagen wurde eine signifikante Korrelation festgestellt. Für den überwiegenden Anteil der Transkripte mit weniger als zehn Kopien (96%) konnte eine qualitative Detektion nachgewiesen werden. Dieses hoch sensitive Verfahren wurde im Folgenden angewendet um zwei spezifische neurobiologische Fragestellungen zu untersuchen.

Das erste inhaltliche Projekt befasst sich mit der Neurogenese, die der Generierung von exzitatorischen Projektionsneuronen im Kortex zu Grunde liegt. Diese Neurone werden zum Großteil bereits auf Vorläufer-Ebene durch eine Vielzahl an intrinsischen und extrinsischen Faktoren vordeterminiert. In Gerstmann et al. (2015) konnten wir zeigen, dass der Verlust von *EfnA5* zu Veränderungen in der Vorläufer-Produktion und in Folge dessen zu einer Verschiebung der kortikalen Schichten in adulten Mäusen führt. Mit Hilfe der hohen qualitativen Auflösung des verwendeten Einzelzell-Amplifikationsverfahrens war es dabei möglich kortikale Zellen als *EfnA5* Quelle auszuschließen. Stattdessen konnten *EfnA5* Transkripte in axonalen Kompartimenten thalamischer Neurone nachgewiesen werden. In Kombination mit funktionellen *in vitro* Assays, wurden in der vorliegenden Arbeit Belege dafür geliefert, dass *EfnA5* durch die in den Kortex einwachsenden thalamischen Afferenzen importiert wird, was eine Interaktion mit den membrangebundenen EphA4-Rezeptoren der radialen Gliazellen ermöglicht. Die präsentierten Daten beschreiben damit einen Mechanismus einer extra-kortikale Feinabstimmung der kortikalen Vorläufer-Produktion durch das Eph-Rezeptor/ephrin-Liganden System.

Das Einzelzell-Transkriptom-Analyse-Verfahren wurde des Weiteren verwendet um ein Thema im Bereich der Interneuron-Entwicklung zu untersuchen. Es gibt viele

Hinweise, dass psychiatrische Erkrankungen mit Störungen in inhibitorischen Netzwerken verbunden sind und Defekte während der Entwicklung scheinen häufig ursächlich für die Ätiologie der Symptome. Im Gegensatz zu kortikalen Projektionsneuronen, weisen Interneurone eine lange Phase der tangentialen Migration auf, während dessen sie von ihren Bildungszonen im basalen Telencephalon zu ihren Zielarealen wandern. Dies erfordert ein hohes Maß an Regulation um die korrekte Verteilung und Anzahl der Interneurone sicherzustellen, was wiederum Voraussetzung für die ordnungsgemäße Informationsverarbeitung im adulten Gehirn ist. Um Faktoren zu identifizieren, welche diese Prozesse im Speziellen in kortikalen Interneuronen steuern, wurden Einzelzellen analysiert, die aus den verschiedenen Arealen des basalen Telencephalons stammen, welche diese Subtypen produzieren. Mittels differentieller Genexpressionsanalyse wurden verschiedene Vorläuferpopulationen und postmitotische Subtypen charakterisiert. Dabei fiel auf, dass die *DNA Methyltransferase 1 (Dnmt1)* Expression in POA-abstammenden Interneuronen aufwies, welche in den Kortex migrieren. Die Deletion von *Dnmt1* in dieser spezifischen Interneuron-Population führte zu anormaler Migration und drastisch reduzierter Interneuronanzahl im adulten Kortex. Vergleichende *Next Generation Sequencing* Analysen von embryonalen, FAC-sortierten *Dnmt1* Wildtyp und *Dnmt1* Knockout Mäusen offenbarte eine DNMT1-abhängige Repression von Genen, die in späte Reifungsprozesse, wie Neuritenwachstum, involviert sind. In Übereinstimmung damit zeigten weitere Experimente, dass DNMT1 die migratorische Kapazität von postmitotischen GABAergen Interneuronen zum Teil durch eine negative Regulation von *Pak6* aufrechterhält, welches seinerseits Neuritenwachstum stimuliert.

Zusammenfassend wurde in dieser Arbeit gezeigt, dass die NanoString basierte Analyse von repräsentativen Einzelzell-cDNA-Bibliotheken, welche durch exponentielle Amplifikation erstellt wurden, sehr gut geeignet ist um Einzelzell-Transkriptome innerhalb komplexer Gewebe zu untersuchen. Es wurde eine valide Analysestrategie erstellt um verschiedene neuronale Subtypen innerhalb einer heterogenen Zellpopulation zu identifizieren. Dabei konnten spezifische Genexpressionsprofile erstellt werden und es wurden zwei neue Mechanismen während der embryonalen Gehirnentwicklung entdeckt. Dieses Verfahren ist gleichermaßen geeignet um die Heterogenität anderer komplexer Gewebe zu ergründen, was auch das Untersuchen von individuellen Zellen in Krankheitsrelevanten Biopsien betreffen könnte.

3 Introduction

3.1 Development of the neocortex

The neuronal network of the adult brain represents the most complex structure for data processing known by far. Thereby, the neocortex as seat of higher cognitive functions including cognition, sensory perception and sophisticated motor control is in the focus of scientific interest. Dysfunctional cortical networks or abnormal cortical development are often involved in neuropsychiatric or neurodevelopmental diseases. However, these remain poorly understood and hence largely untreated (Marin 2012). Already minor alterations in the subtype composition or function of individual neuronal populations can lead to severe neuropsychiatric diseases like epilepsy or schizophrenia (Marin 2012, Benes 2015). Various genes involved in the pathology of such diseases have also been described to have important function also during embryonic brain development (Rubenstein and Merzenich 2003, Dani et al. 2005, Levitt 2005, Lewis et al. 2005). In this context, for several neuropsychiatric diseases, including autism (Rubenstein and Merzenich 2003, Levitt et al. 2004), schizophrenia (Lewis 2000, Benes and Berretta 2001) and anxiety disorder (Jetty et al. 2001), abnormal development and function of cortical interneurons have been implicated. Hence, comprehension of gene function during development could be beneficial to understand adult projection neuron as well as interneuron diversity, the principles of their integration into neuronal networks, but also the causes for dysfunctions.

As a unique phylogenetic feature of all mammals, the neocortex is roughly segmented into six distinct layers and consists of 70-80% excitatory projection neurons and 20-30% at most inhibitory interneurons (Wonders and Anderson 2006, Merot et al. 2009, Gelman and Marin 2010, Kepecs and Fishell 2014). While projection neurons are generated inside the ventricular zone (VZ) and subventricular zone (SVZ) of the neocortex subsequently establishing the cortical plate (CP; Takahashi et al. 1996, Polleux et al. 1997, Gotz and Huttner 2005, Dehay and Kennedy 2007, Merot et al. 2009), the proliferative zones of cortical interneurons are localized inside the basal telencephalon of rodents, as well as primates (Fig. 1A, B; Porteus et al. 1994, de Carlos et al. 1996, Clowry 2015, Arshad et al. 2016). During embryonic brain development multipotent progenitors generate a variety of neurons with distinct morphologic and functional characteristics (Campbell 2005, Flames and Marin 2005, Rakic 2009, Gelman and Marin 2010, Marin and Muller 2014). To ensure the correct number,

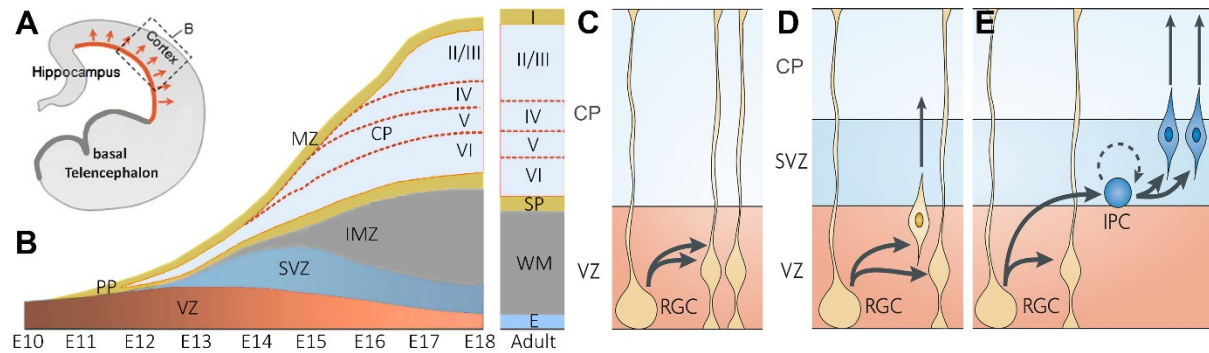


Figure 1 - Cortical projection neuron development. (A) Scheme of sagittal mouse brain section. Projection neurons arise from progenitors in the dorsal-lateral ventricular wall (red line) and migrate radially to populate the nascent cortex (red arrows). (B) Scheme depicting the temporal generation of projection neurons from progenitors located in the VZ and SVZ consecutively establishing the cortical layers. (C-E) Summary of the proliferative behavior and progeny of cortical progenitors. Cortical neurons are mainly generated from two types of precursors: radial glia cells (RGCs) and intermediate progenitor cells (IPCs). (C) RGCs undergo several types of symmetrical and asymmetrical divisions, as indicated by the arrows, including self-renewing ones (C) or neurogenic divisions (D). (E) Through asymmetrical divisions, RGCs give rise to IPCs that migrate to the subventricular zone (SVZ). IPCs divide away from the ventricular surface in the VZ and in the SVZ. IPCs have been reported to undergo mostly neurogenic divisions with a small fraction undergoing symmetrical proliferative divisions (as indicated by the dotted circular arrow). CP, cortical plate; E, ependymal; IMZ, intermediate zone; MZ, marginal zone; PP, preplate; SP, subplate; WM, white matter. (A-B modified according to Merot et al., 2009; C-E modified according to Dehay and Kennedy, 2007)

localization and connectivity of the different neuronal populations, precise control over developmental processes like proliferation, differentiation, apoptosis, migration, axon formation and synaptogenesis is required. Numerous intrinsic as well as extrinsic factors are involved in the regulation of these processes.

3.1.1 Development of cortical excitatory projection neurons

The neocortex of mammals is organized in areas, horizontal layers and vertical columns (Rakic 1988, Mountcastle 1997, Casanova and Trippe 2006, Rakic 2009, Costa and Hedin-Pereira 2010). The allocation into areas is based on their respective cytoarchitectural composition and functionality. Furthermore, the six major horizontal layers are mainly characterized according to their neuronal subtype composition, cell density and connectivity pattern (Rakic 1988, Mountcastle 1997). The neurons of the different layers display distinct morphological as well as functional properties and each layer forms specific intrinsic and extrinsic connections (Lund and Mustari 1977, Gotz and Bolz 1992). In addition to the laminar organization, the cortex is also structured into vertical columns (Mountcastle 1997). Some decades ago Hubel and Wiesel (1962) recognized that neurons of distinct cortical columns inside the visual cortex reply together to stimuli like color or the orientation of light. In this context, it has already been described that excitatory projection neurons originating from the same cortical progenitor are taking the same path during their radial migration into the cortical plate and are localized in the same column at adult stages (Reid et al. 1995, Torii et al. 2009). On the other hand, simultaneously produced neurons are positioned in the

same cortical layer afterwards (McConnell 1995). Thus, the different aspects of projection neurons like their position but also morphology and connectivity pattern reflect their specific function (McConnell 1995, Campbell 2005).

The cortical excitatory projection neurons originate in the neural epithelium near the ventricle. Multipotent neuronal precursors contained therein, display a polarized morphology. Their apical process reaches into the ventricle and their basal process spans the whole cortex up to the basal lamina (Fishell and Kriegstein 2003, Kriegstein and Gotz 2003, Gotz and Huttner 2005). As a consequence, they are called radial glia cells (RGC) or apical progenitors, in regard to their position near the ventricle. Prior to the generation of the first cohorts of neurons, the apical progenitors are proliferating symmetrically to increase the population of multipotent stem cells (Fig. 1C; McConnell 1995, Rakic 1995). The neurogenesis of cortical projection neurons extends from embryonic day 12 (E12) to E18 (Takahashi et al. 1996, Polleux et al. 1997, Merot et al. 2009). The first cohorts of postmitotic neurons are generated by asymmetric division of the apical progenitors producing a postmitotic neuron and an apical progenitor (Fig. 1D; Dehay and Kennedy 2007). The resulting neurons migrate radially out of the VZ leading to the formation of a transient pre-plate (Marin-Padilla 1971, Rickmann et al. 1977). Subsequently generated neurons split this pre-plate into the marginal zone and the sub-plate, which will later develop to layer I and VI (Fig. 1B; Aboitiz et al. 2005, Casanova and Trippe 2006). During the proceeding development the newly produced neurons will integrate between these two layers and form layer V to II in a so called inside-out pattern (Fig. 1B; Angevine and Sidman 1961, McConnell 1989, Polleux et al. 1997). According to this concept, early born neurons form the deep layers and all subsequently generated projection neurons contribute to the overlying layers. Thereby, the birth date of an individual neuron largely determines its subsequent position in the cortical layers and its functional identity. The direct neuronal production of RGCs is limited to 10-20% of the total number of excitatory projection neurons (Kowalczyk et al. 2009, Vasistha et al. 2014). Most excitatory neurons instead derive from a second type of progenitor, called intermediate progenitor, which is produced by asymmetric division of apical progenitors (Fig. 1E; Haubensak et al. 2004, Miyata et al. 2004, Noctor et al. 2004). These progenitor types translocate their cell bodies into the SVZ losing the radial processes connecting the apical progenitors with the ventricle and the basal lamina (Fig. 1E). Due to their relative position closer to the basal lamina, they are also called basal progenitors. Most of the intermediate progenitors produce two

postmitotic neurons by a terminal symmetric division. However, it has also been described, that a distinct proportion performs symmetric proliferative division thereby increasing the pool of intermediate progenitors (Haubensak et al. 2004, Noctor et al. 2004, Gotz and Huttner 2005). After leaving the cell cycle, the postmitotic projection neurons start radial migration to reach their final positions inside the cortical plate. During early neurogenesis the new born neurons mainly migrate without using the scaffold provided by the radial glia cells (Miyata et al. 2001, Nadarajah et al. 2001). Thereby, they establish a pioneer process pointing towards the cortical surface followed by a translocation of the soma (Book and Morest 1990, Morris et al. 1998). When corticogenesis proceeds, the migration mode switches and the newly born projection neurons use the radial glia processes as scaffold for their locomotion (Nadarajah and Parnavelas 2002, Cooper et al. 2008).

At adult stages, the cortex exposed various intracortical, interhemispheric as well as extracortical connections (Price et al. 2006). From E13 on the intermediate zone (IMZ), which will later form the white matter, is established between the VZ and the cortical plate by afferences and efferences connecting the different cortical areas as well as extracortical regions like the thalamus (Fig. 1B; Auladell et al. 2000, Gerstmann et al. 2015). Several signal molecules and transcription factors exert control over axonal outgrowth and guidance. Surface molecules like ephrins, semaphorins or cadherins are involved in the guidance of thalamic axons projecting to the cortex (Lopez-Bendito et al. 2003, Bolz et al. 2004). In addition, transcription factors like *Pax6* and *Emx2* have been described to participate in the generation of thalamocortical projections (Lopez-Bendito et al. 2002, Pratt et al. 2002). First thalamocortical projections reach the cortex as early as E13, when they tangentially invade the IMZ (Auladell et al. 2000). Already at E14 most thalamic fibers have reached their final area-specific position in the IMZ, right beneath their destination in the cortical plate (Price et al. 2006). Some of these fibers are already traceable inside the cortical plate from E15 on (Auladell et al. 2000), but the majority of axons maintain a stand-by position in the IMZ and do not invade the CP before E18 (Molnar et al. 1998).

3.1.2 Development of cortical interneurons

In contrast to the principal neurons which exert excitatory function to the postsynaptic cells, most interneurons perform inhibitory actions (Kepecs and Fishell 2014, Lodato and Arlotta 2015). Thereby, the majority of cortical interneurons uses the inhibitory

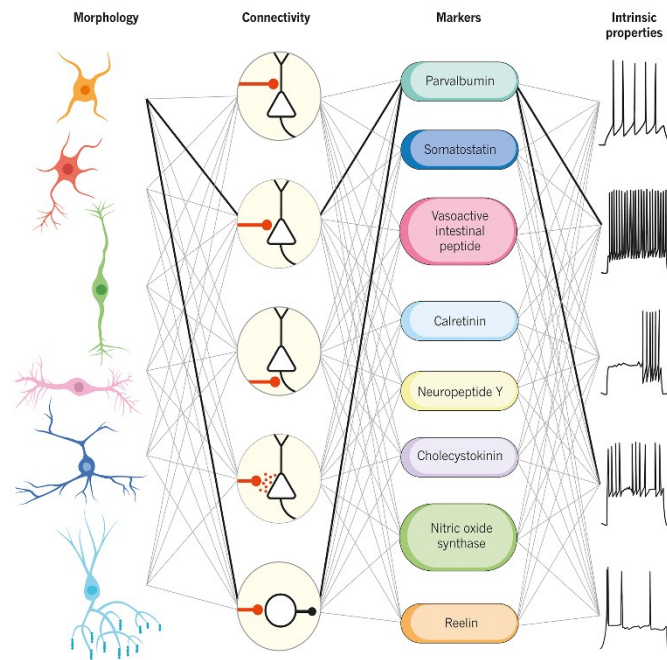


Figure 2 - Multiple dimensions of interneuron diversity. Interneuron cell types are usually defined using a combination of criteria based on morphology, connectivity pattern, synaptic properties, marker expression and intrinsic firing properties. The highlighted connections define fast-spiking cortical basket cells. (according to Kepecs & Fishell, 2014)

neurotransmitter γ -aminobutyric acid (GABA) synthesized by the enzyme glutamate decarboxylase, which is evident as two different isoforms (GAD65 and GAD67; Erlander et al. 1991, Lodato and Arlotta 2015). Cortical GABAergic interneurons are highly diverse according to their morphology, connectivity pattern, expression of molecular markers and electrophysiological properties (Fig. 2; Wonders and Anderson 2006, Kepecs and Fishell 2014). The different subtypes are involved in the synchronization and modulation of the activity of principle neurons (Druga 2009, Marin 2012, Kelsom and Lu 2013). Although interneurons are a minor population within the cortex, they are crucial for the control of neuronal network activity. In mice, they are born from E11 to E17 in different parts of the basal telencephalon, including the medial and caudal ganglionic eminences (MGE and CGE, respectively) as well as the preoptic area (POA; Fig. 3; Anderson et al. 2001, Marin and Rubenstein 2001, Marin et al. 2001, Wichterle et al. 2001, Flames et al. 2007, Corbin and Butt 2011, Marin 2013). Contemporary, the proliferative zones of the basal telencephalon also produce neurons for other destinations, like for the hippocampus, amygdala, septum, striatum or the olfactory bulb (Butt et al. 2008, Nobrega-Pereira et al. 2008, Gelman et al. 2009, Gelman et al. 2011) as well as subsets of oligodendrocytes (Fig. 3A; Qi et al. 2002). Around 60% of all cortical interneurons originate from the MGE expressing parvalbumin (PV) or somatostatin (SST; Fig. 3A; Xu et al. 2004, Butt et al. 2005, Miyoshi et al. 2007, Gelman et al. 2011). Another 25-35% is generated in the CGE,

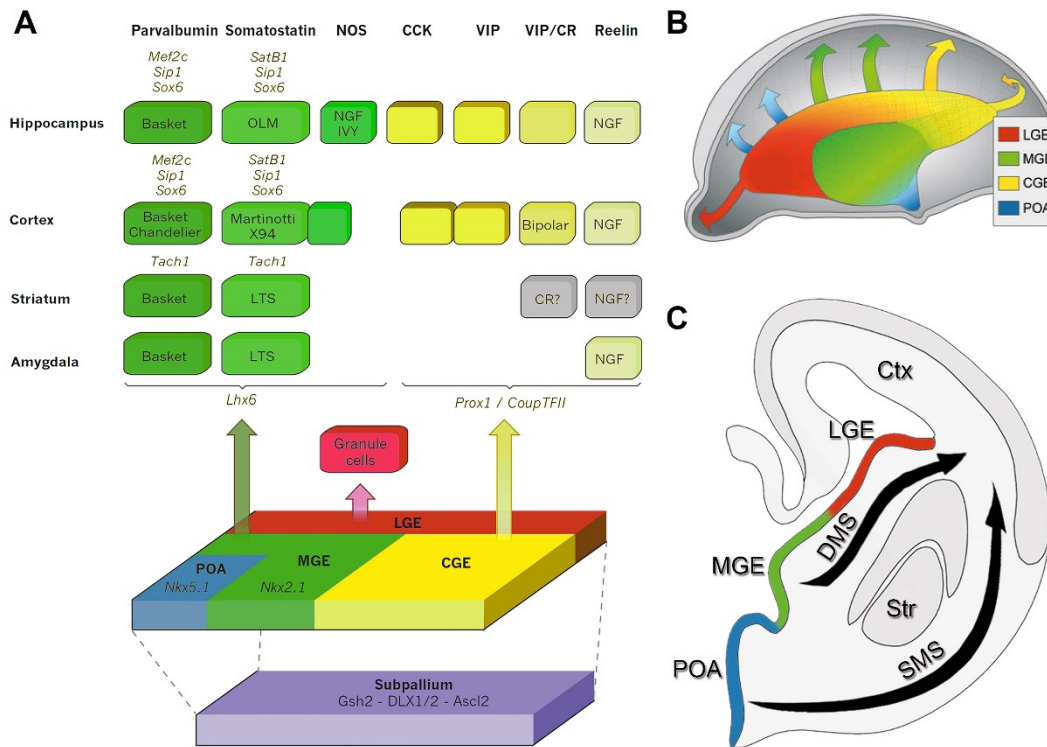


Figure 3 - Interneuron subtypes are generated from discrete proliferative regions within the subpallium. (A) The progressive development of the telencephalon from an undifferentiated epithelium (purple) into discrete proliferative zones that produce particular interneuron populations. The majority of cortical interneurons are generated inside the medial ganglionic eminence (MGE, green), caudal ganglionic eminence (CGE, yellow) and the pre optic area (POA, blue). Interestingly, although common proliferative zones produce the entire diversity of interneurons across all telencephalic structures, unique cell types and gene expression are seen in interneuron populations that reside in particular telencephalic structures. (B) Cortical interneurons are born in distinct structures within the subpallium and migrate tangentially to the cortex. The scheme represents an E13.5 embryo brain hemisection. The arrows show representative migratory routes. For simplicity, the septum and the thalamus are not depicted in the scheme. (C) A sagittal section of an embryonic mouse brain hemisphere depicting the superficial and deep migratory stream (SVZ and DMS, respectively) used by interneurons fating for the cortex. CCK, cholecystokinin; CR, calretinin; LGE, lateral ganglionic eminence; LTS, low threshold spike; NGF, nerve growth factor; NOS, nitric oxide synthase; OLM, oriens/lacunosum moleculare; VIP, vasointestinal peptide. (A modified according to Kepecs & Fishell, 2014; B according to Gelman & Marin 2010; C basic shape retained from Zimmer et al., 2011)

which represents the posterior fusion of the medial and lateral ganglionic eminence in the caudal basal telencephalon (Fig. 3A, B). Cortical interneurons originated from the CGE express the vasoactive intestinal peptide (VIP) and/or the calcium-binding protein calretinin (CR). Alternatively they are positive for neuropeptide Y (NPY; Fig. 3A; Lopez-Bendito et al. 2004, Xu et al. 2004, Butt et al. 2005, Fogarty et al. 2007, Miyoshi et al. 2010).

Using a Cre line under the promoter of *Hmx3* (*Nkx5.1*), which is a postmitotic transcription factor exclusively expressed in the POA inside the basal telencephalon, Gelman et al. (2009) have demonstrated that this region also contributes to cortical interneuron production. The POA is located at the most ventral part of the basal telencephalon (Fig. 3B, C; Anderson et al. 2001, Marin and Rubenstein 2001, Gelman et al. 2009, Zimmer et al. 2011). While a minor fraction of the GABAergic cortical interneurons derived from this lineage expresses NPY, most of them could not be classified according to the established molecular markers like PV, CR, SST or VIP.

However, they show uniform electrophysiological properties (Gelman et al. 2009). *Hmx3* is expressed at an early postmitotic stage and subsequently downregulated. According to genetic lineage tracing experiments this population contributes to cortical interneurons, as well as interneurons for the olfactory bulb and the POA itself (Gelman et al. 2009). In addition, the POA as well as the MGE, also give rise to cholinergic, striatal interneurons, which express the insulin gene enhancer protein (*Islet1* or *Isl1*) during the developmental time course (Elshatory and Gan 2008).

3.1.2.1 Transcriptional code of interneuron subtypes

The intrinsic properties defining a particular interneuron subtype are mainly based on the transcriptional code of gene sets expressed at progenitor level as well as during postmitotic development (Lodato and Arlotta 2015). The initial commitment to the GABAergic lineage is determined by the activity of the transcription factors *Dlx1/2*, whose expression is under control of the proneuronal gene *Mash1* (Fig. 3A; Casarosa et al. 1999, Stuhmer et al. 2002). Later on, the homeobox gene NK2 homeobox 1 (*Nkx2-1*), encoding for the thyroid transcription factor 1 (TTF-1), is expressed inside the MGE as well as in parts of the POA. Fate-mapping studies have demonstrated, that this transcription factor is involved in the generation of several interneuron subtypes. Striatal NPY-positive or SST-positive interneurons originate from this native population, as well as several subtypes fating for the hippocampus (Fig. 3A). The subsequent postmitotic development of MGE-derived cortical interneurons relies on the activity of the *Lhx6* transcription factor which itself is controlled by *Nkx2-1* (Lavdas et al. 1999, Butt et al. 2008, Du et al. 2008, Nobrega-Pereira et al. 2008, Zhao et al. 2008). Interestingly, LHX6 is an upstream regulator of *Sox6*. Its absence results in a drastic loss of PV and SST expression. Instead, increased NPY expression takes place suggesting that even at postmitotic stages cell fate determination is still dynamic (Azim et al. 2009, Batista-Brito et al. 2009).

As suggested by Flames et al. (2007), the high diversity of interneuron subtypes seems to be at least partially achieved by coexpression of several regulatory elements dynamically expressed in overlapping patterns inside the basal telencephalon. Hence, in addition to the anatomical domains (LGE, MGE, CGE and POA) the basal telencephalon is further segmented into compartments characterized by distinct gene expression patterns (Flames et al. 2007). Consistent with these subdivisions it has been proposed that PV-ergic cortical interneurons are generated especially in the

ventral part of the MGE (Wonders and Anderson 2006). In contrast, the dorsal area of the MGE was suggested to give rise to a different class of interneurons expressing SST and/or CR (Liodis et al. 2007, Du et al. 2008). Moreover, genetic fate-mapping as well as transplantation studies support a model in which the localization of progenitors and the timing of neurogenesis have at least predictive value for interneuron cell fate (Xu et al. 2004). Hence, several groups favor a model, whereby distinct adult interneuron subtypes derived from particular precursor populations with a unique pattern of transcription factor expression (Jessell 2000, Lee and Pfaff 2001, Dessaud et al. 2008, Corbin and Butt 2011).

3.1.2.2 Complex postmitotic phase of cortical interneuron maturation

Cortical interneurons have a quite complex and long phase of postmitotic maturation. Based on the transcriptional code several different developmental processes are initiated and controlled (Corbin and Butt 2011). Regarding cortical interneurons as well as subtypes destined for other regions, these processes mainly involve migration, requiring comprehensive reorganization of the morphology by cytoskeleton remodeling to achieve migratory capacity (Martini et al. 2009, Cooper 2013) as well as the expression of guidance receptors and ligands determining the path for distinct interneuron subtypes (Rudolph et al. 2010, Antypa et al. 2011, Zimmer et al. 2011, Marin 2013, van den Berghe et al. 2013, Rudolph et al. 2014, Steinecke et al. 2014, Zito et al. 2014). Two main migratory streams have been identified for cortical interneurons (Lavdas et al. 1999, Anderson et al. 2001, Marin and Rubenstein 2001), which are separated by the developing striatum. MGE-derived cortical interneurons mainly migrate along the deep migratory stream (DMS) through the SVZ of the MGE and LGE (Fig. 3C; Zimmer et al. 2011, Marin 2013). In contrast, POA-derived cortical interneurons use the superficial migratory stream (SMS) along the mantle of the IMZ of the basal telencephalon. Reaching the pallial-subpallial border marks the termination of a phase in the migratory program of cortical interneurons, as the subpallium becomes refractory to cortical interneurons once they have entered the pallium (Marin et al. 2003). Inside the cortex most interneurons migrate either along a superficial route that runs through the marginal zone (MZ) or along a deep route that largely overlaps with the SVZ and IMZ of the cortex (Lavdas et al. 1999, Wichterle et al. 2001).

The final migratory phase of cortical interneurons corresponds to their allocation to specific layers inside the cortex. This process continues until the first postnatal days (Pla et al. 2006, Miyoshi and Fishell 2011). Early cortical interneurons populate the cortex in an inside-out mode comparable to the integration pattern of projection neurons (Valcanis and Tan 2003, Rymar and Sadikot 2007). In contrast, later waves of cortical interneurons are mainly localized in supra-granular layers, independently of their birthdate (Xu et al. 2004, Rymar and Sadikot 2007, Miyoshi et al. 2010). Moreover, all interneurons derived from the CGE seem to preferentially populate the most superficial layers (Miyoshi et al. 2010). Incidentally, the cortical interneuron fraction of the *Hmx3* lineage used in this thesis has been described to integrate mainly into the superficial layers (Layer II-IV; Gelman et al. 2009). Since the time and place of origin seem to be no general predictors of the final specification and lamination of cortical interneurons, the mechanisms determining the proper cortical integration of interneurons are still illusive.

After reaching their final laminar position the interneurons will start to differentiate by establishing their dendritic and axonal arborizations. Arborization is achieved by neurite branching requiring broad cytoskeleton rearrangements, distinct from migratory processes (Cobos et al. 2007, Guillemot 2007). In this context, Cobos et al. (2007) show that PAK3, a member of the p21- activated serine/threonine kinases (PAKs) family, is relevant for branching in MGE derived interneurons. During tangential migration cortical interneurons display low levels of PAK3 expression, whereas PAK3 expression is up-regulated *in vivo* once they start to differentiate at their final position inside the cortical layers (Cobos et al. 2007). PAK kinases are major downstream effectors of the Rho-family GTPases RAC1 and CDC42 (Bokoch 2003, Hofmann et al. 2004, Kumar et al. 2006), which integrate different extracellular and intracellular signals to orchestrate the changes in cytoskeleton necessary for cell motility, neurite outgrowth, as well as for axon and dendrite guidance (Luo 2000, Govek et al. 2005, Rossman et al. 2005). In *Drosophila*, PAK kinases exert essential roles in axon guidance (Hing et al. 1999, Fan et al. 2003). Further, they have been described to regulate neurite outgrowth, cell migration, spine morphogenesis and synapse formation in mammalian brains (Bokoch 2003, Hofmann et al. 2004, Boda et al. 2006). In general, in mammalian neurons high expression levels of PAK kinases seem to promote neurite outgrowth (Daniels et al. 1998, Rashid et al. 2001, Cobos et al. 2007)

and are involved in dendrite spine morphogenesis and synapse formation as well as plasticity (Boda et al. 2004, Meng et al. 2005, Zhang et al. 2005).

3.1.2.3 What defines interneuron subtype identity? Extrinsic versus intrinsic determination.

Insights into the mechanisms controlling subtype determination at progenitor as well as at postmitotic stages are essential to develop potential treatments strategies for neurodevelopmental diseases like cell replacement based therapies (Marin 2012, Southwell et al. 2014). Up to now it is not entirely clear to which extent an interneuron subtype is already pre-specified at precursor level due to intrinsic properties and how relevant extrinsic events are during postmitotic maturation for cell fate determination (Corbin and Butt 2011). The importance of intrinsic determination for cortical interneurons was already highlighted in the last chapters. Consequently, it has been hypothesized for a long time, that their cell fate is already predefined when they leave the cell cycle as previous studies had shown that similar to principle neurons, clonally related interneurons seem to form distinct columns inside the cortex (Nery et al. 2002, Butt et al. 2005, Marin and Muller 2014). But according to current published tracing experiments of individual clonally related cells, there is no broad spatial relationship of interneurons. If anything they are widely dispersed over all cortical areas as well as destinations inside the basal telencephalon (Harwell et al. 2015, Mayer et al. 2015). If there is any kind of clustering observed, this seems to be due to the fact, that clonally related cells are produced in a similar environment. Consequently, the clustering would not be due to lineage relationships, but resulting of similar environmental cues during their postmitotic maturation (Harwell et al. 2015, Mayer et al. 2015). Therefore, the distinct spatial and temporal pattern of interneuron generation might play an instructive role for final positioning and fine tuning of cell fate determination (Ciceri et al. 2013, Marin and Muller 2014), as the immature neurons are exposed to a specific environment dependent on their time and place of generation. In this context it has been shown, that even region-specific migration can be altered at post-mitotic stages (McKinsey et al. 2013, van den Berghe et al. 2013) and that the final layer positioning of cortical interneurons depends to a large extent on the correct distribution of excitatory projection neurons and molecules secreted from the meninges (Tiveron et al. 2006, Li et al. 2008, Lodato et al. 2011). Moreover, it has been demonstrated that electrical activity can influence the migration of cortical interneurons (Bortone and

Polleux 2009, De Marco Garcia et al. 2011). These postmitotic events do not change the interneuron subtype fundamentally, being indicative that intrinsic properties are instructive for the rough subtype determination. Yet, they can alter the distribution and integration of interneuron subtypes, which are also important classifiers determining an interneuron subtype and its prospective function. Hence, intrinsic as well as extrinsic properties seem to be essential to establish a fully functional and integrated interneuron at the default position.

3.2 Multifunctional molecules involved in brain development

Several mechanisms are involved in the control of postmitotic maturation, including tangential and radial migration as well as final differentiation and network integration. While detailed knowledge is very limited for factors and systems that regulate the migration of CGE- and POA-derived interneurons, several mechanisms regulating MGE-derived interneuron migration have already been identified. For instance, it has been described that, MGE-derived interneurons follow a gradient of increasing permissivity towards the cortex, most likely created by the diffusion of long-range chemo attractive cues from the pallium (Marin et al. 2003, Wichterle et al. 2003). Two isoforms of neuregulin act as short- and long-term attractants that demarcate the migratory route of cortical interneurons. ERBB4, a receptor of the ErbB tyrosine kinase family has been identified as the corresponding receptor expressed in MGE-derived interneurons fated for the cortex (Yau et al. 2003, Flames et al. 2004). In contrast, cortical interneurons avoid the striatum based on a repulsive signaling. Class III semaphorine 3A expressed inside the striatum mediates a repulsive action on migrating cortical interneurons carrying the neuropilin receptor NRP1 and NRP2 (Marin et al. 2001, Zimmer et al. 2010). Moreover, several factors such as brain-derived neurotrophic factor (BDNF), neurotrophins (NT4) as well as hepatocyte growth factor (HGF) serve as motogens for interneurons, initiating and promoting their migration (Brunstrom et al. 1997, Powell et al. 2001).

3.2.1 The role of ephrins during brain development

The sorting of interneurons into the superficial or deep migratory stream during their way up to the cortex is partially achieved by two members of the Eph-receptor/ephrin-ligand system. In more detail, Zimmer et al. (2011) showed that due to a repulsive interaction of EFNB3 and EPHA4 the majority of *EphA4*-expressing MGE-derived cortical interneurons enter the deep migratory stream, whereas *efnB3*-expressing

POA-derived cortical subtypes are enforced to follow the superficial migratory stream (Fig. 3C; Zimmer et al. 2011). Similar, previous studies demonstrated repulsive responses after EphA activation in retinal ganglion cells and cortical neurons mediated by Src family kinases (Klinghoffer et al. 1999). These kinases have been associated to cell migration (Klinghoffer et al. 1999), and are suggested to regulate integrin function and rearrangements of the cytoskeleton required for migratory processes (Huang et al. 1997, Felsenfeld et al. 1999). Remarkably, both the Eph-receptors and the ephrin-ligands are able to induce signaling cascades allowing bidirectional signal transduction (Holland et al. 1996, Bruckner et al. 1997). A signaling cascade induced in the receptor expressing cell is designated as forward signaling, whereas reverse signaling is established in the ligand expressing cell (Wilkinson 2001, Kullander and Klein 2002, Murai and Pasquale 2003). In the case of B ligands, the receptor binding leads to phosphorylation of the cytoplasmic domain of the ligand initiating the reverse signaling. Though A ligands do not exhibit an intracellular binding domain, it has been described that a reverse signaling could be triggered by adaptor proteins (Anderson et al. 1998, Davy et al. 1999).

In addition to their functions during postmitotic migration, Eph-receptor/ephrin-ligand interactions have been described to regulate proliferation and differentiation as well as axon guidance and synaptogenesis (Bolz and Castellani 1997, Flanagan and Vanderhaeghen 1998, Knoll and Drescher 2002, Kullander and Klein 2002, Qiu et al. 2008, North et al. 2009, Rudolph et al. 2010, Zimmer et al. 2011). It has further been shown, that ephrins promote branching of thalamic afferences (Castellani and Bolz 1996, Uziel et al. 2008), affect the adhesive properties of cortical cells (Holmberg et al. 2000, Zimmer et al. 2007) and regulate the topographic organization of the cerebral cortex (Kullander and Klein 2002, Bolz et al. 2004). Hence, Eph receptor and ephrin ligands are broadly expressed in the embryonic brain (Liebl et al. 2003, Yun et al. 2003). However, for interaction direct cell to cell contact is required as both components are anchored inside the membrane (Davis et al. 1994). So far 15 Eph receptors and 9 ephrin ligands have been identified (Fig. 4A). Based on their structure the ephrin ligands are divided into two classes (Gale et al. 1996). Ephrin A ligands

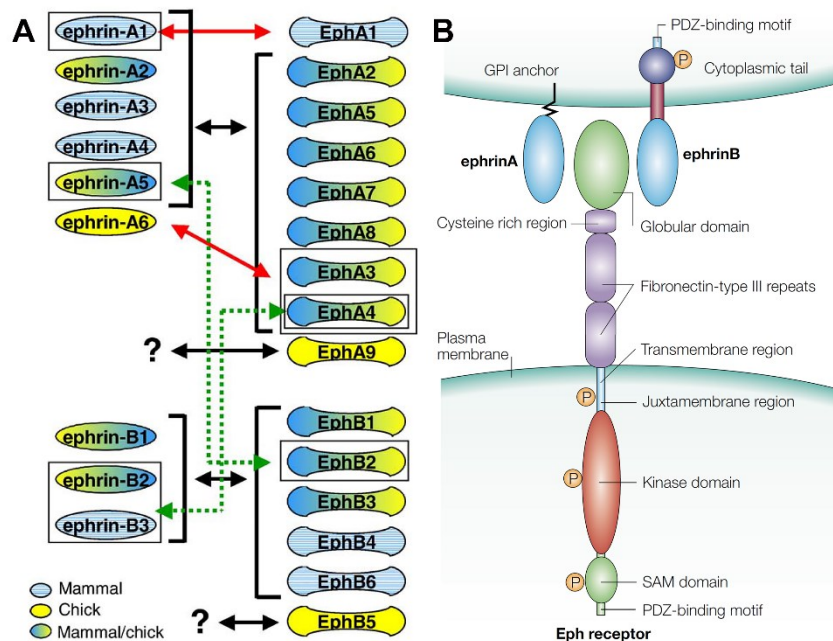


Figure 4 - General features and binding abilities of Eph receptors and ephrins. (A) Structural classes of Eph receptors and ephrins and their binding specificities. Despite some described high affinity ligand/receptor interactions (red arrows), binding is mostly promiscuous within each of the ephrin/Eph specificity classes (black arrows). In addition, there are two exceptions that show low affinities between members of distinct subclasses (green arrows). Ligands for EphA9 and EphB5 receptors have still not been described. Ligands and receptors have been characterized in mammals (blue), chick (yellow) or both (blue/yellow). **(B)** A schematic diagram, which shows an ephrin-expressing cell (top) interacting with Eph-expressing cell (bottom) and the different components of the Eph-receptors and the two distinct types of ligands (ephrin A and ephrin B). GPI, glycosylphosphatidylinositol; SAM, sterile α -motif **(A)** according to Martinez and Soriano, 2005; **(B)** according to Kullander & Klein, 2002)

have a GPI-anchor (glycosylphosphatidylinositol), whereas B ligands exhibit a transmembrane domain as well as an intracellular PDZ-binding domain (Fig. 4B; Torres et al. 1998, Song et al. 2002). In contrast, the Eph receptors have a quite similar structure with an extra-cellular, N-terminal binding domain enabling specific ligand interaction (Labrador et al. 1997), as well as a cysteine-rich region and two type-II fibronectin-domains, mediating interaction with other proteins (Fig. 4B; Dalva et al. 2000). In addition, Eph receptors have a highly conserved juxtamembrane motif and a kinase domain required for auto phosphorylation. Both are necessary, as Eph receptor tyrosine kinases are monomeric receptors, which dimerize upon ligand binding (Flanagan and Vanderhaeghen 1998, Lackmann et al. 1998, Torres et al. 1998, Murai and Pasquale 2003). Further, a c-terminal SAM domain enables the agglomeration of dimers and oligomers (Torres et al. 1998, Kullander and Klein 2002). The Eph receptors were categorized based on sequence homologies and binding properties to distinct type A or B ligands, although a few exceptions exist (Fig. 4A; Gale et al. 1996, Martinez and Soriano 2005). For instance, the receptor EPHB2, that normally binds to B ligands, is also able to interact with EFNA5. In contrast, EPHA4 displays additional binding affinity to EFNB2 as well as to EFNB3 (Fig. 4A; Gale et al. 1996, Flanagan and Vanderhaeghen 1998, Martinez and Soriano 2005). Furthermore, different binding

affinities for distinct receptor-ligand combinations have been described. For example, EFNA5 is a high affinity binding partner of EPHA4, whereas the interaction with EPHA3 is significantly weaker (Monschau et al. 1997).

3.2.2 Epigenetic regulation of gene expression

The distinct steps and the extended period of cortical interneuron maturation underline the relevance of postmitotic regulatory mechanisms, which control initiation, motility, directionality and termination of interneuron migration. Recent literature had shown that maintaining the proliferating capabilities of stem cells requires the epigenetic suppression of neuronal and glial gene sets, whereas differentiation is based on removal of epigenetic suppression of genes necessary for neuronal or glial fate specification (Hsieh and Eisch 2010, Jobe et al. 2012, Sharma et al. 2016).

Several epigenetic pathways, such as mediators of DNA methylation, chromatin remodeling systems and non-coding RNA modulators seems to play an important role during neurogenesis (Jobe et al. 2012, Tuncdemir et al. 2015). Modification of histone proteins, such as the methylation of lysine and arginine residues, influences the higher order of chromatin leading to gene activation or silencing (Zhou et al. 2011, Roidl and Hacker 2014). Several groups have provided evidence, that histone modifications are important regulators of gene expression at the transition from progenitor level to neuronal differentiation (Azuara et al. 2006, Bernstein et al. 2006, Mikkelsen et al. 2007, Mohn et al. 2008). Further, in a recent study, Tuncdemir et al. (2015) suggest that miRNAs also exert epigenetic control over postmitotic cortical interneuron maturation (Tuncdemir et al. 2015).

DNA methylation represents another major epigenetic mechanism, which is performed by DNA methyltransferases (DNMTs) and in general leads to gene silencing (Razin and Shemer 1995, Robertson 2002, Jiang et al. 2008), It has been shown to control gene expression during development, ageing and disease (Hirabayashi and Gotoh 2010, Adefuin et al. 2014). DNMT1, which was long time thought to be limited to maintenance of methylation profiles during cell division (Inano et al. 2000), has been described to be critical for cortical projection neuron maturation and synaptic function (Feng and Fan 2009, Feng et al. 2010), also suggesting a role in postmitotic cells. In addition, deregulated *Dnmt1* expression and DNMT1 activity in cortical GABAergic interneurons are implicated in the pathophysiology of psychiatric diseases (Benes 2015, Dong et al. 2015). This appears, at least in part, to be linked to developmental

defects since prenatally induced changes in the *Dnmt1* expression level in murine GABAergic interneurons elicit schizophrenia-like phenotypes in mice (Matrisciano et al. 2013). However, its role in postmitotic but immature cortical interneurons during their prolonged phase of maturation is completely unknown yet.

3.3 Single cell analysis is required to reveal subtype specific developmental mechanisms

The elaborated functions of the mammalian cerebral cortex rely on the specific connectivity of many different neuronal subtypes. The sites of origin of cortical projection neurons as well as interneurons in the murine telencephalon are enormously complex mosaics (Arlotta et al. 2005, Merot et al. 2009, Kelsom and Lu 2013, Lodato and Arlotta 2015), which contemporaneously produce a variety of neuronal subtypes. In addition, gene expression changes throughout the cell cycle as well as during different stages of postmitotic maturation (Kawaguchi et al. 2008, Xue et al. 2013, Zopf et al. 2013, Trapnell et al. 2014, Treutlein et al. 2014, Kolodziejczyk et al. 2015b). For this, single-cell based global transcriptome analysis is essential to decipher the regulators of neuronal heterogeneity orchestrating their cell fate and maturation. The transcriptome is defined as the actually expressed mRNA inside a cell or tissue. The mRNA composes only 5% of all RNA, which corresponds to around 0.5-1.5 pg mRNA per cell, assuming a total RNA quantity of 5-30 pg (Kurimoto et al. 2006, Haag 2009). To date, no method exists, that would allow a direct analysis of such low mRNA quantities. Instead, several approaches have been developed, which are based on amplification prior to downstream analysis (Brady and Iscove 1993, Wagatsuma et al. 2005, Kurimoto et al. 2006, Lao et al. 2009, Tang et al. 2009, Islam et al. 2011, Hashimshony et al. 2012, Pollen et al. 2014, Macosko et al. 2015, Liu and Trapnell 2016).

To gain single cell transcriptome information, exponential amplification has major advantages in regard to efficiency and methodological simplicity (Brady et al. 1990, Dulac and Axel 1995, Iscove et al. 2002, Petalidis et al. 2003) over multiple-round linear amplification (Eberwine et al. 1992, Iscove et al. 2002, Kamme et al. 2003). However, as exponential amplification has been shown to bias abundance relationships due to different lengths and base compositions of transcripts (Freeman et al. 1999, Phillips and Lipski 2000, Baugh et al. 2001), length restriction during reverse transcription was suggested to minimize this amplification-induced bias

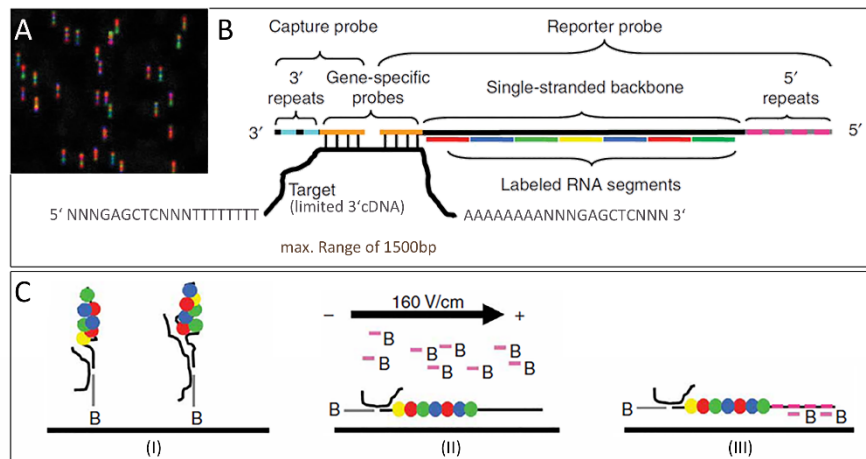


Figure 5 - Overview of NanoString nCounter gene expression system. (A) False-color image of immobilized reporter probes captured by the NanoString digital analyzer. (B) A schematic representation of the hybridized complex. The capture probe and reporter probe hybridize to a complementary target mRNA via the gene-specific sequences. After hybridization, the complex is affinity-purified first by the 3'-repeat sequence and then by the 5'-repeat sequence to remove excess reporter and capture probes, respectively. (C) Schematic representation of binding, electrophoresis, and immobilization. (I) The purified complexes are attached to a streptavidin-coated slide via biotinylated capture probes. (II) Voltage is applied to elongate and align the molecules. Biotinylated anti-5' oligonucleotides that hybridize to the 5'-repeat sequence are added. (III) The stretched reporters are immobilized by the binding of the anti-5' oligonucleotides to the slide surface via the biotin. Voltage is turned off and the immobilized reporters are prepared for imaging and counting. (modified according to Geiss et al., 2008)

(Iscove et al. 2002, Kurimoto et al. 2006). In the protocol used in this thesis, the original transcriptome size distribution of 1.5 – 10 kb (Okayama and Berg 1982, Wellenreuther et al. 2004), has been limited to a maximum fragment size of around 2000 bp (Brady and Iscove 1993, Iscove et al. 2002, Haag 2009, Pensold 2012). The initial reverse transcription starting from the 3' end of each poly-A tagged mRNA, is limited in time and dNTP concentration, which leads to size-limited mRNA fragments of the 3' end (Brady and Iscove 1993, Iscove et al. 2002, Haag 2009, Pensold 2012). As a consequence, all downstream analysis have to be restricted to this sequence parts. Variations of this protocol have already been used in several studies (Dulac and Axel 1995, Klein et al. 2002, Chiang and Melton 2003, Tietjen et al. 2003, Haag 2009). So far, the preservation of original transcript abundancies has been proven with southern- and northern-blot (Haag 2009) and with micro-arrays (Brady and Iscove 1993, Iscove et al. 2002), which are relative insensitive in regard to quantitative measurements.

In 2008, Geiss et al. published a method, which enables highly quantitative measurements of RNA and DNA, the NanoString nCounter technology (Fig. 5), which was used in the study presented here, to validate the amplification protocol and profile distinct interneuron subtypes. The system is based on hybridization of two probes on a custom target sequence (Fig. 5B). Thereby, each particular reporter probe exhibits a distinct fluorescently labeled barcode with seven color-coded positions. Using four distinct colors this enables a potential analysis of up to 16.000 genes within a single codeset ($4^7 = 16,348$). The second probe per target is a biotinylated capture probe.

Both probes include additional 3'- or 5'-prime repeats, which are necessary for purification (Fig. 5B, C). After hybridization and purification with magnetic beads, the triple hybridization complex of target sequence, reporter probe and biotinylated capture probe will bind to a streptavidin surface. An electric field is applied to elongate the hybridization complex to linearize the color code. During this step biotinylated anti-5'-prime-repeat oligonucleotides targeting the reporter probe are added, to fix the whole complex in its linearized state (Fig. 5B, C). Afterwards the NanoString nCounter digital analyzer is used to scan the surface (Fig. 5A) and automatically count the color codes, which are associated to distinct target sequences. According to Geiss et al. (2008) the number of reads obtained for a particular target is equivalent to 1% of the amount contained in the native suspension. The accuracy and detection limit achieved with this system is comparable to quantitative RT-PCR, requiring significant less input material than standard next generation sequencing or micro-array (Geiss et al. 2008). Therefore, the NanoString nCounter technology represents a straight forward method for single cell analysis with the additional benefits of having multiplexing capabilities and the option to do direct measurements without an additional enzymatic bias.

3.4 Aims

The investigation of complex tissue with a heterogeneous cellular composition often requires single cell resolution to reveal subtype specific mechanisms. Therefore, in this study a single cell transcriptome analysis approach should be validated and applied to two distinct neurodevelopmental issues.

1st Part – Validation of the single cell transcriptome analysis approach:

- A single cell approach had to be tested in regard of quantitative representation of the original RNA abundancies and for the detection limits of low abundant genes using the NanoString nCounter technology

2nd Part – Impact of *EfnA5* during the development of cortical excitatory projection neurons:

- *EfnA5* knockout lead to a shift in cortical layer distribution with expanded deep layers at the expense of the upper layers via changes in cortical progenitor output (Gerstmann et al. 2015)
- By application of the single cell approach the source of *EfnA5* inside the cortex has to be revealed

- The mechanism leading to altered output of cortical progenitors should be elucidated by *in vitro* experiments

3rd Part – Mechanisms controlling interneuron migration and maturation:

- Embryonic interneuron subtype diversity will be analyzed using a custom designed NanoString codeset
- Genes revealed by differential gene expression analysis will be tested *in situ* to confirm their expression pattern
- Including cells from a *Hmx3-Cre/tdTomato* reporter line will highlight the expression profile of postmitotic POA-derived interneurons, leading to the observation of negative correlation of *Pak6*, a gene involved in post-migratory maturation and *Dnmt1*, an epigenetic modifying factor
- *Dnmt1* knockout in postmitotic interneurons (*Hmx3-Cre* lineage) will be analyzed in regard to cell distribution and subtype identity at adult stages as well as during embryonic development
- Changes in gene expression of *Dnmt1* knockout during embryonic development has to be tested by enrichment *Hmx3-Cre/tdTomato/Dnmt1* wild-type as well as *Hmx3-Cre/tdTomato/Dnmt1 loxP²* mice and comparative analysis using next generation sequencing and qRT-PCR

4 Methods

4.1 Animals

The following mouse strains were used: C57BL/6 wild-type mice and transgenic mice on the C57/BL6 background including *Hmx3-Cre/tdTomato/Dnmt1* wild-type as well as *Hmx3-Cre/tdTomato/Dnmt1 loxP²* mice. Transgenic mice will be abbreviated as *Dnmt1* WT and *Dnmt1* KO in the figures. The transgenic mice were established by crossing the *Hmx3-Cre* line (obtained from Oscar Marin, King's College, London, UK and described in Gelman et al. (2009)) with the tdTomato transgenic reporter mice (obtained from Christian Hübner, University Hospital Jena, Germany and described in Madisen et al. (2010)) and *Dnmt1 loxP²* mice, (B6;129S-Dnmt1tm4Jae/J, Jaenisch laboratory, Whitehead Institute; U.S.A. Jackson-Grusby et al. (2001)). The *Dnmt1 loxP²* mice had LoxP-sites flanking exons 4 and 5 of the *Dnmt1* gen. Cre-mediated deletion led to out-of-frame slicing from exon 3 to exon 6, resulting in a null *Dnmt1* allele (Jackson-Grusby et al. 2001). For staging of mouse embryos, the day of insemination was considered as embryonic day 1 (E1).

All animal procedures were performed in accordance with guidelines for the care and use of laboratory animals of the Friedrich Schiller University Jena and the University Hospital Jena, Germany. Animals were housed under 12 h light/dark conditions with access to food and water *ad libitum*.

4.2 General considerations for working in sterile and in ribonuclease-(RNase)-free conditions

All procedures including living tissue or dissociated single cells were performed in sterile conditions as far as possible using sterile buffer and media unless otherwise stated. Dissecting sets and work surfaces were disinfected with 70% ethanol prior to use. Plastic material (Eppendorf-tubes, pipette tips, etc.) and glassware (bottles, glass-petridishes, measuring cylinders, etc.) were autoclaved for 20 min at 121 °C and the latter were sterilized for 6 h at 180 °C. In addition, sterile disposable material like petri dishes, pipettes and reaction tubes were used.

When working with RNA special measures had to be taken to protect the RNA molecules from degradation by ribonuclease (RNase). *Aqua bidest* and all solutions without nucleophilic substances were treated with 0.1% Diethylpyrocarbonat (DEPC v/v) for at minimum 60 min/l and autoclaved afterwards. All remaining buffers used in

RNA approaches were prepared with DEPC-treated water under RNase-free conditions. Working surfaces were cleaned with 70% ethanol followed by RNase decontamination solution (100 mM NaOH, 0.5% SDS).

4.3 Brain and tissue preparation

Mice were deeply anesthetized (150 μ l) for perfusion or killed by applying an overdose (1 ml) of 10% chloral hydrate in phosphate buffered saline (PBS; pH 7.4) intraperitoneally. For preparation of adult brains, mice were transcardially perfused with PBS (pH 7.4) followed by 4% paraformaldehyde (PFA) in PBS (pH 7.4) prior to removal of brains and post-fixation overnight in 4% PFA at 4 °C. Cryoprotection with 10% and 30% sucrose in PBS overnight was performed before freezing in liquid nitrogen and storage at -80 °C. Embryos of anesthetized time pregnant dams were prepared as described in Zimmer et al. (2010). For *in situ* hybridization experiments, freshly prepared brains were immediately frozen in liquid nitrogen and stored at -80 °C. For immunohistochemistry, brains were fixed in 4% PFA for 5 h at room temperature for E14.5 and E16.5, prior to cryoprotection and storage at -80 °C.

4.4 Primary Cell culture

4.4.1 Preparation of dissociated single cells

Dissociated cortical as well as POA- and MGE-derived single cells for primary culture and single cell transcriptome analysis were prepared from cortical, POA or MGE explants, respectively, according to Zimmer et al. (2008). Briefly, after preparation, brains were embedded in Low-Melt-Agarose (Carl Roth, Germany) and coronal living-brain sections (300 μ m, VT1000S, Leica, Germany) were performed. The target area was dissected from the slices and collected in ice-cold Hank's balanced salt solution (HBSS w/o Ca^{2+} and Mg^{2+} ; Invitrogen, Germany) supplemented with 0.65% glucose. After incubation with 0.4% trypsin in HBSS for 15 min at 37 °C, the tissue was dissociated into single cells via trituration and filtered through a nylon gauze (180 μ m, Merck Millipore, Germany) to remove cell aggregates. Cells were then isolated for transcriptome analysis or cultured in Dulbecco's Modified Eagle Medium (DMEM) supplemented with 10% fetal bovine serum (FBS), 100 U/ml penicillin, 100 mg/ml streptomycin and 0.4 mM l-glutamine at 37 °C, 5% CO_2 (Sigma, Germany) in a humid atmosphere for 2 days *in vitro*. Cells were seeded at a density of 300 cells/ mm^2 for immunohistochemistry and stimulation experiments. The whole basal telencephalon of

E16.5 living brains was subjected to cell dissociation for FACS-mediated enrichment of tdTomato cells.

4.4.2 Pair-cell assay

E13.5 cortical cells were plated on coverslips coated with 19 µg/ml laminine (Sigma-Aldrich, U.S.A.) and 5 µg/ml poly-L-lysine (Thermo Fisher Scientific, U.S.A.) at clonal density in DMEM/F12 supplemented with 10% FBS, 0.4% methyl cellulose, 0.065% glucose, 100 U/ml penicillin, 100 µg/ml streptomycin and 0.4 mM L-glutamine. After incubation for 24 h *in vitro*, the medium was supplemented with either 5 µg/ml EFNA5-FC (R&D Systems, U.S.A.) or FC protein as control (Rockland Immunochemicals, U.S.A.) clustered with 50 µg/ml anti-human IgG antibody (Alexis Biochemicals, U.S.A.). Cell pair identity was determined after 24 h *in vitro* by immunostaining with antibodies against NES and TUBB3 for neuronal precursors and early postmitotic neurons, respectively (Michalczyk and Ziman 2005, Pacal and Bremner 2012). In addition to pairs of two NES-positive, two TUBB3-positive cells as well as mixed pairs of a TUBB3 and a NES positive cell, also cell pairs composed of one cell positive for either NES or TUBB3 and an unlabeled cell were obtained. Only cell pairs showing exclusive staining of both cells were included in the analysis that showed exclusive staining of both cells.

4.4.3 Cultivation of thalamic explants

Thalamic explants were prepared according to Ruediger et al. (2013) with slight modifications. Briefly, to obtain explants, the thalamic tissue was cut into 200 µm³ cubes using a scalpel, followed by incubation at 37 °C and 5% CO₂ for minimum 2 h in serum-free medium consisting of 100 U/ml penicillin, 100 mg/ml streptomycin, 2 mM L-glutamine, 6.5 mg/ml glucose in Neurobasal (all from Thermo Fisher Scientific, U.S.A.). Thalamic explants were then placed on coverslips coated with 19 µg/ml laminine and 5 µg/ml poly-L-lysine (Thermo Fisher Scientific, U.S.A.) and incubated at 37 °C and 5% CO₂ for 10-30 min, so that the explants were only slightly covered with medium and could adhere. Finally, a co-culture with cortical cells or cultivation in DMEM/F12 supplemented with 10% FBS, 0.4% methyl cellulose, 0.065% glucose, 100 U/ml penicillin, 100 µg/ml streptomycin and 0.4 mM L-glutamine for 24 h at 37 °C and 5% CO₂ prior to fiber isolation was performed.

4.4.4 Co-culture of thalamic explants with cortical single cells

To easily discriminate the cortical cells from migrating cells out of the thalamic explants, dissociated E13.5 cortical cells were treated with Cell Tracker Green (Thermo Fisher Scientific, U.S.A.) and washed before adding to already adhered E13.5 thalamic explants (see 4.4.3) at clonal density in DMEM/F12 supplemented with 10% FBS, 0.4% methyl cellulose, 0.065% glucose, 100 U/ml penicillin, 100 µg/ml streptomycin and 0.4 mM L-glutamine. After 24 h at 37 °C and 5% CO₂, 5 µg/ml EPHA3-FC (R&D Systems, U.S.A.) pre-clustered with 50 µg/ml Alexa 488-conjugated anti-human IgG (Alexis Biochemicals, U.S.A.) was added for 30 min at 37 °C. After fixation in 4% PFA in PBS for 30 min, cell pair identity was determined by immunostaining against NES and TUBB3 according to chapter 4.4.2. Only pairs located clearly within the axons and stained with Cell Tracker Green (for cortical cells) were taken into consideration.

4.4.5 Pak6 siRNA transfections in primary neuronal culture and verification of siRNA treatment in cell culture.

For siRNA transfections of dissociated POA cells (E14.5, E16.5), Lipofectamine RNAiMAX (Invitrogen, U.S.A.) was used for reverse lipofection according to the manufacturer's protocol and as described in Zimmer et al. (2011). 50 nM mouse *Pak6* siRNA containing a pool of three target-specific 20–25 nt siRNAs to knockdown gene expression (Santa Cruz Biotechnology, U.S.A.) or 50 nM control siRNA (BLOCK-iT Alexa Fluor red fluorescent oligo; Invitrogen, U.S.A.) was applied for 5 h in antibiotics-free Opti-MEM® I Reduced Serum Medium (Thermo Fisher Scientific, U.S.A.) at 37 °C, 95% H₂O and 5% CO₂.

To verify *Pak6* downregulation upon siRNA treatment, COS-7 cell were co-transfected with *Pak6-Gfp* expression construct (PS100010, Origene, U.S.A.) and either *Pak6* siRNA (Santa Cruz Biotechnology, U.S.A.) or control siRNA (BLOCK-iT Alexa Fluor red fluorescent oligo; Thermo Fisher Scientific, U.S.A.) with Lipofectamine RNAiMAX (Thermo Fisher Scientific, U.S.A.) overnight in antibiotics-free Opti-MEM® I Reduced Serum Medium (Thermo Fisher Scientific, U.S.A.) at 37 °C, 95% H₂O and 5% CO₂ (Thermo Fisher Scientific, U.S.A.). COS-7 cells were fixated for 5 min in 4% PFA in PBS (pH 7.4) and coverslips were embedded in Mowiol (Roth, Germany). The *Pak6* siRNA lead to a downregulation of fluorescence intensity of about 80% (Fig. 6). Of note, *Pak6-Gfp* transfection together with control siRNA caused an atypical morphology of COS-7 cells inducing strong filopodia formation, which was reversed by

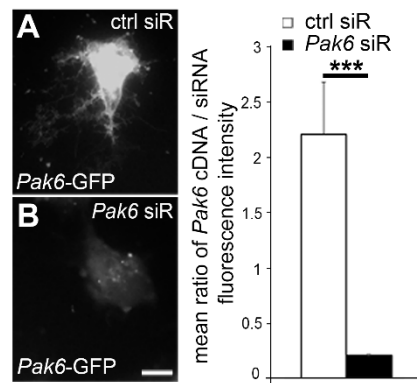


Figure 6 - Validation of *Pak6* siRNA knockdown efficiency in COS-7 cells. (A-B) COS-7 cells co-transfected with *Pak6-GFP* cDNA and either control siRNA (A) or *Pak6* siRNA (B). (C) Normalized fluorescence intensity measurements revealed significant decrease of *Pak6-GFP* expression upon *Pak6* siRNA co-transfection (n=22 cells) compared to control siRNA co-transfections (n=21, ***p<0.001; Student's T-test). Of note, *Pak6-GFP* transfection together with control siRNA caused the adoption of an atypical morphology of COS-7 cells inducing strong filopodia formation (A), which was reversed by co-transfection with *Pak6* siRNA (B). Scale bars: 10 μ m in (A, B).

co-transfection with *Pak6* siRNA (Fig. 6A, B). All siRNA treatment experiments were performed by Judit Symmank.

4.4.6 FACS enrichment of tdTomato cells

Cell suspensions subjected to FACS, were prepared from the basal telencephalon as described in chapter 4.4.1. After addition of DAPI, the cells were sorted using an ARIA III FACS sorter from BD Bioscience (U.S.A.) with a maximal flow rate of 6 (about 45 μ l/min). The tdTomato reporter was excited by a 561 nm yellow/green solid state laser and the emission signal was detected in a range of 579 nm to 593 nm. According to their FCS/SSC (Forward scatter/ Side scatter) criteria followed by cell doublet exclusion via a FSC-H vs. FSC-W criteria, DAPI-negative living cells were sorted based on a distinctive tdTomato signal. Cells of interest were collected in culture medium (see 4.4.1) at 4 $^{\circ}$ C, pelleted by centrifugation and substituted with 500 μ l Trizol®Reagent (Thermo Fisher Scientific, U.S.A.) and subsequently frozen on dry ice prior to RNA isolation. The FACS experiments were performed in cooperation with the Leibniz Institute for Age Research - Fritz Lipmann Institute (FLI, Jena, Germany).

4.5 Molecular biology methods

4.5.1 RNA isolation of tissue and FAC-sorted cells

E14.5 or E16.5 POA and MGE explants were dissected from coronal living brain sections (300 μ m) according to Zimmer et al. (2007) and collected in ice-cold HBSS supplemented with 0.65% glucose and pelleted by centrifugation (5 min, 70x g, 4 $^{\circ}$ C). The tissue was then subjected to standard RNA isolation procedure using Trizol®Reagent (Thermo Fisher Scientific, U.S.A.), digested with RNase-free DNase (Qiagen, Netherlands) and checked for integrity by capillary gel electrophoresis

(Bioanalyzer, Agilent Technologies, Inc., U.S.A.). The FACS enriched tdTomato cells were processed similarly, with adding GlycoBlue (Thermo Fisher Scientific, U.S.A.) to a final concentration of 0.2% during RNA precipitation for better visualization of the pellet.

4.5.2 Amplification protocols

PCR was performed either with a T-Gradient PCR machine (Bio-rad, U.S.A.), a T3000 thermocycler from Biometra (Germany) or for qRT-PCR with a CFX96 qPCR system (Bio-rad, U.S.A.). If necessary, the PCR products were subsequently separated by agarose gel-electrophoresis and the fragment sizes analyzed on an UV table Benchtop 2UV Transilluminator equipped with VisiDoc-iT Imaging System (UVP, Germany).

4.5.2.1 Genotyping and Standard PCR

Genotyping was performed on DNA isolated from mice tail biopsies by alkaline lysis (75 μ l 25 mM NaOH, 0.2 mM EDTA in H₂O for 45 min at 95 °C, neutralized with 75 μ l 40 mM Tris-HCl in H₂O). The PCR was performed in a volume of 20 μ l with 0.1-1 μ g template-DNA, using 1.5 U Taq DNA polymerase (Invitrogen, U.S.A.), 10 pmol of each primer and 0.5 mM of each dNTP. The used primers and reaction conditions are listed in Table 1.

Dnmt1 loxP site genotyping

PCR program:		primer sequence:	
	4°C, ∞	<i>Dnmt1</i> F:	GGGCCAGTTGTGTGACTTGG
┐	95°C, 30s	<i>Dnmt1</i> R:	CCTGGGCCTGGATCTTGGGGA
37x	58°C, 25s	resulting fragment size:	
└	72°C, 30s	wild type:	334 bp
	72°C, 2 min	<i>Dnmt1</i> loxP ² :	368 bp
	4°C, ∞		

tdTomato genotyping

PCR program:		primer sequence:	
┐	95°C, 30 s	oIMR9020-wt-F:	AAG GGA GCT GCA GTG GAG TA
35x	61°C, 30 s	oIMR9021-wt-R:	CCG AAA ATC TGT GGG AAG TC
└	72°C, 1 min	oIMR9103-mu-R:	GGC ATT AAA GCA GCG TAT CC
	72°C, 7 min	oIMR9105-mu-F:	CTG TTC CTG TAC GGC ATG G
	4°C, ∞	resulting fragment size:	
		wild type:	297 bp
		mutant:	196 bp

Hmx3 Cre genotyping

PCR program:		primer sequence:	
	4°C, ∞	<i>iCre</i> F:	CTC TGA CAG ATG CCA GGA CA
	94°C, 5min	<i>iCre</i> R:	TCT CTG CCC AGA GTC ATC CT
┌	94°C, 30s	<i>Ano6</i> F:	ctg gta aac gtg gaa gag cac
	67°C, 30s, -0,5°+0:00	<i>Ano6</i> R:	gct tta tag cca ccc ctt aca g
9x	R=3,0°/s+0:00°/s	resulting fragment size:	
	G=0,0°	<i>iCre</i> :	394 bp
L	72°C, 30s	<i>Ano6</i> :	198 bp
┌	94°C, 30s		
25x	62°C,30s		
L	72°C, 30s		
	72°C, 5min		
	4°C, ∞		

Table 1 - PCR conditions for genotyping of *Dnmt1* loxP sites, *tdTomato* and *Hmx3* Cre. Primer are indicated as 5' → 3'. *Ano6* was used as positive control for *Hmx3* Cre genotyping. F, forward primer; R, reverse primer.

4.5.2.2 Quantitative reverse transcription PCR (qRT-PCR)

RNA of FAC-sorted cells was used in a one-step qRT-PCR reaction using SuperScript III Platinum SYBR Green One-Step qRT-PCR Kit according to the manufacture's guide (Invitrogen, U.S.A.) with the following primer sequences listed in Table 2.

<u><i>Dnmt1</i></u>	
F primer:	TGAGCATCGATGAGGAGATG
R primer:	CGCATGGAACATCATCTGAC
temperature/fragment: 60°C/134 bp	
<u><i>Pak6</i></u>	
F primer:	CTGTACGCTACTGAGGTGGA
R primer:	GTACCAGCATCCGATCCAGG
temperature/fragment: 60°C/193 bp	
<u><i>Rps29</i></u>	
F primer:	GAAGTTCGGCCAGGGTTCC
R primer:	GAAGCCTATGTCCTTCGCGT
temperature/fragment: 60°C/121 bp	

Table 2 - Primer sequences, used temperature and resulting fragment size for qRT-PCR. Sequences are indicated as 5' → 3'. F, forward primer; R, reverse primer.

Obtained data were normalized to *Rps29* mRNA levels and diagramed as fold induction. Results were analyzed via the $\Delta\Delta C_t$ -method (Livak and Schmittgen 2001).

4.5.2.3 cDNA synthesis from single cells, thalamic fibers and tissue-RNA dilution

As published in Gerstmann et al. (2015), single-cell suspensions (50.000 cells/ml in HBSS, free of Ca^{2+} and Mg^{2+} ; 1%FBS) were plated onto siliconized (Silicone solution, SERVA, Germany) glass coverslips. Cells were individually collected by micromanipulation under visual control (inverted transmitted-light microscope CellObserver, 100x optical magnification, NA=0.3, Carl Zeiss Microscopy, Germany) using fire-polished, FBS-coated glass capillaries (40 μm tip diameter; Hilgenberg or Science products, Germany) and a microinjection device (CellTram® vario, Eppendorf, Germany). Each cell was washed twice in fresh buffer (HBSS, free of Ca^{2+} and Mg^{2+} ; 1% FBS) before transfer in a maximum volume of 0.5 μl to a PCR vial containing 4.5 μl lysis & first strand buffer (50 mM Tris-HCl (pH 8.3); 75 mM KCl; 3 mM MgCl_2 ; 1 mM DTT; 0.5% (v/v) Igepal CA-630; 100 $\mu\text{g/ml}$ acetylated bovine serum albumine (BSA, Sigma-Aldrich, Germany); 10 μM each of dATP, dCTP, dGTP und dTTP; 3.5 nM SR-T₂₄-Primer (5'-GTAACTCGAGAATTCT₂₄-3'); 0.04 U/ μl RiboLock™ RNase inhibitor (Fermentas, Germany); 0.03 U/ μl SuperaseIn™ RNase inhibitor (Thermo Fisher Scientific, U.S.A.) followed by immediate freezing in liquid nitrogen. The SR-T₂₄-Primer (5'-GTAACTCGAGAATTCT₂₄-3') included an adapter sequence for cloning, which was not used in the scope of this project but was kept as the protocol was optimized also in regard to primer concentration and efficiency.

To obtain axonal compartments, the fibers from cultured thalamic explants were scratched using glass capillaries and collected in lysis and first-strand buffer under visual control ensuring cell soma free isolation. In addition to single cells and thalamic compartments, whole-tissue RNA dilutions from E14.5/E16.5 MGE and POA (300 pg, 50 pg, 5 pg) were subjected to global cDNA synthesis and exponential amplification for the validation procedure. To minimize dilution errors, which might bias the significance of the validation, subsequent dilution of the RNA to 300 pg, 50 pg and 5 pg in three independent samples were performed, which were pooled again prior to template extraction and the next dilution step (Fig. 8).

To circumvent shifts in representation or loss of low abundant transcripts during amplification due to variations in RNA fragment-size and base compositions, the applied protocol for global cDNA synthesis and amplification is based on limited reverse transcription prior to exponential amplification (Brady and Iscove 1993, Haag

2009, Gerstmann et al. 2015). Briefly, cell lysis was performed at 65 °C for 90 sec followed by reverse transcription at 42 °C for 15 min (100 U M-MuLV reverse transcriptase; RevertAid™ H Minus, Fermentas, Germany). After heat inactivation (10 min, 70 °C), RNase H (5 U, New England Biolabs, U.K.) and MgCl₂ to 9 mM were added and incubated for 15 min at 37 °C, followed by cDNA denaturation for 2 min at 95 °C. 5'-end tailing was performed in 5 mM potassium-phosphate buffer (pH 7.0) containing 750 μM dATP and 10 U terminal transferase (New England Biolabs, U.K.) for 15 min at 37 °C. After heat inactivation (65 °C, 10 min), samples were cooled to 4 °C and PCR1-mix (67 mM Tris-HCl (pH 8.8), 16 mM (NH₄)₂SO₄, 0.01% Tween 20, 1.5 mM MgCl₂, 200 μM of each dNTP, 10 μM SR-T₂₄-primer) with 2.5 U HotStart Taq-DNA polymerase (Genaxxon bioscience, Germany) and 0.05 U HotStart Pfu Turbo DNA-Polymerase (Agilent Technologies, U.S.A.) was added to a total volume of 75 μl, subsequently split into triplicated of 25 μl each. First, second strand synthesis was performed (95 °C, 2 min; 52 °C, 2 min; 72 °C, 2 min) prior to 35 cycles of amplification (94 °C, 45 secs; 60 °C, 1 min; 72 °C, 1 min). For the optional second round of PCR (PCR2), 0.4 μl of PCR1 product was re-amplified for 30 additional cycles (95 °C, 2 min; 30x [94 °C, 45 secs; 60 °C, 1 min; 72 °C, 2 min]; 72 °C, 10 min) using 49.6 μl PCR2-mix, equal to PCR1-mix except a lower concentration of 2.5 μM SR-T₂₄-primer and containing 5 U HotStart Taq-DNA polymerase (Genaxxon bioscience, Germany) and 0.1 U HotStart Pfu Turbo DNA-Polymerase (Agilent Technologies, U.S.A.).

The 3' limited cDNAs were analyzed with capillary gel electrophoresis (Bioanalyzer, Agilent Technologies, Inc., U.S.A.) to determine the mean fragment size of the PCR fragments (486 ± 18 bp; n=37; Pensold 2012).

4.5.2.4 Qualitative evaluation of amplified cDNAs from single-cells and thalamic axons

To classify the amplified 3' cDNA libraries from single-cells and thalamic axons for distinct gene expression, qualitative evaluation was done by PCR amplification using Hot Start Taq (PeqLab, Germany). To account for the fragment size obtained by the limited reverse transcription, 3' located specific primers were used for relevant transcripts and housekeeping genes (listed in Table 3). As a positive control, cDNA libraries generated from single cell equivalent dilutions (5 pg) of E14.5/E16.5 RNA isolated from whole brain tissue were used, to validate the functionality of the respective primer in limited 3' cDNA libraries. As negative controls reaction products

of „clean“ controls, containing freshly prepared isolation buffer as template as well as “picked” controls were used. For the latter, whole manual cell isolation procedure was performed without collecting a cell (Pensold 2012). As an additional control the cDNA-synthesis protocol was applied to a cell-containing sample without adding the reverse transcription enzyme to check for DNA contamination. Samples from isolation experiments with positive housekeeping gene expression in any of the controls were excluded from further processing.

ActB

F primer: CAGCATTGCTTCTGTGTAATTATG

R primer: GCACTTTTATTGGTCTCAAGTCAGT

temperature/fragment: 60°C/223 bp

EfnA5

F primer: CTTTTGAAAATCGCCTCCAC

R primer: AGACAGACCTGCCATTAC

temperature/fragment: 60°C/292 bp

EphA4

F primer: AAATCAAGCCGTTTCACCAC

R primer: CGTCCCCTTCACAGATGAAT

temperature/fragment: 60°C/168 bp

HuD

F primer: TGCACATTGAAGAGGCAAAC

R primer: TCCAAAACCGAAAAGAGGA

temperature/fragment: 60°C/129 bp

Pax6

F primer: CGGATCTGTGTTGCTCATGT

R primer: CAACCTTTGGAAAACCAACA

temperature/fragment: 59°C/221 bp

Tbr2

F primer: CCTGGTGGTGTGTTTGTG

R primer: AATCCAGCACCTTGAACGAC

temperature/fragment: 60°C/220 bp

Table 3 - Primer sequences, used temperature and resulting fragment size for 3'limited cDNA libraries. Sequences are indicated as 5'→3'.
F, forward primer; R, reverse primer.

4.5.3 Next Generation Sequencing

Next Generation Sequencing (NGS) and initial data analysis, including all steps necessary to obtain normalized read counts, were performed by the Transcriptome and Genome Analysis Laboratory (TAL), Göttingen, within the scope of collaboration. Data analysis regarding differential gene expression analysis and GO-enrichment (gene ontology) was provided by Anne Hahn.

4.5.3.1 Library preparation and data processing of tissue RNA

RNA-Seq was applied for E14.5/E16.5 MGE and POA tissues. Library preparation was performed using the TruSeq RNA Sample Preparation Kit (Cat. N°RS-122-2002, Illumina, U.S.A.). Accurate quantitation of cDNA libraries was ensured via the QuantiFluor™ dsDNA System (Promega, U.S.A.), followed by size range determination on a Bioanalyzer 2100 (DNA 1000 Chip; Agilent). cDNA libraries were amplified and sequenced by using the cBot and HiSeq2000 from Illumina (PE; 2x100 bp; ca. 30 million reads per sample).

Sequence images were transformed with Illumina software BaseCaller to bcl files, which were demultiplexed to fastq files with CASAVA v1.8.2. Quality check was done via fastqc (v. 0.10.0; Babraham Bioinformatics). Sequences were aligned by Bowtie2 (v2.0.2; Langmead and Salzberg 2012) to the UCSC mouse reference genome mm10. Counting the reads mapped to each gene of the UCSC gene annotation file was done via HTSeq Python scripts (v.0.5.3p9; Anders et al. 2015) filtering for exonic reads. Data were preprocessed and analyzed in the R/Bioconductor environment (v.2.15.2; Bioconductor) loading edgeR (v.3.0.4, Bioconductor; Robinson et al. 2010) and further R-packages (i.e. lattice, estrogen, gplots, colorRamps; Huber and Gentleman 2006, Sarkar 2008, Keitt 2012). Normalization of data was done by trimmed Mean of M-values (TMM), estimation of dispersions and testing for differentially expressed genes based on a generalized linear model likelihood ratio test assuming negative binomial data distribution and computed via edgeR. Candidate genes were filtered to a minimum of 2-fold change and an FDR-corrected (false discovery rate) p-value < 0.05.

4.5.3.2 Library preparation and data processing of 3'limited cDNA

For 3'limited cDNA the library preparation was performed using the TruSeq Nano DNA LT Library Preparation Kit for low-throughput studies from Illumina (U.S.A.) Cat. N° FC-121-4002 according to manufacturer's instructions. Libraries sizing averages were analyzed using the fragment Analyzer (320 bp). For library quantitation, the QuantiFluor Assay from Invitrogen (Germany) was used. Libraries were diluted at 8 pM and sequenced on the MiSeq using the MiSeq Reagent Kits v2 from Illumina Cat N°MS-102-2002.

The adapter sequence 5'-GTAACTCGAGAATTCTTTT-3' included in the SR-T₂₄-primer was trimmed from fastq reads applying the software Cutadapt (v1.7; Martin 2011) and stripped of long poly-A/T homonucleotides. Trimmed reads were aligned to the GRCm38 cDNA reference sequence using BWA-MEM (v0.7.12; Li 2014). Aligning sequence reads, clone sequences and assembly contigs with BWA-MEM. arXiv:1303.3997v1 [q-bio.GN]."), read alignments marked as "secondary" were discarded, and reads summarized by transcript isoform count. Reads were mapped to 12,144 genes in total across all cells. These genes were ranked according to their variance across cells and only 70% of all genes (n=8501) with high variance were admitted to further processing. Principle component analysis (PCA) was performed to confirm clustering of the cells similar as observed in NanoString data-based clustering. For correlation analysis, the Pearson Correlation Coefficient (R_{Pearson}) was calculated between the across-cells expression profile of *Dnmt1* and each of the remaining 8500 genes.

Genes with expression profiles positively correlated ($R_{\text{Pearson}} > 0.7$, n=315) or negatively correlated ($R_{\text{Pearson}} < -0.3$, n=280) to the *Dnmt1* profile were submitted to the Database for Annotation, Visualization and Integrated Discovery (DAVID, <https://david.ncifcrf.gov>) for GO- term enrichment analysis. The statistic was corrected using Fisher's exact test. For 27 (positive correlation) and 34 genes (negative correlation), no GO annotation was available. Results of GO enrichment analysis were visualized using Cytoscape 3.2.1 and the EnrichmentMap plugin (Merico et al. 2010). Terms were linked with edges if the Overlap Coefficient of the genes associated with each of the terms was > 0.5 . The resulting network was manually curated to exclude highly non-significant nodes.

4.6 NanoString Codeset design

Due to the mean fragment size of the generated cDNA libraries (486 ± 18 bp; see 4.5.2.3), transcript specific probes were directed against regions within a maximum range of 500-600 bps from the 3'end. Probe position and isoform coverage are summarized in Appendix Table 1-3.

For the validation experiments it was necessary to design a codeset containing probes directed against relatively high abundant genes in the tissue used as RNA template, as only these kind of genes are reliably present in the enormous dilution that served as templates for amplification due to the heterogeneity of the tissue (Eberwine et al.

1992, Monyer and Lambolez 1995, Freeman et al. 1999) as described in the introduction. Most prominently expressed genes evident in MGE and POA domain of the embryonic brain were revealed by NGS, followed by multifactorial likelihood ratio tests allowing for a paired-design experiment. The expression patterns of the 100 transcripts with the highest number of reads in all tissue samples were then verified by database research (<http://www.genepaint.org/>, <http://www.stjudebgem.org>). Out of this combined analysis 32 transcripts were chosen to design the NanoString codeset for the validation of the representative amplification of single cell equivalent mRNA quantities (codeset details are listed in Appendix Table 2).

The same RNA sequencing data were analyzed regarding differential gene expression between MGE and POA tissue to reveal transcripts potentially expressed by distinct MGE and POA subtypes. Based on these data and literature research, 96 genes were chosen for the NanoString codeset design, which are potentially involved in subtype-specific development, in addition to house-keeping genes as well as known marker transcripts (codeset details are listed in Appendix Table 3).

4.7 NanoString hybridization, data processing and analysis

About 200 ng of tissue RNA were used and processed according to the manufacturer's instructions provided by NanoString nCounter technology (U.S.A.). Five μ l of amplified cDNA material from single cells and replicates of diluted tissue RNA were applied and subjected to denaturation (95 °C, 5 min) prior to hybridization. Further sample processing was performed automatically by the NanoString nCounter PrepStation.

Altogether, 147 single cell libraries were tested with the profiling codeset. The NanoString nCounter data were pre-processed in three steps (probe-level back-ground correction, code-count normalization and concentration prediction) using the nSolver software (v2.0, NanoString Inc., U.S.A.) to normalize results against internal controls. A threshold of at least 50 counts per probe was applied setting all probes beneath that threshold to 0. This was done to ensure robust transcript detection and to reduce stochastic noise (Kharchenko et al. 2014). Furthermore, samples with less than 10% gene expression profile represented by the 96 probes of the codeset, were excluded resulting in 92 cells used for further analysis. This was necessary, as these cells formed a separate cluster in the subsequently performed clustering, which is a consequence of overestimated power of missing genes in regard to the cluster formation. Hence, no biological meaningful clustering was achieved when these

samples were included (data not shown). But in general, cells with sparse gene expression profiles revealed comparable level of housekeeping gene expression (data not shown). This fact pointed to subtype specific gene expression not covered by the codeset rather than failure during amplification.

The following analyses were performed with the statistical programming language R (v.2.15.2, Bioconductor) applying different R-packages. To reduce the dimension of the dataset and to reveal correlated gene expression pattern among the cells a principal component analysis (PCA) was performed on \log_2 -transformed normalized NanoString data using R-package FactoMineR (v.1.31.4; Lê et al. 2008). The PCA converted potentially correlated variables (genes) to sets of linearly uncorrelated values (principal components, pc), where the first pc explains the greatest amount of the variance in the data. This approach helps to explore and visualize high dimensional data. To obtain information about affiliation of cells to distinct populations, an agglomerative hierarchical clustering was performed on these data using Ward's method with Euclidean metric. Consecutive, statistics for differential gene expression between cells of a specific cluster and the remaining samples were obtained using R-package NanoStringNorm (v1.1.19; Waggott et al. 2012) on normalized NanoString counts. The box plots, illustrating gene expression distribution inside distinct cluster were done using ggplot2 (Wickham 2009). Pearson Correlation Coefficient (R_{Pearson}) for single cell expression data were calculated based on \log_2 -transformed normalized NanoString counts and illustrated applying R-package corrplot (v.0.73; Wei and Wei 2016).

4.8 Validation using NanoString

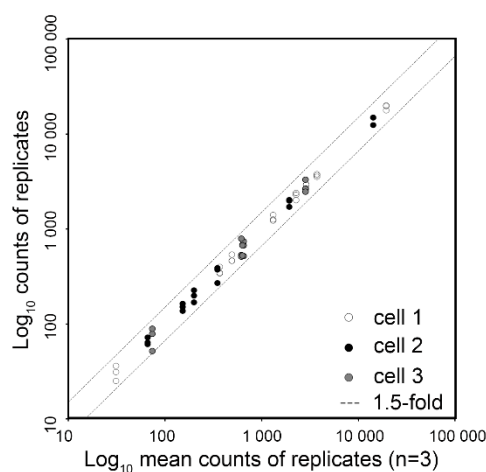


Figure 7 - NanoString reproducibility for non-purified single cell cDNAs. Triplicates of detected counts for three single cell libraries analyzed with codeset No.1 are plotted against the calculated mean counts of replicates for each transcript. Dashed lines indicate a 1.5-fold change range.

The cDNA libraries obtained from the amplification protocol were directly used for NanoString analysis. In addition to the cDNA, these samples included all enzymes and high concentration of ions due to the one-tube-reaction. To ensure highly quantitative and reproducible measurements technical triplicates of 3' limited cDNA preparations from single cells were performed. All Transcript counts of replicates were found within 1.5-fold change range (Fig. 7), comparable to the reported reproducibility of NanoString for detection of purified RNA (Geiss et al. 2008). Since the accuracy for technical replicates reported for qRT-PCR (Higuchi et al. 1993) and NanoString (Geiss et al. 2008) already lies within a 2-fold change, transcript representations within a 4-fold change was defined as not significantly different, in accordance with other studies (Kurimoto et al. 2006, Tang et al. 2009).

Normalization was performed as stated for the single cells (see 4.7). The theoretical copy number for each transcript species analyzed was calculated on the basis of their specific mean counts in the original RNA, the dilution factor prior to amplification and the observation that 1% of all RNA molecules in a given sample are detected with NanoString (Geiss et al. 2008). For statistical comparison of E14.5/E16.5 MGE/POA tissue RNA counts with detected counts in amplicates generated from the different dilution of the original RNA pool, regression analysis for all valid probes with theoretical transcript copies above ten prior to amplification was performed. Based on the analysis, a connection between the distance of the probes from the 3'end and the reproducibility of the counts in the different replicates could be observed (Fig. 8 and Appendix Tab. 3). In more detail, the NanoString probe for *Spna2* was directed against a region with a distance of 486 bps from the 3'end being equivalent to the mean fragment size of the 3' limited cDNA's. Thereby, the individual counts for *Spna2*, which were represent at low transcripts levels in the 5 pg dilution, showed highly inconsistent values in the 9 independent replicates (Fig. 9C probe number 12). This was also reflected by the mean value of the counts of all 9 replicates, which was deceeding the 4-fold change. In contrast, the probes detecting *Gnb1*, *Tubb5* and *Agrn* transcripts, which had an even lower theoretical transcript number of only ten for *Gnb1* and 11 transcripts for *Tubb5* and *Agrn* in the 5 pg dilution (Fig. 9C probe number 9-11), were directed against regions closer to the 3'end (252 bps for *Gnb1*, 252bps for *Tubb5* and 314 bps for *Agrn*; Appendix Tab. 3). Except for 4 of 27 values, all amplified replicates of the three probes were plotted within the 4-fold change, indicating that a representative amplification even at very low transcript numbers was received, when

the NanoString probe binds to transcript positions, which do not exceed 400 bps from the 3' end (Fig. 9C probe number 9-11). According to this, only probes directed against transcript regions with less than 400 bps from the 3' end were included for correlation analysis (excluded probes: 2,3,15,20,22; see Appendix Tab. 3). In addition, *Smarca4* was excluded due to a low detection level in the RNA (0.3 theoretical copies in the 5 pg dilution).

4.9 Immunohistochemistry and immunocytochemistry

For immunohistochemistry in fixed embryonic brains, 20 µm coronal cryosections were prepared at -20 °C (CM1510, Leica Biosystems, Germany) as described in Zimmer et al. (2011). For immunohistochemistry in adult brain sections, 30 µm free-floating sagittal sections were done by a sliding microtome (SM2000R, Leica, Germany). Sections were washed in PBS/0.2% Triton-X-100 and for free-floating sections an antigen-retrieval was carried out for 20 min at 90 °C in 10 mM citrate buffer with 0.05% Tween20 (pH 6.0), prior to blocking with 10% normal goat serum, 4% BSA in PBS/0.2% Triton X-100 for 1 hour. In addition, HCl treatment was performed for DNMT1 immunostaining (10 min at 4 °C in 1N HCL, 10 min at room temperature (RT) in 2N HCL, 20 min at 37 °C in 2N HCL followed by neutralization in 10 mM borate buffer (pH 8.8) for 12 min at RT).

Primary antibodies were applied over night at 4 °C for cryosections and over 2 nights for free-floating sections. After washing in PBS/Triton-X-100, the secondary antibody was applied for 2 hours. After nuclei staining with DAPI (100 ng/ml in PBS; Molecular Probes, U.S.A.) for 15 minutes, sections were embedded in Mowiol (Roth, Germany). For immunocytochemistry on dissociated cells, fixation and blocking occurred for 5 min and 30 min, respectively. Primary antibodies were applied for 2 h, secondary antibodies for 45 min, and DAPI staining was performed for 2 min. Following primary antibodies were used: rabbit anti-CB (Swant, Swiss, 1:500), rabbit anti-DNMT1 (Santa Cruz Biotechnology, U.S.A., 1:100), mouse anti ISL1/2 (DSHB, U.S.A., 1:500), mouse anti-NES (Millipore, U.S.A., 1:500), rabbit anti-NPY (Immunostar, U.S.A., 1:1000), mouse anti-RFP (Thermo Fisher Scientific, U.S.A., 1:500), rabbit anti-TUBB3 (Sigma, Germany, 1:500). Following secondary antibodies were applied: goat Cy5 anti-rabbit (Thermo Fisher Scientific, U.S.A., 1:1000), goat Cy5 anti-mouse (Thermo Fisher Scientific, U.S.A., 1:1000), donkey DyLight488 anti-rabbit (Jackson ImmunoResearch, U.S.A., 1:1000).

4.10 *In situ* hybridization

For *in situ* hybridizations fresh embryonic brains were cryo-sectioned coronally at -20 °C (20 µm, CM1850, Leica, Germany). *In situ* hybridizations were performed as described by Zimmer et al. (2011) using digoxigenin-labeled riboprobes. The primers listed in Table 4 were used to generate the riboprobes via *in vitro* transcription using DIG-11-UTP (Roche, Germany) from cDNA fragments cloned in pBluescript I KS (Stratagene, U.S.A.). The *in situ* hybridization data were kindly provided by Judit Symmank, Anne Rotzsch, Katrin Gerstmann or obtained from www.genepaint.org.

<u>Dnmt1</u>	<u>Maf</u>
F primer: TTCCTGTGCAGAAGGCAAG	F primer: AAGGAGGAGGTGATCCGACT
R primer: CACCTGCCGGTGTCTGTC	R primer: ACTAGCAAGCCCACTCAGGA
<u>Tcf4</u>	<u>Tbr1</u>
F primer: GCCTCCTCTTGACTTTGCTT	F primer: CCCCACCACTTAGAGACAGC
R primer: GCAGCTATGTGTACAGTCGC	R primer: ACCCACGTTTAGACCCTGAA
<u>Glcci1</u>	<u>Ccdc184</u>
F primer: CGCTCCCTGCTCACTACA	F primer: AGATCATGACCAAGGACGGC
R primer: ACGCCATTCCTCAAAGACC	R primer: CGTCCTCGTCTTCATCAGGA
<u>Abrac1</u>	<u>Zic3</u>
F primer: GGTGGAGGAAATTCATCGCC	F primer: TGTAAGTGGATCGAGGAGGC
R primer: CAGGACTTCTCAACAAGCCC	R primer: CTCGGGTGTGTGTAGGACTT
<u>Lhx6</u>	<u>Zic4</u>
F primer: TTCAGGGGATGCCATTTATC	F primer: AAGCCCTTCCCTTGTCCCTT
R primer: AAAGTTCCTTCTGGGGTGT	R primer: TGCAAGCAACATCATTGCT
<u>Epha4</u>	
F primer: TGAGAGGCTGCCTTGCTTAT	
R primer: GTGAAACGGCTTGATTTGGT	

Table 4 - Primer sequences used to create *in situ* probes. Sequences are indicated as 5' → 3'. F, forward primer; R, reverse primer.

4.11 Microscopy and image analysis

Image acquisition of *in situ* hybridization was performed using the Axio Cell observer Z1 (Zeiss, Germany) equipped with MosaiX module for tile scanning. Immunohistochemistry staining's of embryonic or adult tissue were recorded either with a confocal laser scanning microscope TCS SP5 (Leica Microsystems, Germany) or with the Axio CellObserver Z1 (Zeiss, Germany). Images of immunocytochemistry on dissociated cells were taken with the TCS SP5. ImageJ and Photoshop CS5 were applied for analysis and editing of the images, respectively.

Analysis of the cell number in embryonic cryosections and adult free floating sections was performed with ImageJs cell counter plugin. The distribution of embryonic cells

was depicted in schemes over all cryosections considering the coordinates of each cell in regard to the center of the POA region. For adult sections cells of a representative samples per genotype and staining were depicted in schemes modified according to Paxinos (2001). Counted numbers of tdTomato cells or double labelled NPY/tdTomato cells were normalized to the area of the whole cortex and the basal telencephalon measured with ImageJ. The distance of migrating E16.5 embryonic tdTomato cells was normalized to the extension between the center of the POA and the beginning of the cerebral cortex. For morphological analysis of siRNA and cDNA transfected dissociated neurons and COS-7 cells, the length of all neurites was measured with ImageJ and the longest neurite was defined as leading or main process. To validate the *Pak6* siRNA efficiency, GFP fluorescence intensity was measured in COS-7 cells co-transfected with a *Pak6-Gfp* expression construct and the Alexa Fluor red labelled control siRNA alone or together with *Pak6* siRNA, over the whole cellular area and normalized to the background using ImageJ. The mean ratio of background-corrected fluorescence intensities of *Pak6-Gfp* and Alexa Fluor red labelled siRNA was determined.

4.12 Statistical analysis

The number “n” refers to the number of analyzed cells or replicates (single cell RT-PCR, *Pak6* siRNA experiments, embryonic and adult phenotypic analysis of *Hmx3-Cre/tdTomato/Dnmt1 loxP²* and wild-type mice), cell pairs (pair cell assay and co-culture of thalamic explants with cortical single cells), explants or sections of at least three independent experiments. In terms of FACS-enriched samples “n” refers to the number of brains used for isolation (qRT-PCR and sequencing).

Student’s t-test and Fisher’s exact test (GO-enrichment analysis) were used for statistical analysis with the following significance level (*, $p < 0.05$; **, $p < 0.01$; ***, $p < 0.001$). Regarding the validation experiments, the Spearman Correlation Coefficient (R_{Spearman}) was calculated for all valid probes and its statistical relevance was tested via Student's t-test. For statistical comparison of transcript counts in PCR1 and PCR2 products, the Pearson Correlation Coefficient (R_{Pearson}) was calculated. The p-values obtained from differential analysis of sequencing data were corrected according to the Benjamini-Hochberg procedure (FDR correction).

5 Results

The results section is divided into three parts. In the first part, the results of the validation of the single cell transcriptome amplification protocol in regard to quantitative terms and detection limits are described. The second and third part describe applications of this method for neuroscientific questions. In part two, the source of *EfnA5* inside the cortex is identified taking advantage of the high sensitivity of the transcriptome amplification protocol. This helps to elucidate a model of extracortical regulation of excitatory projection neuron production, which was already published in Gerstmann et al. (2015). Whereas, the last chapter focus on the topic of postmitotic cortical interneuron maturation. Here, the single cell amplification protocol is applied to characterize distinct interneuron subtypes and to identify regulators of their postmitotic development.

5.1 Validation of the single cell amplification protocol

In a first set of experiments, a method for a time-efficient global transcriptome profiling of single cells was validated using the highly quantitative NanoString nCounter technology (Geiss et al. 2008). Due to its high sensitivity comparable to quantitative real time PCR (Geiss et al. 2008), reproducibility and straightforward sample preparation without any additional amplification or steps leading to loss of samples, the NanoString nCounter technology was chosen for the verification of quantitative transcript representation. An amplification protocol published by (Haag 2009), which is based on a strategy of (Brady and Iscove 1993) was used to produce 3' limited cDNA libraries. Transcript counts of RNA prepared from native brain tissue (MGE/POA tissue of E14.5 and E16.5) were compared with transcript level of cDNA libraries obtained by limited reverse transcription and amplification of single-cell equivalent dilutions of the same tissue RNA. A schematic workflow of the experimental design is illustrated in Figure 8. According to literature, single cell equivalent quantities of total RNA are estimated to about 5 to 30 pg, containing approximately 0.2 to 0.5 pg mRNA (Kurimoto et al. 2006, Haag 2009, Islam et al. 2011). However, as the mRNA content of an individual cell was reported to fluctuate over several orders of magnitude dependent on its transcriptional state and due to intrinsic transcriptional burst expression (Raj et al. 2006, Baserga 2007, Bengtsson et al. 2008, Eldar and Elowitz 2010), three different RNA amounts (5, 50 and 300 pg total RNA) as templates for cDNA synthesis and

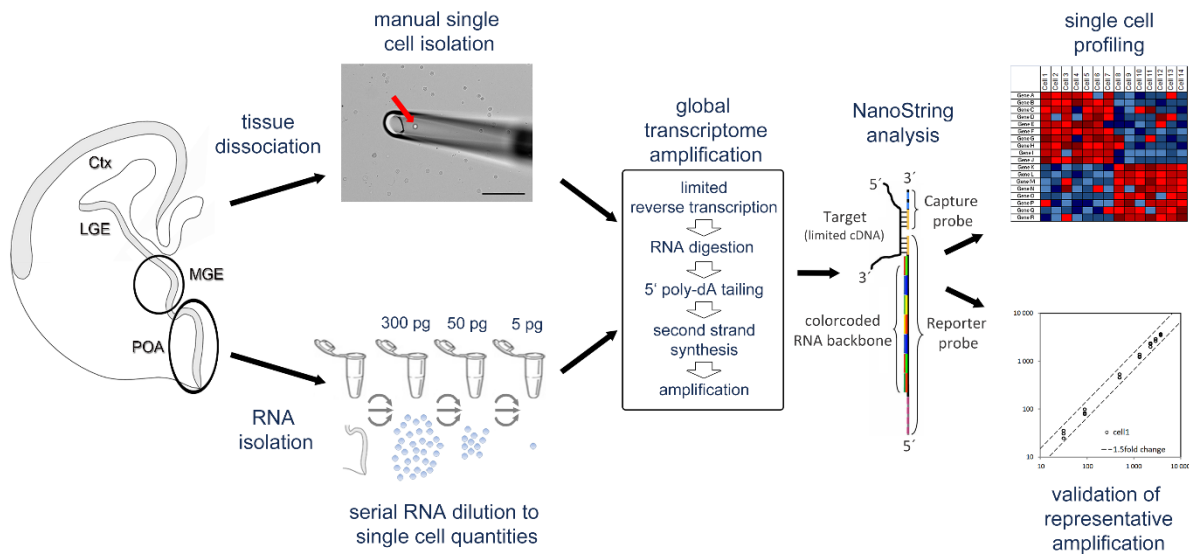


Figure 8 - Schematic workflow of the experimental design. Embryonic tissue from MGE and POA neurogenic domains was used either directly for RNA isolation or as single cell preparations. The serial RNA dilutions were performed in triplicates to minimize dilution artifacts. Single cells or samples with 300 pg, 50 pg or 5 pg RNA amount were subjected to global reverse transcription and amplification to generate global transcriptome cDNA libraries. Different NanoString codesets were applied to validate the cDNA synthesis and amplification procedure regarding transcript representation and to profile transcriptomes of neuronal subtypes. MGE, medial ganglionic eminence; POA, pre optic area.

amplification were tested. For the 5 pg RNA template nine independent samples were amplified, for the 50 pg and 300 pg RNA solutions six parallel replicates were generated. A validation codeset was designed based on Next Generation Sequencing (NGS) information of embryonic POA and MGE tissue, which was used as template in the following validation approach. In order to minimize the problem of transcript dilution below one copy per single cell equivalent (5 pg dilution) due to the heterogeneity evident in this native tissue (Flames et al. 2007, Gelman et al. 2012), highly expressed transcripts were identified by RNA sequencing and chosen for the codeset (Codeset details are listed in Appendix Tab. 2).

5.1.1 Correlation of native tissue RNA with amplicates from diluted templates

The theoretical copy numbers of the distinct transcript species chosen for the validation analysis covered a wide range of transcript quantities from several thousands down to only one in the different dilutions (Appendix Tab. 4), similar to what had been previously described for estimated single cell transcriptomes (Bengtsson et al. 2008, Islam et al. 2011, Liu and Trapnell 2016). The correlation between mean transcript expression levels in the original RNA sample ($n=3$, technical replicates) and the replicates of the cDNA preparations from the three distinct RNA dilutions is illustrated in Figure 9 A-C. For all three RNA concentrations, transcripts with copy numbers of 10 and more were well represented in the cDNA preparations compared to the original RNA pool (Fig. 9 A-C). Transcript counts of the 300 pg RNA template revealed a

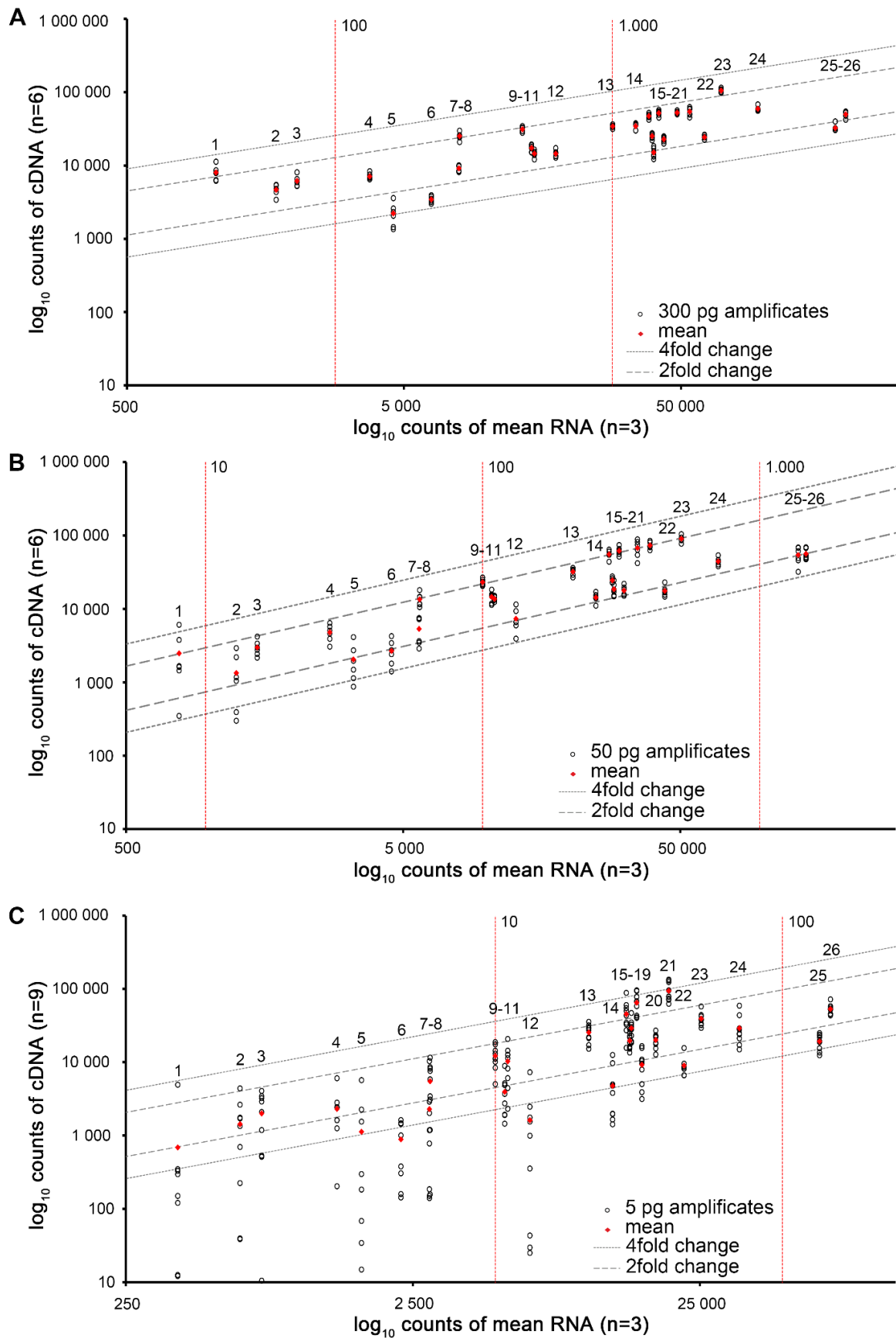


Figure 9 - NanoString-based validation of transcript abundance relationships in amplified cDNA libraries from single-cell RNA equivalents. (A-C) Mean counts of RNA from embryonic brain tissue (E14.5/E16.5) prepared from the MGE and POA compared to respective amplified cDNA libraries generated from (A) 300 pg (n=6), (B) 50 pg (n=6) and (C) 5 pg (n=9) total RNA template. Vertical dotted lines (red) separate amplicons of transcripts representing genes with copy numbers below 10, 100 and 1000 in the respective RNA templates. Numbers refer to detected transcripts listed in **Appendix Tab. 4**. Dashed and dotted lines (grey) represent the 2- and 4-fold regression, respectively. MGE, medial ganglionic eminence; POA, preoptic area.

significant correlation ($R=0.81$, $p \leq 0.01$), which indicates a preserved transcript representation for RNA species of all expression levels (Fig. 9A). About 98.1% of all transcript counts are plotted within a 4-fold change range (Table 4; includes additional fold-change information). This was considered to be an acceptable fold-change in agreement with other studies (Kurimoto et al. 2006, Tang et al. 2009). Comparably, 97.3% of transcript species of the 50 pg RNA samples with copy numbers as low as 10 were detected within a 4-fold change range ($R=0.86$, $p \leq 0.01$; Fig. 9B). A significant correlation ($R=0.80$, $p \leq 0.01$) was also determined for the 5 pg samples, although 5 pg RNA had previously been considered as an extremely low amount of RNA (Hashimshony et al. 2012) revealing various low copy transcripts (Appendix Tab. 4). In general, for RNA species with a copy number lower than 10, variations between the different cDNA replicates were observed, which were particularly evident in the 5 pg replicates (Fig. 9C probe numbers 1-8). However, these low copy number transcripts of the 5 pg dilution were well represented in the cDNA generated from the 50 pg and 300 pg RNA sample (Fig. 9A, B probe numbers 1-8). This observation pointed to dilution artefacts, which likely had a strong impact on these low level transcripts. Due to the fact that issues regarding mRNA capturing by the SR-T₂₄ primer especially for rare transcripts leading to reduced amplification could not be completely excluded, the quantitative validity of the amplification protocol cannot be reliably judged for transcript species with a copy number below 10 in the RNA template. For this reason, all probes with theoretically transcripts below 10 were excluded from quantitative regression and correlation analysis.

	% counts 2-fold	% counts 4-fold	% counts 5-fold	% counts 10-fold
5 pg RNA template	54.9	81.5	89.5	95.7
50 pg RNA template	65.3	97.3	99.3	100.0
300 pg RNA template	75.6	98.1	98.7	100.0

Table 5 - Summary of fold-changes. Percentages of obtained transcript counts in amplified cDNA samples plotted within 2-fold, 4-fold, 5-fold and 10-fold changes of regression for different amounts of input RNA template (5 pg, 50 pg and 300 pg).

The detection of rare transcript species is a central issue for nearly all available single cell methods (Liu and Trapnell 2016). Most protocols especially for NGS were described to detect approximately 10% of the whole transcriptome of a single cell making them unable to reliably detect low-abundant mRNA species (Deng et al. 2014, Islam et al. 2014, Saliba et al. 2014). In this context, the protocol described here outperformed existing approaches as even for probes with theoretical transcript counts below 10, a robust amplification above the threshold was detected for almost all

replicates (about 96% of all replicates in the 5 pg dilution, Fig. 9C probe numbers 1-8). Moreover, about 54.2% of these low level transcripts were detected within the tolerated 4-fold range of change. In more detail, the transcripts for *Lars2*, *Tuba1c* and *Malat1* were theoretically represented with roughly one transcript in the 5 pg dilution (Appendix Tab. 4). In two thirds of the replicates for *Lars2*, for all but one replicates for *Tuba1c* and in all replicates of *Malat1* transcript counts above the threshold were measured (Fig. 9C probe numbers 1-3).

5.1.2 Transcript representation was preserved after additional amplification

The validation experiments described above were performed with the single-cell PCR1 products (scPCR1) after 35 cycles of amplification, which generates sufficient material for several analytical trials of transcriptome analysis with NanoString. As for multiple experimental procedures involving also other methods like NGS, even higher amounts of single-cell cDNA may be required, less than 1% of the scRT-PCR1 products of seven individual cells were re-amplified and processed with different codesets. As shown in Figure 10, the representation of transcripts highly correlated between scPCR1 and scPCR2 products of all cDNA preparations tested ($R=0.96$, $p \leq 0.01$), indicating a preserved transcript representation after additional 30 cycles of amplification.

Taken together, these results demonstrated that the amplification protocol applied here in combination with the NanoString technology is suitable to generate valid and representative cDNA libraries enabling quantitative detection of transcript levels ranging from copy numbers as low as 10 to several thousands. Moreover, even at

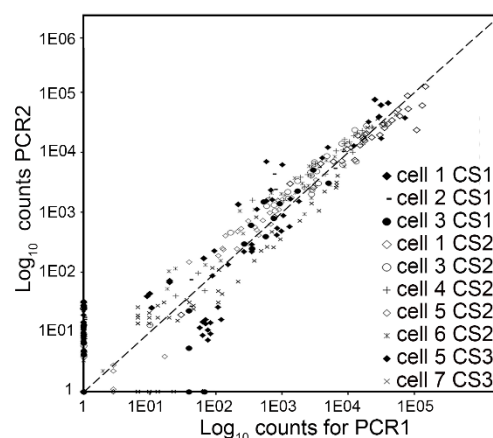


Figure 10 - Validation of second round amplification. Quantitative analysis of transcript counts in PCR1 (35 PCR cycles) and PCR2 (additional 30 PCR cycles) products of seven different single cell libraries generated from isolated cells of the MGE and POA and tested with different codesets, revealed a significant correlation $R_{\text{Spearman}} = 0.963$ (** $p \leq 0.001$, Student's t-test). Codeset details are listed in Appendix Tab. 1-3. CS, codeset; MGE, medial ganglionic eminence; POA, preoptic area.

transcript levels down to one, amplified cDNAs were detected in 90.3% of all replicates over threshold, indicating that this protocol is appropriate for amplification and detection of even very low abundant transcripts.

5.2 Regulation of cortical progenitor division by thalamic fibers expressing *EfnA5*

As outlined in the introduction, the generation of cortical projection neurons is a highly complex process requiring several mechanisms, which exert control over the whole developmental process. The Eph-receptor/ephrin-ligand system has already been described to participate in the regulation of processes like proliferation and differentiation during neurogenesis (Bolz and Castellani 1997, Flanagan and Vanderhaeghen 1998, Knoll and Drescher 2002, Kullander and Klein 2002, Qiu et al. 2008, North et al. 2009, Rudolph et al. 2010, Zimmer et al. 2011). In this context, phenotypic analysis of *EfnA5* deficient mice provided evidence that this membrane bound ligand regulates cortical progenitor division during embryogenesis, thereby affecting cortical layer formation (Gerstmann et al. 2015). *EfnA5* deletion led to a shift from proliferative to neurogenic progenitor division at early stages of corticogenesis causing enlarged infragranular cortical layers IV and V. This occurred at the expense of the progenitor pool generating neurons of the superficial layers at later stages, which were consistently reduced in thickness in *EfnA5* knockout mice (Gerstmann et al. 2015). In the following chapters the single cell amplification protocol was applied to identify the cell type that expresses *EfnA5* in the developing telencephalon.

5.2.1 EFNA5 affects the division mode of cortical progenitors

The phenotype observed in *EfnA5* deficient mice could be achieved via a direct interaction on cortical progenitors or as a secondary mediated effect. Interaction between Eph-receptors and their corresponding ligand required direct cell-to-cell contact for proper signal transduction (Davis et al. 1994, Bruckner et al. 1997, Flanagan and Vanderhaeghen 1998). A pair-cell assay was performed, to test if the changes observed in the *EfnA5* knockout strain occur based on primary effects of EFNA5 on cortical progenitors. According to Gerstmann et al. (2015), first alterations were observed at E13.5 in the *EfnA5* knockout model. Therefore, cells prepared from E13.5 cortices were seeded at clonal density and stimulated with either recombinant

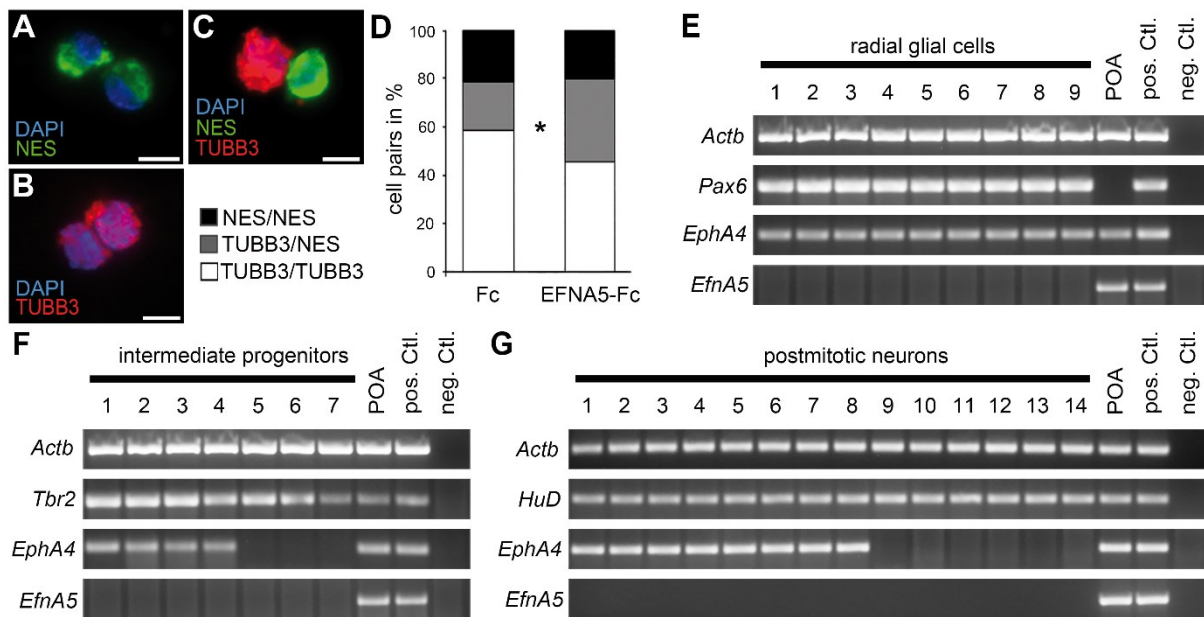


Figure 11 - EFNA5 effects on cortical cells and expression pattern at single cell level. (A-D) Pair-cell assay with E13.5 cortical cells after 24 h *in vitro* followed by immunostaining against NES and TUBB3 for progenitors and postmitotic neurons, respectively. Formed cell pairs were analyzed according to their staining pattern of either two NES-positive cells (A), two TUBB3-positive cells (B) or mixed pairs of a TUBB3 and a NES positive cell (C). (D) Upon EFNA5-Fc stimulation (n=154 cell pairs) the proportion of TUBB3/NES-positive cell pairs increased at the expense of TUBB3/TUBB3-positive cell pairs, as compared to Fc application (n=141; five independent experiments; *p<0.05, Student's t-test). (E-G) Single-cell RT-PCR of E16.5 cortical progenitors (E, F) and postmitotic cortical neurons (G). *EfnA5* transcripts were absent from cortical progenitors, as identified by *Pax6* expression for RGCs (n=15; E) and by *Tbr2* signal for IPCs (n=7; F), as well as from *HuD*-expressing postmitotic neurons (n=17; G). In contrast, *EphA4*-receptor expression was confirmed in *Pax6*-positive and *Tbr2*-positive cortical progenitors at the single-cell level (E, F). Pre optic area (POA)-derived single-cell libraries (E14.5, n=3; E-G) and cDNA libraries of whole brain tissue RNA (E14.5) served as positive controls (pos. Ctl.); the negative control (neg. Ctl.) lacked cDNA template. *Actb*, β -actin. Scale bars: 25 μ m in (A-C).

clustered EFNA5-FC or control-FC. After 24 hours *in vitro*, division of the progenitor cells led to formation of cell pairs, which were analyzed by immunostaining against NES for progenitors and TUBB3 for early postmitotic neurons. The analysis of the proportional appearance of cell pairs consisting of two NES-positive, two TUBB3-positive cells as well as mixed pairs of a TUBB3 and a NES positive cell (Fig. 11A-C) revealed a significant reduction of TUBB3 postmitotic cell pairs after EFNA5-FC stimulation compared to control treated cells (Fig. 11D; p<0.05). The results were opposed to the phenotype observed in *EfnA5* deficient animals revealing increased numbers of postmitotic neurons at E13.5 (Gerstmann et al. 2015) and hence consistent, as the stimulation with recombinant EFNA5-FC protein represented a gain of function assay.

5.2.2 *EfnA5* transcripts were not detected in cortical cells by single cell-based expression analysis while *EphA4* was confirmed in progenitors

The EFNA5 gain and loss of function studies provided evidence for an effect of EFNA5 on cortical progenitors (Fig. 11A-D; Gerstmann et al. 2015). In the study of Gerstmann et al. (2015), EPHA4 was identified as the interacting receptor, as of all potential binding partners of EFNA5 only *EphA4* revealed a strong expression in the cortical

ventricular zone (VZ), where the progenitors reside. In addition, the layer shift observed in *EfnA5* deficient animals was phenocopied in *EphA4*-knockout mice (Gerstmann et al. 2015), further suggesting EPHA4 as the corresponding receptor. Eph-ephrin signaling was already described to promote and maintain proliferation of cortical progenitors by paracrine activation (Qiu et al. 2008, North et al. 2009) giving reason to expect *EfnA5* expression in progenitor cells located in the VZ of the cortex.

While *EfnA5* transcripts were detected in embryonic cortical tissue with RT-PCR, non-radioactive *in situ* hybridization did not reveal reliable signals in embryonic pallial structures (Gerstmann et al. 2015), suggesting that cortical *EfnA5* expression might be below the detection limit for this particular technique. Hence, in a next set of experiments embryonic cortical single cells were isolated and applied to the 3' limited single cell amplification protocol to investigate *EfnA5* expression at a cellular level. In addition to its high sensitivity, this approach allows to discriminate between different subtypes of cortical progenitors and postmitotic neurons. To this end, PCR with sequence specific primers against *Pax6*, *Tbr2* and *HuD* was performed, in order to identify apical and basal progenitors as well as postmitotic neurons, respectively (Englund et al. 2005, Gauthier-Fisher et al. 2009, Fujiwara et al. 2011). Of all tested cells (n=63, exemplarily shown in Fig. 11E-G), about one fourth was positive for *Pax6* (n=15) representing apical progenitors (Fig. 11E; Gotz et al. 1998, Englund et al. 2005). Most of them also express *EphA4* (Fig. 11E), confirming the immunostaining data presented in Gerstmann et al. (2015), which showed *EphA4* expression in cortical progenitors. Further, basal progenitor cells were identified based on their expression of *Tbr2* (n=7; Fig. 11F; Englund et al. 2005), from those four cells were positive for *EphA4*. In contrast, *EfnA5* was neither detected in apical nor in basal progenitors. As a positive control for *EfnA5* detection, single cell libraries isolated from the POA known to express this ligand (n=3; Fig. 11E-F; Zimmer et al. 2008), as well as cDNAs generated from single cell equivalent dilutions (5 pg quantities) of embryonic brain tissue RNA, were included in the analysis. Since *EfnA5* expression was not detected in cortical progenitors a paracrine activation of the EPHA4 receptor by neighboring progenitor cells expressing *EfnA5* appeared to be unlikely.

A feedback signaling by postmitotic neurons was another conceivable mechanism. Here the radial processes of the progenitors could serve as a scaffold passing the signal to the ventricular zone (VZ). In support of this, Parthasarathy et al. (2014)

provided evidence that the neurotrophin *Ntf3* expressed by postmitotic cells inside the cortical plate signal back to the VZ and thereby regulating progenitor division. In support of this, Gerstmann et al. (2015) showed EPHA4-receptor expression along the radial processes of the apical progenitors spanning through the whole cortical plate. Nevertheless, it was not possible to detect *EfnA5* signals in postmitotic cortical transcriptomes, which were classified according to *HuD*-expression (n=17; Fig. 11G; Gauthier-Fisher et al. 2009, Fujiwara et al. 2011). Hence, a feedback mechanism mediated by postmitotic neurons as suggested by several groups (Seuntjens et al. 2009, Parthasarathy et al. 2014, Toma et al. 2014) did not seem responsible in this particular case. In conclusion, consistent with the *in situ* hybridization data provided by Gerstmann et al. (2015), *EfnA5* expression could not be observed in any of the 63 individual cortical cells. In turn, the expression of the corresponding *EphA4* receptor was confirmed in apical (n=13 of 15) and basal (n=4 of 7) progenitors.

5.2.3 *EfnA5* transcripts were detected in axonal compartments of the thalamus

As it was not possible to detect *EfnA5* expression in cortical cells, we hypothesized an extra-cortical source importing *EfnA5* into the cortex. In this context, it was verified by our group and others that first thalamic axons reached the developing cortex as early as E13.5 (Auladell et al. 2000, Gerstmann et al. 2015), when initial defects in the *EfnA5* knockout mice were observed (Gerstmann et al. 2015). Furthermore, the embryonic thalamus was shown to express *EfnA5* already during early stages (Gerstmann et al. 2015). Thus, the next question was whether *EfnA5* expressed by invading thalamic fibers could regulate the mitotic activity of cortical precursors. First, to show the expression of ephrin A-ligands along thalamic fibers, thalamic explants were cultured for 24 hours to allow axonal outgrowth. Following this, Alexa488 labelled recombinant EPHA3-FC protein was applied, due to the lack of specific antibodies for EFNA5. In contrast to the EPHA4 receptor, EPHA3 does not interact with ephrin B ligands and was therefore used to specifically visualize ephrin A-ligands, according to previous studies (Zimmer et al. 2011). Indeed, EPHA3-FC binding sites were detected along thalamic axons stained with TUBB3, indicating the presence of ephrin A-protein expression (Fig. 12A-D).

As axon-located protein synthesis has already been described and hence the presence of respective mRNAs (Jung et al. 2012), thalamic fibers were tested specifically for the presence of *EfnA5* mRNA. For this, axonal compartments of E14.5 thalamic explants

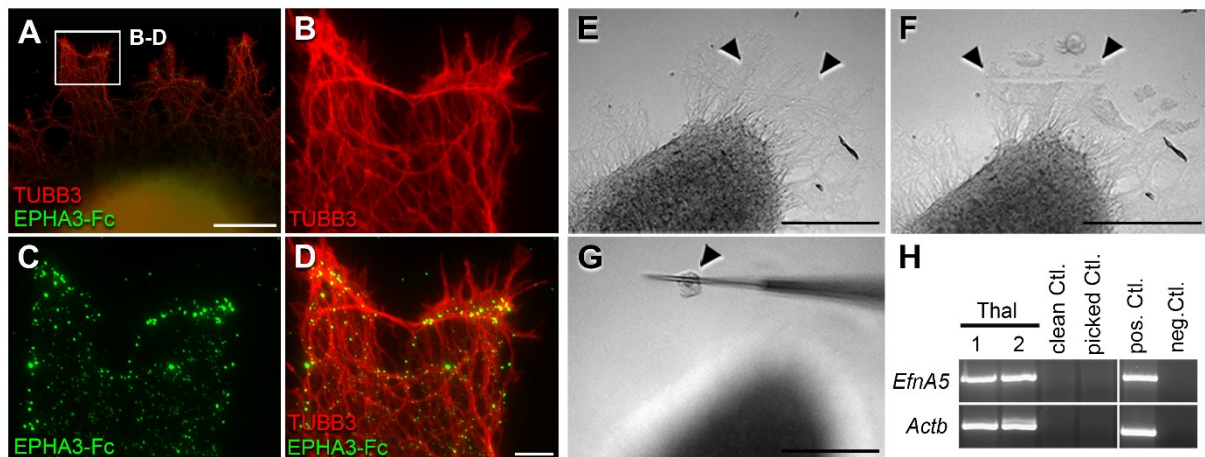


Figure 12 - Evidence for *EfnA5* expression in thalamic axons. (A-D) Axons of thalamic explants (E14.5+1div) express ephrin A ligands as revealed by EPHA3-Fc binding sites. Thalamic explants were treated with EPHA3-Fc prior to immunostaining for TUBB3. The boxed region is magnified in (B-D). (B) Immunostaining against TUBB3. (C) EPHA3-Fc binding sites visualized with an Alexa 488-labeled anti-Fc antibody. (D) Overlay of (B) and (C). (E-H) Isolated axonal compartments from thalamic explants without soma contamination (E14.5+1div) (E-G; arrowheads indicate isolated axons) contained *EfnA5* transcripts as revealed by RT-PCR (H); the housekeeping gene β -actin (*Actb*) provided a loading control. Single cell libraries of preoptic area-derived cells and limited cDNA generated from E14.5/E16.5 embryonic brain tissue served as positive controls (pos. Ctl.); the negative control (neg. Ctl.) lacked cDNA template. 1 and 2 refer to the axonal samples. Clean Ctl. and picked Ctl. refer to control conditions in which freshly prepared isolation buffer (clean control) and isolation buffer of the explants after axon isolation (picked control) were used as templates for cDNA synthesis to check for potential RNA contamination. Scale bars: 500 μ m in (E-G); 100 μ m in (A); 10 μ m in (D).

cultured for 24 hours were manually isolated under visual control (Fig. 12E-G) ensuring no cellular contamination. The samples were applied to the same sensitive amplification protocol used for single cells. *Actb* was used as house-keeping gene, which was detected in axonal samples but not in the negative controls. As negative controls either freshly prepared isolation buffer (clean Ctl.) or the isolation buffer of the explants after axon isolation (picked Ctl.; Fig. 12H) were used. As illustrated in Figure 12H, *EfnA5* transcripts were indeed detected in the axonal compartments of thalamic explants with primer specific PCR, which confirmed the EPHA3 binding assay showing ephrin A-protein expression.

In summary, these results demonstrate that *EfnA5* is expressed by embryonic thalamic fibers, which reach the cortex as early as E13.5, when the first effects were observed, leading to increased numbers of basal progenitors in *EfnA5* deficient animals (Gerstmann et al. 2015). Thereby, the sensitivity of the amplification protocol solved a major issue in this study, as *EfnA5* transcripts were detected with RT-PCR in cortical tissue but could neither be confirmed with *in situ* hybridization (Gerstmann et al. 2015) or the analysis of cortical single cells (see chapter 5.2.2). Moreover, these data provided evidence, that extra-cortical *EfnA5* imported by invading thalamic axons could regulate cortical progenitor division.

5.2.4 Ephrin A-ligand expressing thalamocortical axons affected cortical progenitor division

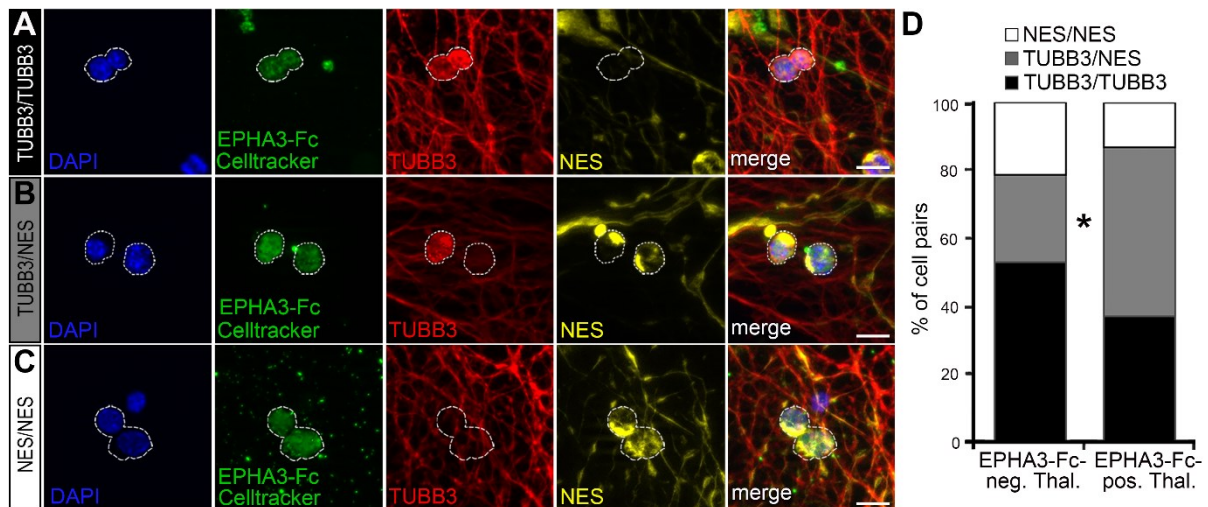


Figure 13 - Ephrin A-ligand expressing thalamic fibers regulate progenitor proliferation. (A-C) Cell Tracker Green-labeled E13.5 single cortical cells co-cultured with either EPHA3-Fc-negative (A, B) or EPHA3-Fc-positive (C) E13.5 thalamic explants for 24 h *in vitro* and labeled by NES/TUBB3 double staining (yellow and red, respectively). Cell Tracker Green labeling the whole cell body and the dotted clustered EPHA3-Fc/Alexa 488 signal is shown in green. Cell pairs are outlined. (D) Quantification of the proportion of cell pairs shows an increased proportion of TUBB3/NES-positive cell pairs in response to EPHA3-positive (n=38 cell pairs) versus EPHA3-negative thalamic axons (n=40 cell pairs; four independent experiments; *p<0.05, Student's t-test). Scale bars: 10 μ m in A-C.

To test if ephrin A-expressing thalamic fibers are capable of influencing cortical progenitor division, a modified pair cell assay was performed. Briefly, E13.5 thalamic explants were co-cultured for 24 hours with cortical single cells (E13.5) at clonal density. To distinguish between cortical cells and thalamic cells emigrating from the explants, the cortical cells were labelled with Cell Tracker Green resulting in a complete soma staining (Fig. 13A-C). In order to further discriminate ephrin A-ligand-positive thalamic axons from negative ones, recombinant EPHA3-FC clustered with an Alexa 488-labeled anti-human IgG antibody was applied, leading to a spotty staining of positive fibers (Fig. 13C). Similar to the pair cell assay described above immunostaining against NES and TUBB3 was performed and the Cell Tracker Green positive cortical cell pairs located within the area covered by thalamic axons were analyzed in regard to their composition (Fig. 13A-C). An increase in the proportion of the mixed NES/TUBB3-positive cell pairs in the presence of EPHA3-FC positive axonal fibers compared to EPHA3-FC negative explants was observed (Fig. 13D). Accordingly, decreased proportions of double TUBB3-positive and double NES-positive cell pairs were evident for cell pairs influenced by ephrin A-expressing fibers. These *in vitro* data resemble the results obtained by the stimulation of cortical cells with recombinant EFNA5-FC protein, which also resulted in an increased proportion of NES/TUBB3 cell pairs (Fig. 11D).

Taken together, the combination of cellular as well as subcellular expression analysis and functional *in vitro* data indicate that the proliferation and differentiation of cortical progenitors is affected by EFNA5 ligands imported by invading thalamic axons. Thereby, the extra-cortical regulation of progenitor division by EFNA5 represents a novel mechanism controlling the proper laminar organization of the cerebral cortex (Gerstmann et al. 2015).

5.3 DNMT1 is required for the migration of POA-derived cortical interneurons

5.3.1 Approaching the diversity of neurons generated in the embryonic subpallium with NanoString-based single cell analysis

The research of interneuron development is another issue, which already benefits from single cell transcriptome analysis as most of the neuronal diversity in the mature telencephalon derives from progenitor cells of the subpallium (Cauli et al. 2000, Nelson et al. 2006, Zeisel et al. 2015). In contrast to cortical projection neurons, interneurons fated for the cortex are characterized by a prolonged maturation due to their phase of tangential migration. In the last decades quite a lot knowledge has been acquired regarding the mechanism controlling the tangential migration like cytoskeleton remodeling or distinct guidance receptor expression (Abo et al. 1998, Rashid et al. 2001, Antypa et al. 2011, Cooper 2013, van den Berghe et al. 2013, Rane and Minden 2014, Rudolph et al. 2014, Steinecke et al. 2014, Zito et al. 2014, Boitard et al. 2015, Peyre et al. 2015). But what are the superordinate control instances? To get insights into the processes regulating migratory capacities of cortical interneurons, we focused our analysis on POA subtypes, because fate mapping studies revealed that POA-derived cells expressing the transcription factor *Hmx3* give rise to cortical populations as well as to residual subtypes populating the mantle zone of the POA (Gelman et al. 2009). If it is possible to discriminate migrating subtypes from residual populations based on their single cell transcriptome, this would be beneficial for finding key regulators of tangential migration. So far it has been described, that in addition to the diverse inhibitory interneurons of the cortex (Gelman et al. 2009, Gelman et al. 2011), this region also give rise to neurons destined for the olfactory bulb, amygdala and striatum (Elshatory and Gan 2008, Garcia-Lopez et al. 2008, Bupesh et al. 2011). Nevertheless, the POA still represents a black box to a great extent, regarding the diversity of neuronal subtypes produced therein and the mechanism exerting control

over their maturation and differentiation. Therefore, cells isolated from MGE derivatives were included into the analysis to serve as internal control of the profiling strategy.

5.3.1.1 Discriminating MGE and POA subtypes by single cell-based principal component analysis

To find potential regulators of postmitotic development especially orchestrating the period of migration, quantitative NanoString based single cell transcriptome analysis was performed. Applying the strategy validated in chapter 5.1, distinct neuronal subsets generated in the MGE and POA at embryonic day E14.5 were profiled. For this, 96 genes were selected for the NanoString codeset No3 based on differential gene expression analysis obtained by Next Generation Sequencing of RNA from E14.5 MGE and POA tissue (further details are described in methods 4.6; Appendix Tab. 3). In addition to house-keeping genes and known marker transcripts, probes were included in the codeset against genes encoding for chromatin/DNA binding factors, intracellular membrane bound signaling molecules, cytoskeleton associated proteins, cytokines and secreted factors as well as for proteins of unknown function, which could be potentially relevant for postmitotic development. For MGE-derivatives, important marker transcripts of distinct interneuron subtypes are already identified (Marin et al. 2000, Alifragis et al. 2004, Flames et al. 2007, Zimmer et al. 2011), some of which were included in the codeset.

The molecular signatures of different neuronal subtypes were investigated by unbiased clustering of 92 single cell libraries obtained from the MGE (n=21 cells) and POA (n=71 cells) revealing 6 major groups (Fig. 14). The clustering was based on principal component analysis (PCA), converting potentially correlated variables (genes) to sets of linearly uncorrelated values (principal components) to reduce the dimension of the dataset and to reveal population specific gene expression pattern. Thereby, the first principal component (PC) captures genes with the largest variance and each succeeding component includes the highest remaining variance as illustrated in the scree plot (Fig. 14 scree plot at the top left side; Lê et al. 2008). In addition, a gene clustering was performed to reveal sets of genes characterizing the different cell cluster. The PCA is free of any presuppositions like the origin of prepared cells or the expression of known markers. However, considering the information about the source of preparation, most cells clustered together according to their site of origin. As illustrated in Figure 14, cells prepared from the MGE mainly cluster in group II and III

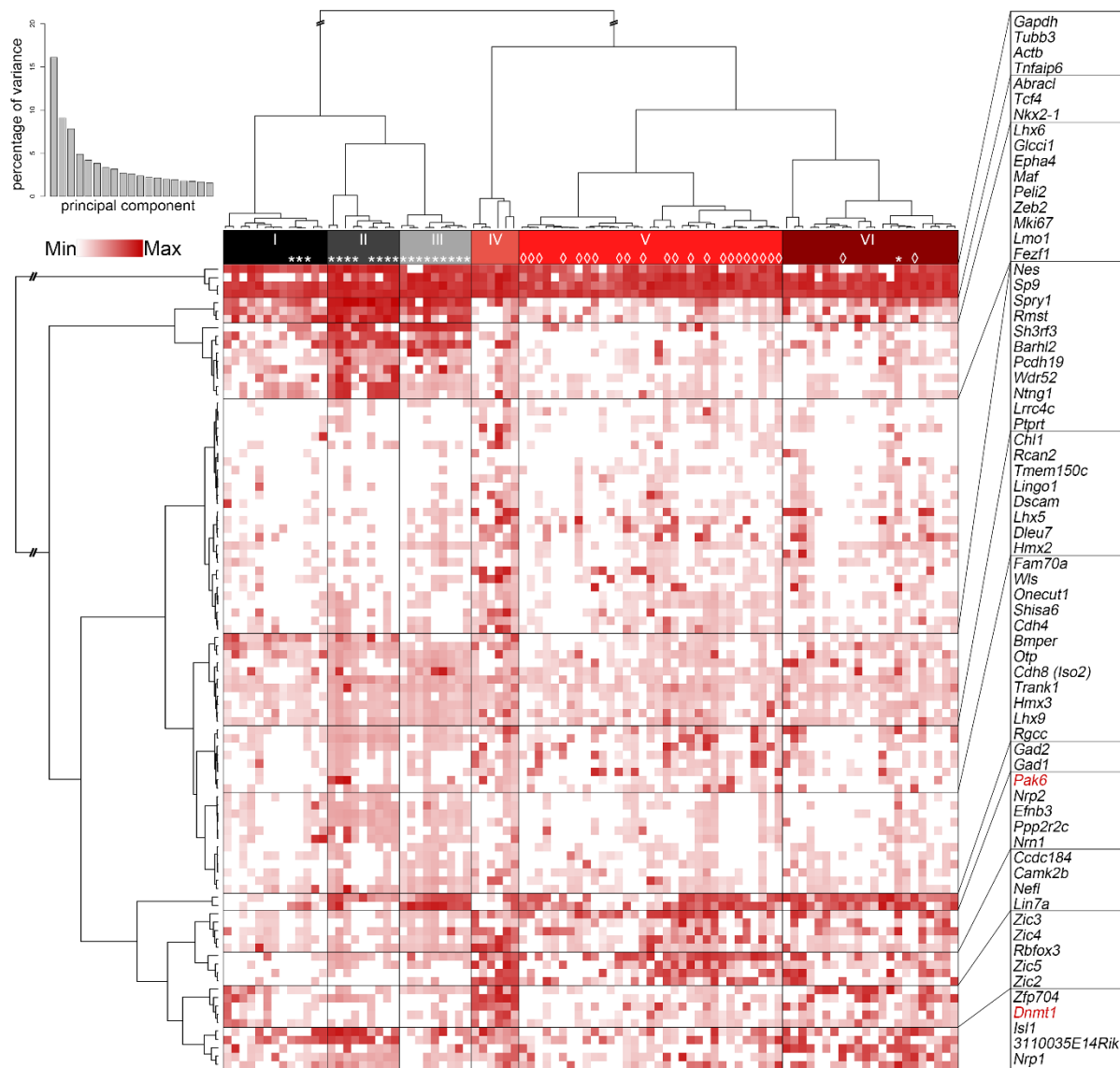


Figure 14 - Gene expression profiles of MGE- and POA-derived cells revealed by NanoString-based single-cell transcriptomics. The heat map illustrates the expression level of 96 genes in 92 cells isolated from the MGE and the region of the POA of E14.5 brains. Principal component analysis (PCA)-based hierarchical clustering revealed six major groups, labelled by Roman numerals. Thereby, the first principal component (PC) captures the largest variance and each succeeding component includes the highest remaining variance as shown by the scree plot (top left). Post-mitotic POA-derived *Hmx3-Cre/tdTomato* cells (labelled by diamond symbols underneath the cluster designation) mainly belong to cluster V, representing post-mitotic POA cells. Cells of MGE origin are labelled by stars (labels underneath the cluster designation). Non-labelled cells derive from POA preparations. MGE, medial ganglionic eminence; POA, preoptic area.

(star symbols). Cells obtained from POA preparations (cells without any symbol or with diamond symbols) are mostly collected in group IV-VI, while group I contains cells from both domains, which segregated into distinct subcluster. Moreover, *Hmx3-Cre/tdTomato*-expressing postmitotic POA cells were included as an additional control (Gelman et al. 2009), which mainly clustered into group V and VI (n=24 of 71 POA cells, symbolized by diamonds).

The most informative genes contributing to each component and which are consequently highly relevant for the cluster formation are illustrated in the variables factors maps (Fig. 15). According to the cell and gene projections illustrated in

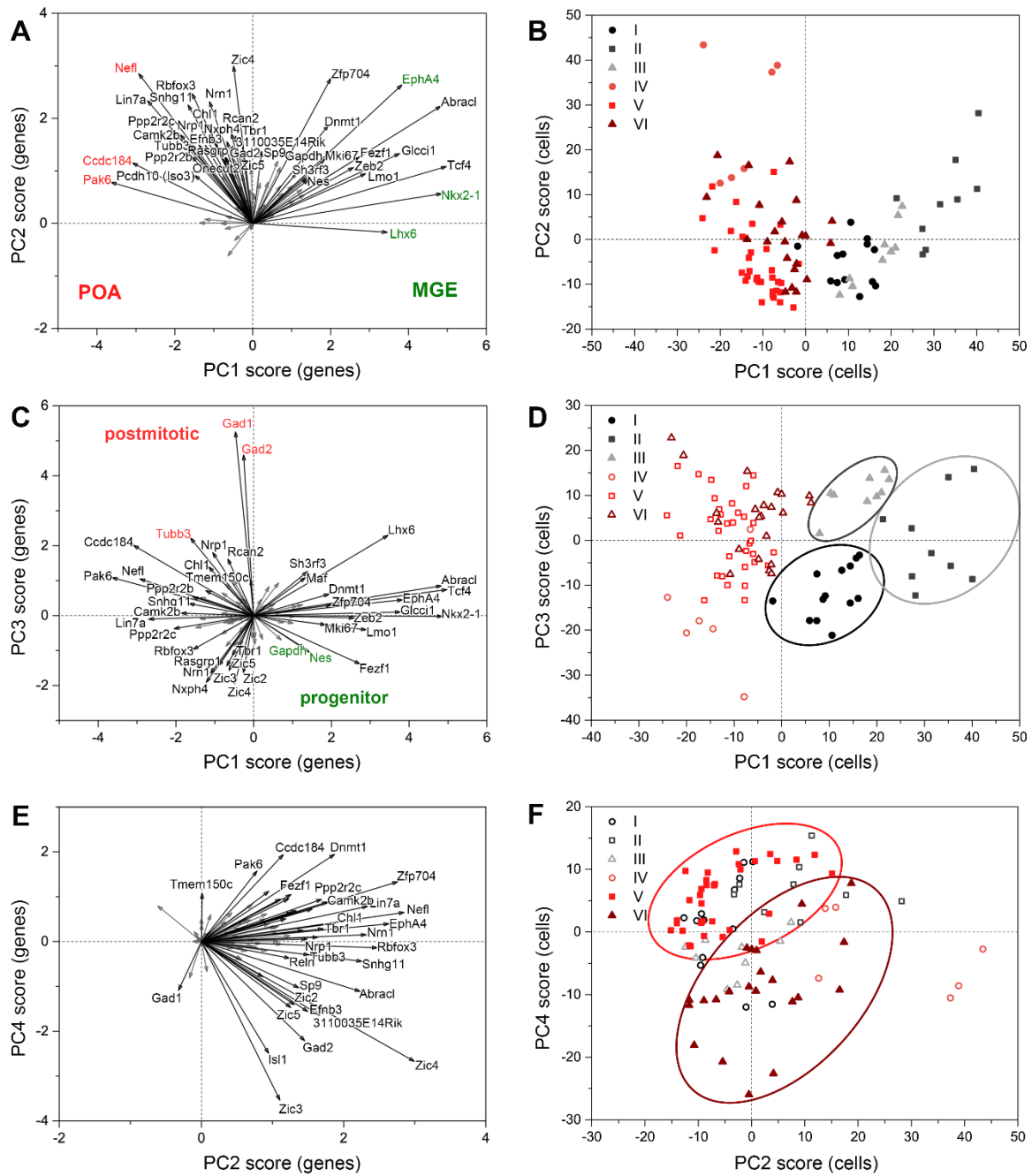


Figure 15 - The contribution of different principal components to the segregation of distinct cellular subsets. The most informative genes contributing to the cluster formation are depicted in variables factor maps (A, C, E). The segregation of the cells into distinct groups based on their expression profile is illustrated by cell projection maps (B, D, F). (A, B) PC1 mainly separates MGE- (clusters II and III) from POA-derived cells (clusters IV-VI). Thereby, genes like *EphA4*, *Nkx2-1* and *Lhx6* (labelled in green) are decisive for MGE populations, whereas genes like *Nefl*, *Ccdc184* or *Pak6* (labeled in red) seems to be relevant for POA-derived cells. The PC2 axis as well as higher PCs instead separate the different subclusters for the MGE (C, D) and the POA pool (E, F). (C, D) The differences between progenitors and postmitotic neurons of the MGE is mainly captured by PC3 as illustrated by the opposing expression of progenitor markers like *Nes* and *Gapdh* (labelled in green) and genes associated to postmitotic development like *Gad1*, *Gad2* or *Tubb3* (labelled in red). (E, F) The segregation of post-mitotic cells of clusters IV-VI is mainly influenced by PC2 and PC4. Thereby, *Nrn1* and *Tbr1* expression define cluster IV, while *Pak6* and *Ccdc184* expression characterize cluster V. In turn, *Isl1* (*Isllet-1*) contributes to cluster VI segregation. MGE, medial ganglionic eminence; PC, principal component; POA, pre optic area.

Figure 15A, B principle component 1 has the strongest impact on the segregation of MGE- and POA-derived cDNA libraries. Well known MGE marker transcripts like *EphA4*, *Nkx2-1* and *Lhx6* (Lavdas et al. 1999, Xu et al. 2004, Zimmer et al. 2011) are enriched in cells obtained from MGE preparations, whereas POA-derived cells

including the *Hmx3-Cre/tdTomato* population (mainly Cluster V) are characterized by strong expression of genes like *Ccdc184*, *Pak6* and *Nefl* (Fig. 15A, B). As the POA is still mostly unclassified in regard to their subtype composition during development, none of those genes were yet described for the POA. Higher components affect the formation of subsets of MGE and POA-derived cells (Fig. 15C-F). Therefore, the PC3 axis seems to be important for the segregation of progenitors from postmitotic cells as typical postmitotic marker like *Gad1*, *Gad2* and *Tubb3* (Erlander et al. 1991, Gelman et al. 2012, Pacal and Bremner 2012) are contrary projected to genes associated with progenitor expression like *Nes* or *Gapdh*, which were already described to be enriched in progenitors (Fig. 15C, D; Meyer-Siegler et al. 1992, Michalczyk and Ziman 2005, Hao et al. 2015). The PCA plots presented so far only provide relative gene expression information between the different cluster, hence as a next step it was necessary to reveal the significantly differentially expressed genes.

5.3.1.2 The profiling strategy confirmed known cellular subtypes of the basal telencephalon

The PCA led to segregation of cells according to their gene expression pattern and the subsequent clustering approach highlights distinct cluster affiliations for each cell based on their PCA-based weighted gene expression. To approach the identity of the clusters, differential gene expression analysis was performed to reveal known and new marker genes for the distinct populations. Group I embraced apical progenitors due to significant expression of *Nes*, a known marker transcript of apically dividing cells during brain development (Tokunaga et al. 2004, Petros et al. 2015). In addition to *Nes*, significant *Gapdh* transcript levels characterized group I identity (Fig. 16A, B). *Gapdh* is usually ubiquitously expressed in tissue and is therefore often used as a housekeeping gene (Barber et al. 2005). However, consistent with other studies, describing *Gapdh* to be enriched in progenitor cells (Meyer-Siegler et al. 1992, Hao et al. 2015), a significantly increased expression of *Gapdh* by progenitor cells was revealed. In support of this, region specific expression demarcating strongly the VZ of the basal telencephalon was observed with *in situ* hybridization (Fig. 16B). According to the source of preparation, group I includes progenitors of the POA as well as the MGE domain (Fig. 14), which are collected in distinct sub-clusters within group I. The integration of POA- and MGE-derived apical progenitors in the same cluster can be explained by the composition of the codeset focusing strongly on postmitotic

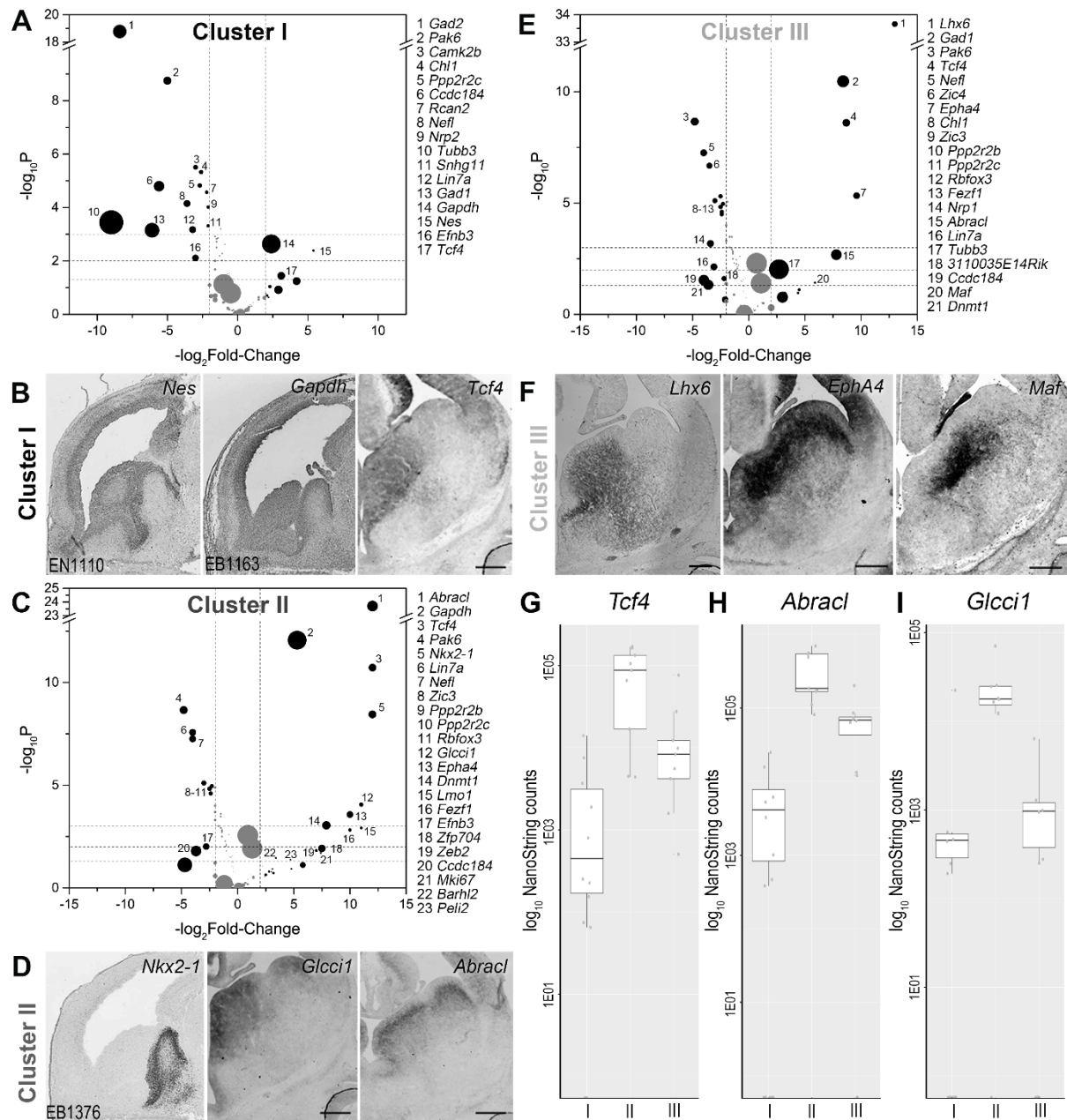


Figure 16 - Differential gene expression analysis of Cluster I to III reveal different maturational stages of MGE-derived cells. (A, C, E) Differential gene expression analysis depicted in volcano plots, based on the comparison of gene expression of the respective cluster compared to all remaining cells. (B, D, F) Validation of region specific expression in E14.5 coronal brain sections with *in situ* hybridization using sequence specific riboprobes. *In situ* hybridization in E14.5 sagittal sections were obtained from genepaint.org, for which the gene accession number is provided. (A, B) Cluster I displays significant *Nes*, *Gapdh* and *Tcf4* expression, representing progenitor marker transcripts with major signal intensity in the ventricular and subventricular zone (VZ and SVZ, respectively). (C, D) Cluster II is characterized by significant expression of progenitor associated transcripts *Gapdh* and *Nkx2-1*. Due to the lack of *Nes* and the significant level of transcripts expressed in the SVZ like *Abracl* and *Glcci1* (D), cluster II likely includes basal progenitors of the MGE. (E, F) Post-mitotic MGE marker transcripts like *Lhx6*, *Epha4* and *Maf* are enriched in cluster III cells. (G-I) For genes like *Tcf4*, *Abracl* and *Glcci1* a cluster specific expression level was observed, which suggest that gene expression levels are subtype dependent. Scale bars: 500µm in (B, D, F).

differentiation and lacking probes against specific marker transcripts for POA- versus MGE-derived apical precursors.

Group II, predominantly composed of MGE-derived cells, was characterized by high levels of progenitor associated marker transcripts (*Gapdh*, *Nkx2-1* and *Mki67*) but lacked significant *Nes* expression (Fig. 16C). This pointed to basally dividing MGE

progenitors of the SVZ, which has already been described for the MGE (Pilz et al. 2013). Consistently, this cluster exhibited significant expression of *Glcci1*, *Abrac1* and *Tcf4*, which were also mainly detected in the SVZ of the MGE (Fig. 16B, D). *Tcf4* has already been described as a downstream transcription factor of the Wnt pathway orchestrating cell fate decision by modulation of gene expression during embryonic development (Faro et al. 2009, Livnat et al. 2010). However, for *Glcci1* and *Abrac1* besides the expression pattern, the functions in neuronal development are unknown according to literature.

Group III cells represented postmitotic MGE-derived interneurons based on significant expression of described marker transcripts like *Gad1*, *Lhx6*, *Maf-1* and *EphA4* (Fig. 16E, F; Zhao et al. 2008, Zimmer et al. 2011, McKinsey et al. 2013, Neves et al. 2013). For instance, the *EphA4* receptor has been described to serve as a guidance factor simultaneously promoting the migration of MGE-derived interneurons to their cortical targets (Steinecke et al. 2014). Also the LIM homeodomain transcription factor *Lhx6* was shown to be essential for proper migration of MGE-derived cortical interneurons mainly along the deep migratory stream through the SVZ of the MGE (Alifragis et al. 2004, Liodis et al. 2007). Furthermore, significant *Tcf4* and *Abrac1* transcript counts characterized these cells (Fig. 16E), indicating that these transcripts are expressed by basal progenitors as well as postmitotic MGE derivatives. However, the expression levels of these genes were cluster specific as illustrated in Figure 16G, H. Consistent with the *in situ* hybridization for *Abrac1* (Fig. 16D), apical progenitors residing in the VZ and collected in cluster I showed low levels of expression, while cluster II representing basal progenitors located in the SVZ showed quite high mean transcript counts for *Abrac1* (Fig. 16H). The postmitotic cluster III cells in turn revealed medium expression (Fig. 16H). Similar results were observed for *Tcf4* and *Glcci1* (Fig. 16G, I) emphasizing the importance of the expression level in the biological context and thereby also for cluster formation.

In agreement with the source of preparation and known marker transcripts, distinct cell types of the MGE domain could be identified with this approach confirming the analysis strategy and exposing interesting biomarkers for eventual investigation. In addition, the identification of cluster specific gene expression levels like for *Glcci1*, *Tcf4* and *Abrac1* demonstrated the relevance of a highly quantitative method for single cell analysis.

5.3.1.3 Cluster IV embraced pallial excitatory neurons invading the POA

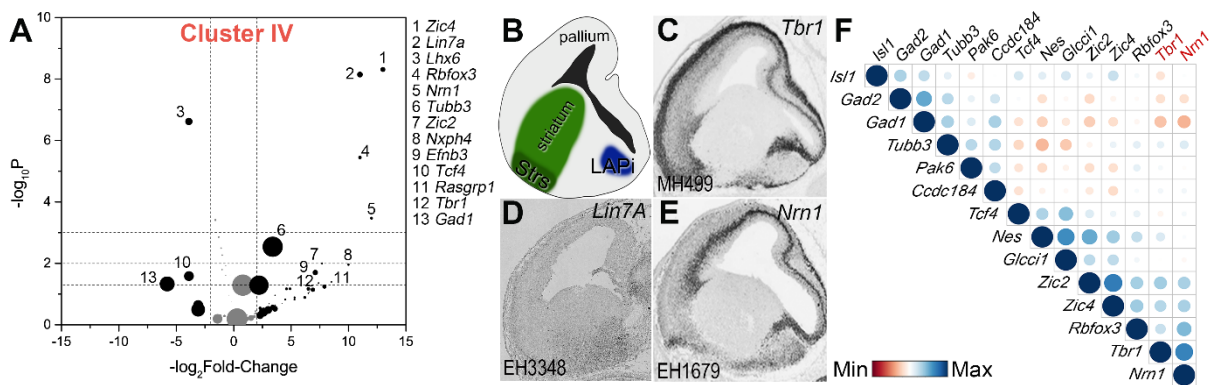


Figure 17 - Cluster IV represents pallial derived excitatory neurons settle into the POA. (A) Cluster IV cells, composed of POA-isolated cells, display significant expression of transcripts accounting for marker of cells with pallial origin including *Tbr1* (C) and *Nrn1* (E). Pallial neurons have already been described to migrate into the basal telencephalon through the intermediate stratum of the lateropallial amygdalopiriform area (LAPi, highlighted in blue in B) or the superficial stratum of the striatum (Strs, highlighted in dark green in B). As suggested by expression of *Rbfox3* and *Lin7A* (D), these neurons seems to have already entered late phase of maturation. (F) Correlation plot of all POA-derived cells showing negative correlation of *Tbr1* and *Nrn1* to GABAergic marker transcripts like *Gad1* and *Gad2*. (C-E) *In situ* hybridization in E14.5 sagittal sections were obtained from genepaint.org. POA, pre optic area.

The basal telencephalon had mostly been described to give rise to neuronal cell types for various targets in the brain (Gelman et al. 2012, Kelsom and Lu 2013, Lodato and Arlotta 2015), but some populations had also been reported to invade the basal telencephalon from other regions (Remedios et al. 2007). In accordance with this, cluster IV exhibited an enrichment of *Tbr1* and *Nrn1* transcripts predominantly expressed in the pallium (Fig. 17A, C, E) suggesting that these cells were of pallial origin. Furthermore, these cells displayed significant *Tubb3* expression and lacked *Gad1* as well as *Gad2* transcripts. This pointed to postmitotic excitatory neurons present in POA preparations. In agreement with this, *Tbr1*-positive pallial neurons had already been reported to invade the basal telencephalon at embryonic stages (Puelles et al. 2000, Remedios et al. 2007). Remedios et al. (2007) described a caudal amygdaloid stream of *Tbr1*-positive cells through the lateropallial amygdalopiriform area (LAPi), which originates in the pallium aiming for the ventral basal telencephalon. In agreement, *Tbr1* as well as *Nrn1* expression was observed in the LAPi as well as along the superficial stratum of the striatum (Strs), in addition to pallial structures (Fig. 17B, C, E). Interestingly, *Nrn1* has already been reported to be relevant for neuronal survival and migration (Fujino et al. 2008, Zito et al. 2014). Thus, due to its particular expression by *Tbr1* positive non-GABAergic cells, *Nrn1* is likely relevant for the development of these pallial cells and represents a new candidate biomarker for cells of pallial origin that can be found in subpallial structures at E14.5. Consistent with their relevance for excitatory neurons during postmitotic maturation, these genes showed no or even negative correlation with genes associated to GABAergic subtypes

or progenitors (Fig. 17F). In addition, these cells exhibited significant expression of *Rbfox3* and *Lin7a* (Fig. 17A, D), which are associated with late postmitotic maturation. *Rbfox3* is initially expressed when neurons start to perform axonal and dendritic targeting (Bohlen and Halbach 2007, Pacal and Bremner 2012), whereas *Lin7a* has been described to be involved in synaptogenesis (Misawa et al. 2001, Karnak et al. 2002, Samuels et al. 2007).

5.3.1.4 Postmitotic POA derived GABAergic cells segregated into two main clusters

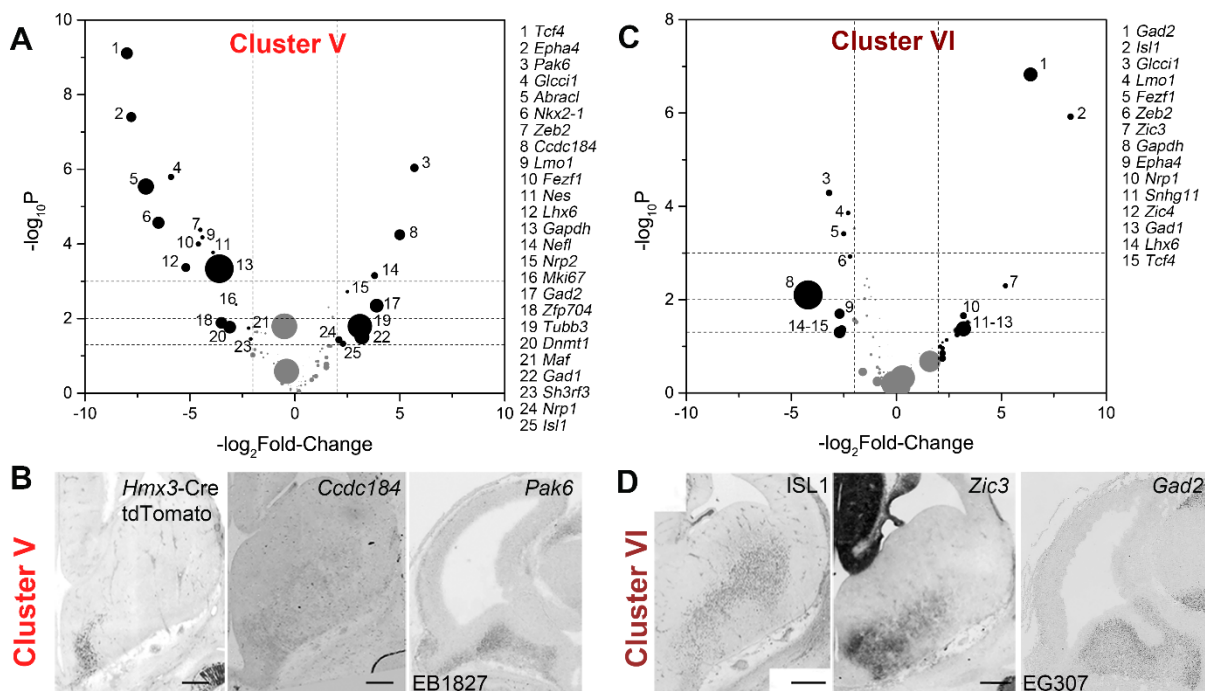


Figure 18 - POA-derived interneurons are enriched in Cluster V and VI. (A) Cluster V contains post-mitotic POA cells due to significant *Tubb3* level and the integration of most *Hmx3-Cre/tdTomato* cells (see Fig. 14, diamond symbols). Due to their high significance, *Ccdc184* and *Pak6* are newly identified marker transcripts for this subset, confirmed in the POA in tissue sections by *in situ* hybridization (B). Striatal fated cells are collected in cluster VI based on significant *Isl1* transcript counts (B). These cells are further characterized by *Zic3* expression, labeling the migration route in tissue sections, which ISL1 immuno-positive cells follow on their way to the developing striatum (D). (B-D) Validation of region specific expression in E14.5 coronal brain sections with *in situ* hybridization using sequence specific riboprobes (gene names in italic) or with immunohistochemistry applying specific antibodies (protein names in capitalized letters). *In situ* hybridization in E14.5 sagittal sections were obtained from genepaint.org, for which the gene accession number is provided. Scale bars: 500µm in (B, D)

Due to the integration of most of the *Hmx3-Cre/tdTomato* cells (22 of 24 cells, symbolized by diamonds, Fig. 14) and significant *Tubb3*, *Gad1* and *Gad2* expression cluster V collected postmitotic GABAergic POA-derived interneurons. These cells were further characterized by significant transcript levels of *Ccdc184*, a gene of unknown function, and *Pak6* (Fig. 18A, B). PAK6 belongs to the p21 activated kinases, involved in neuronal survival and neurite outgrowth (Bokoch 2003, Furnari et al. 2013, Rane and Minden 2014). In addition, significant levels of *Nrp1* and *Nrp2*, known markers of migrating POA derivatives (Zimmer et al. 2011), were further confirmed by differential gene expression analysis for these cells (Fig. 18A).

Finally cluster VI (Fig. 18C) was designated by significant *Islet-1 (Isl1)* expression in addition to *Gad1* and *Gad2*. As shown by Marin et al. (2000), the POA contributed a minor proportion of striatal GABAergic interneurons expressing the transcription factor *Isl1*, in addition to subtypes of the MGE. In support of this ISL1 immunostaining of E14.5 coronal slices labelled cells along the migration route from the POA to the striatum as well as the striatum itself (Fig. 18D; Rudolph et al. 2014). Furthermore, *Zic3* which was enriched in this population, was detected in the POA as well as along the migratory tract to the striatum (Fig. 18C, D).

In summary, in addition to the cluster with immigrated excitatory pallial cells, two clusters for postmitotic GABAergic POA-derived cells were identified by PC-based single cell analysis. A striatal fated population defined by *Isl1* expression and a cluster integrating most of the *Hmx3/tdTomato* cells, that was characterized by the expression *Ccdc184* and *Pak6*.

5.3.2 PAK6 promoted neurite outgrowth and negatively correlated with the expression of the epigenetic modifier *Dnmt1*

One of the most highly significant differentially expressed genes of postmitotic POA cells collected in cluster V was *Pak6* (Fig. 14 and 18A, B). PAK6 has been reported to promote neurite outgrowth and complexity of cortical excitatory neurons (Zhao et al. 2011). In addition, for another member of the p21 activated kinases, PAK3, a function in neurite outgrowth was proposed in post-migratory MGE-derived interneurons (Cobos et al. 2007). Briefly, Olivier et al. (2001) could show that repression of PAK3 by *Dlx1,2* inhibits premature neurite outgrowth necessary for proper migration and formation of the migratory morphology. To test whether PAK6 possessed a similar function in POA-derived neurons, dissociated cells of E14.5 POA tissue were transfected with *Pak6* siRNA or non-silencing control siRNA (see chapter 4.4.5 for the siRNA efficiency in *Pak6* downregulation). After 24 hours cells were fixed and stained against TUBB3 for morphological analysis (Fig. 19A, B). *Pak6* downregulation led to significantly diminished numbers of neurites compared to control transfections (Fig. 19C). In addition, the branching of the longest process was reduced upon *Pak6* siRNA treatment (Fig. 19C). In support of this, forced expression of *Pak6* in COS-7 cells led to the adoption of an atypical cell shape with highly branched filopodium-like structures (see chapter 4.4.5). This *in vitro* study kindly provided by Judit Symmank proposed a similar function for PAK6 in maturing processes like neurite outgrowth and

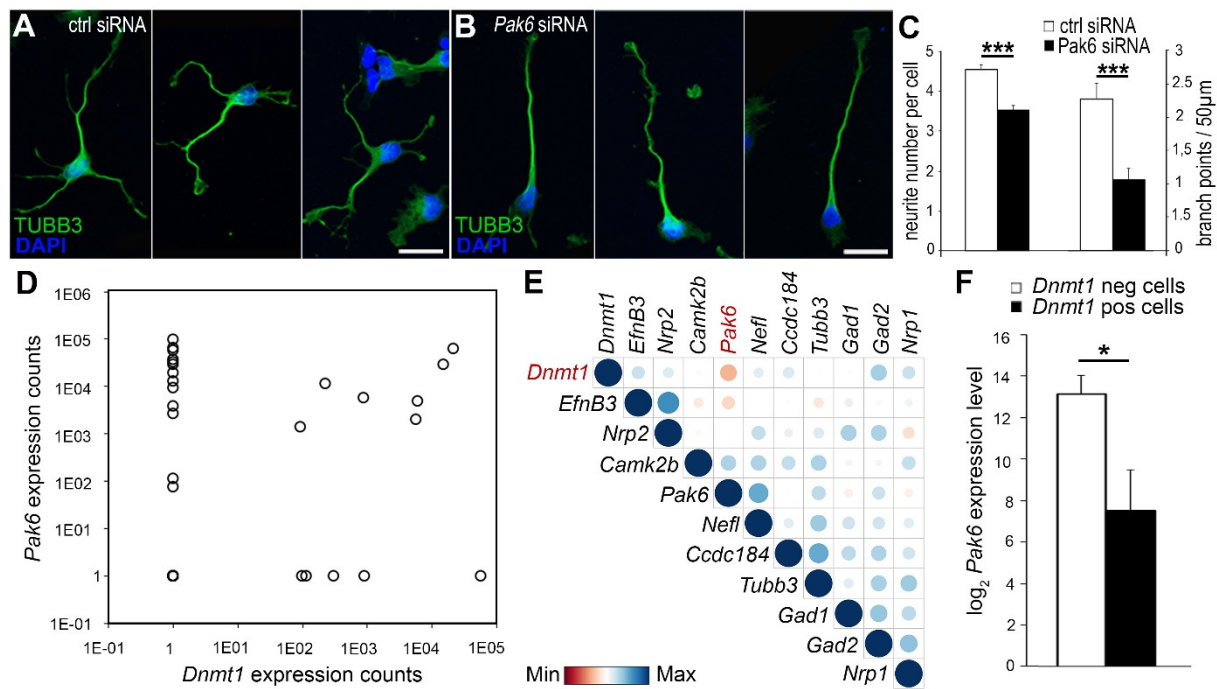


Figure 19 - Pak6 expression alters morphology and is negatively correlated with *Dnmt1* expression. (A-C) Knockdown of *Pak6* with target-specific siRNA in dissociated E14.5 (+1div) POA cells (B) revealed a decreased mean number of neurites per cell and a reduced branching density of the longest process compared to control transfections (A) as quantified in (C) (n=36 cells for control siRNA; n=55 cells for *Pak6* siRNA of three different experiments; ***p<0.001; Student's t-test). (D) Scatter plot illustrating the expression of *Pak6* and *Dnmt1* in different subsets of POA-derived post-mitotic neurons identified in cluster V by NanoString analysis, based on the single cell profiling shown in Fig. 14. (E) Correlation analysis of all cluster V cells exhibiting *Dnmt1* and/or *Pak6* expression revealed negative correlation of *Pak6* and *Dnmt1*. (F) Significant reduction of *Pak6* expression was revealed for *Dnmt1* positive cells (n=12) compared to *Dnmt1* negative cells (n=13) of cluster V (Fig. 14), *p<0.05; Student's t-test. Scale bars: 20 µm in (A, B).

branching in POA cells at post-migratory stages similar to what have been described for the function of PAK6 in cortical projection neurons (Zhao et al. 2011) or for PAK3 in MGE-derived interneurons that have reached the cortex (Cobos et al. 2007).

Of note, *Hmx3*/*tdTomato* cells, mainly integrating into cluster V, were already described to give rise to residual cells populating the mantle zone of the POA as well as to cortical interneurons (Gelman et al. 2009). Based on this information and the fact that PAK6 promoted neurite outgrowth, a process of rather later stages of maturation, the assumption was made that *Pak6* expressing cells represent post-migratory POA fated neurons. Conversely, this implicated that *Pak6*-negative POA-cells most likely represented the migratory cortical interneuron fraction. As one research focus of our group are postmitotic regulators of migration, both fractions were comparatively analyzed. Interestingly, a remarkable fraction of *Pak6*-negative cells expressed *Dnmt1*, encoding for the DNA-methyltransferase 1 (DNMT1; Fig. 19D). DNMT1 is one of the main DNA-methyltransferases (DNMTs) evident in the developing and mature brain, regulating gene expression during normal development, aging and disease mainly by its DNA-methylating activity (Inano et al. 2000, Feng and Fan 2009, Feng et al. 2010, Rhee et al. 2012, Baets et al. 2015). In contrast, the majority of *Pak6* positive cells did

not display detectable *Dnmt1* transcript levels (Fig. 14 and Fig. 19D). In addition, correlation analysis of cluster V cells expressing one or both of these transcripts revealed a negative correlation (Fig. 19E), resulting in a significantly lower mean expression level of *Pak6* in *Dnmt1* positive cluster V cells compared to the *Dnmt1* negative cells (Fig. 19F).

Taken together, these results demonstrate a negative correlation of the epigenetic regulator *Dnmt1* with *Pak6*, which is important for the post-migratory maturation of postmitotic POA-derived interneurons.

5.3.3 Expression of *Dnmt1* correlated with cell motion associated genes and was detected in migrating POA-derived GABAergic interneurons

The negative correlation of *Dnmt1* with *Pak6* expression suggested that DNMT1 is relevant for migrating cells. Due to its potential to control gene expression by canonical DNA-methylation or by non-canonical functions like histone modification (Fuks et al. 2000, Noguchi et al. 2016), DNMT1 represents a potential candidate orchestrating regulatory gene networks that control interneuron migration and maturation at postmitotic level. To test this hypothesis sequencing of individual cDNA libraries of the POA cell pool exhibiting different *Dnmt1* expression level in the NanoString analysis was performed, to obtain the whole transcriptome information.

First, the segregation of the cells was tested using PCA analysis based on the genes defining 70% of the highest variance in the NGS dataset, to check for a clustering comparable to the NanoString data. For this, in addition to cluster V cells, some cells of cluster IV and VI were included into the analysis. The sequencing data result in a segregation of the cells, comparable to the cluster affiliations obtained by the NanoString based profiling (Fig. 20A, B). The genes with the highest contribution to the cluster formation are different from those of the NanoString analysis (arrows and labels in dark grey; Fig. 20C), but among the 2000 genes with the highest impact several genes from the NanoString codeset are represented (arrows and labels in black; Fig. 20C). In a second step, genes that positively correlated with *Dnmt1* expression levels ($R > 0.7$) were functionally condensed by GO enrichment analysis to retrieve a functional profile of these genes, in order to reveal the underlying biological processes. This list of genes includes a significantly enriched number of genes involved in cell motion (Fig. 20D). In accordance with this, DNMT1 was recently reported to regulate gene expression specifically associated to processes like cell

Results

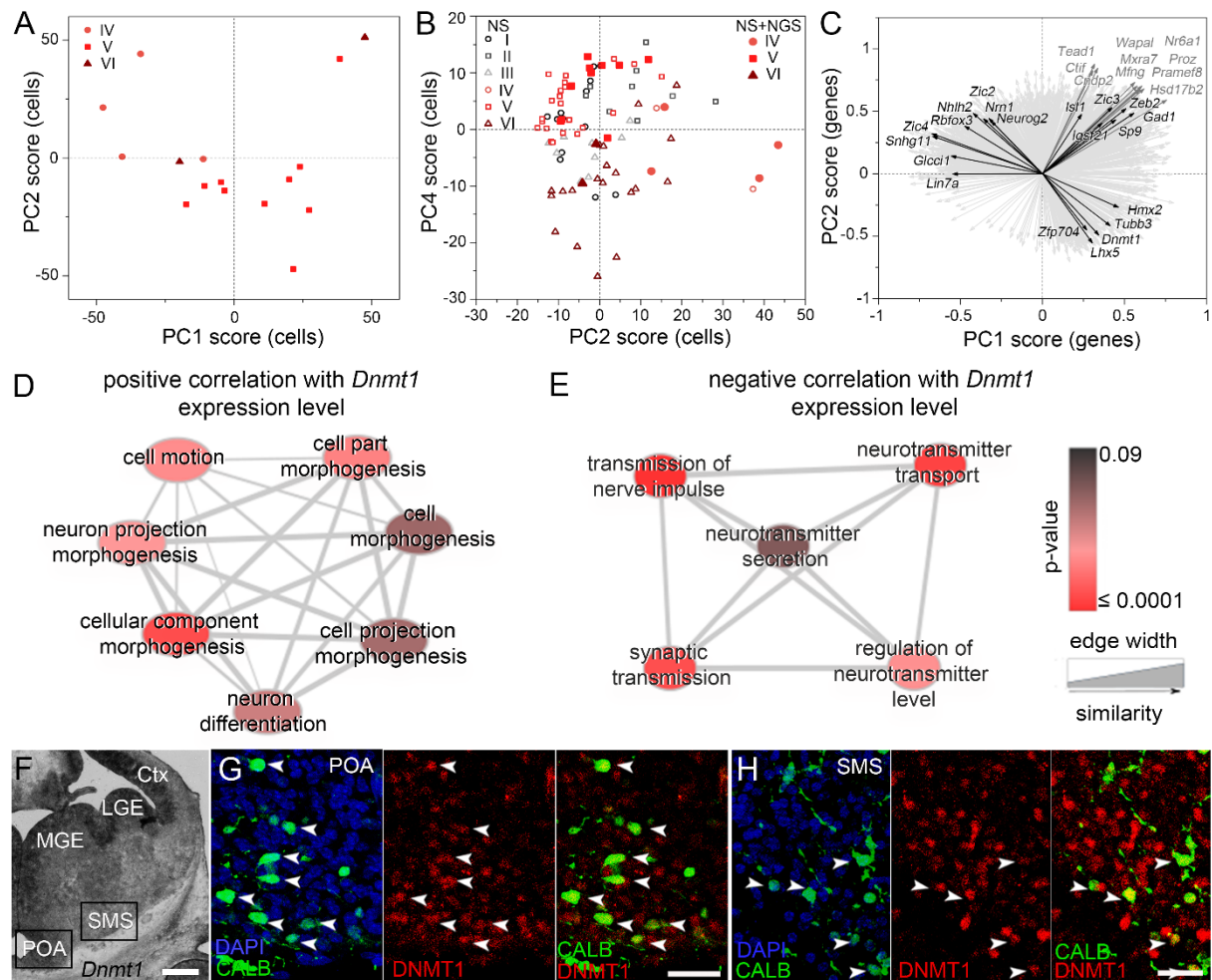


Figure 20 - *Dnmt1* expression in single cells correlated with cell motion associated genes and was detected in migrating POA-derived GABAergic interneurons. (A, B) The PCA plots illustrate a comparable segregation of the single cells based on sequencing data (A) and NanoString data (B). The cluster affiliation in (A) and (B) is obtained from the original PCA-based hierarchical clustering of the NanoString data (see chapter 5.3.1). In (B) the filled symbols highlight the cells analyzed with NanoString (NS) as well as Next Generation Sequencing (NGS). (C) Variables factor map of NGS data representing the 2000 genes with the highest contribution to cell segregation (light grey arrows). Several genes, which were included in the NanoString codeset are among the high impact genes of the sequencing data (black arrows and labels). The ten genes with the highest impact off all are highlighted and labeled in dark grey. (D, E) Correlation analysis was performed based on 70% of genes with the highest variance revealing 315 genes with a positive correlation ($PCC > 0.7$; D) and 280 genes with negative correlation ($PCC < -0.3$; E). Gene Ontology (GO) analysis was then performed with DAVID. GO terms associated to genes with positive correlation are shown in (D) and for negative correlated genes in (E). Connection between nodes require an Overlap Coefficient > 0.5 , a p-Value cutoff 0.09 and a false discovery rate (FDR) q-Value of 0.9. (F) *In situ* hybridization for *Dnmt1* in E14.5 coronal brain sections showed prominent expression in the proliferative zones of the MGE, LGE and POA. (G, H) DNMT1 expression was detected in calbindin-positive migrating interneurons of the POA (G) and along the superficial migratory stream (H) in E14.5 coronal brain sections using antibodies directed against DNMT1 (red) and calbindin (green) (co-labelling indicated by arrowheads). DAPI nuclear staining is shown in blue. The regions presented in (G) and (H) are depicted by black squares in (F). CALB, calbindin; Ctx, cortex; LGE, lateral ganglionic eminence; MGE, medial ganglionic eminence; PC, principal component; POA, pre optic area; SMS, superficial migratory stream. Scale bars: 500 μ m in (F); 25 μ m in (G, H).

migration, mobility, proliferation and focal adhesion in NHI3T3 cells (Estève et al. 2006). In turn, transcripts relevant for synaptic transmission, which is a feature of rather mature stages, negatively correlated with *Dnmt1* expression (Fig. 20E). These results further underline the hypothesis that DNMT1 is expressed in and relevant for migratory active POA cells.

To investigate if *Dnmt1* is indeed expressed in migrating POA-derived interneurons, expression studies in tissue sections were performed. At transcript level *Dnmt1* was most prominently detected in the proliferating zones of the sub-pallium including the

MGE and the POA (Fig. 20F), reflecting its function during division of progenitors (Bestor 2000). However, immunohistochemistry with antibodies directed against the postmitotic interneuron subtype marker calbindin (CB) and DNMT1 revealed double positive immature cortical interneurons in the region of the POA and along the superficial migratory route, which is followed by interneurons generated in this domain (Fig. 20G, H; Zimmer et al. 2011).

In summary, it was shown that *Dnmt1* is expressed in migrating postmitotic POA-derived cortical interneurons and seemed to be relevant for migration associated processes.

5.3.4 Postmitotic *Dnmt1* deletion in the mouse model system led to reduced numbers of cortical interneurons

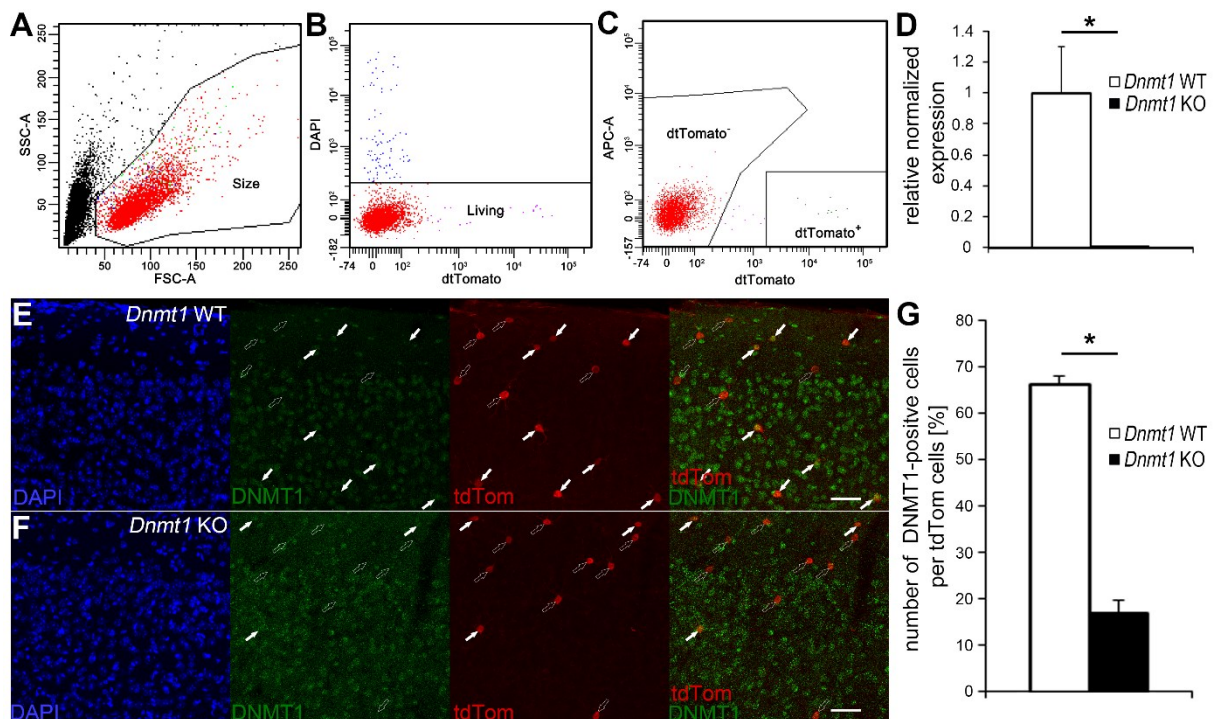


Figure 21 - Validation of *Dnmt1* deletion in *Hmx3-Cre/tdTomato/Dnmt1 loxP²* mice. (A-C) Embryonic (E16.5) *Hmx3-Cre/tdTomato/Dnmt1* wild-type and knockout cells were enriched by FACS. Gating parameters for size, living cells and tdTomato positive fraction are illustrated in (A), (B), and (C) respectively. (D) Quantitative RT-PCR was applied to determine the *Dnmt1* transcript abundance, which were strongly reduced in *Hmx3-Cre/tdTomato/Dnmt1 loxP²* cells. *Dnmt1* expression was normalized to *Rps29* transcript level (WT n=12, KO n=6 brains, *p<0.05; Student's *t*-test). (E-G) Immunohistochemistry with an antibody directed against DNMT1 was performed in tissue sections of the cerebral cortex of wild-type (E) and *Dnmt1* deficient (F) adult mice (DAPI is shown in blue, DNMT1 in green and tdTomato in red). Open arrows point to DNMT1 negative tdTomato cells, filled arrows to DNMT1/tdTomato double positive cells (G) Quantification reveals a strongly decreased number of DNMT1 positive tdTomato cells in the cortex of *Dnmt1* deficient mice (n= 162 cells) compared to wild-type (n=681 cells; from three different brains per genotype; *p<0.05; Student's *t*-test). FSC, forward scatter; SSC, side scatter; Scale bars: 50 μ m in (E, F).

To functionally address the role of DNMT1 in postmitotic interneurons of the POA, a transgenic mouse model was generated, in which *Dnmt1* was conditionally deleted in *Hmx3*-expressing cells (*Hmx3-Cre/tdTomato/Dnmt1 loxP²* mice). The expression of *Hmx3* in the telencephalon is restricted to early postmitotic cells of the POA fated for residual cells of the POA as well as for cortical interneurons performing long-range

tangential migration to the neocortex (Gelman et al. 2009). First, efficient deletion of *Dnmt1* in the triple transgenic mice was confirmed at mRNA level. To this aim, embryonic *Hmx3-Cre/tdTomato/Dnmt1 loxP²* and wild-type cells were enriched by FACS (Fig. 21A-C) and the mRNA was isolated to measure *Dnmt1* transcript levels. As illustrated in Figure 21D, *Dnmt1* deletion led to a nearly complete reduction of *Dnmt1* expression in knockout compared to wild-type cells, as revealed by quantitative real-time PCR. Further, staining in tissue sections with an antibody directed against DMNT1 showed strongly reduced immunoreactivity in *Hmx3-Cre/tdTomato/Dnmt1*

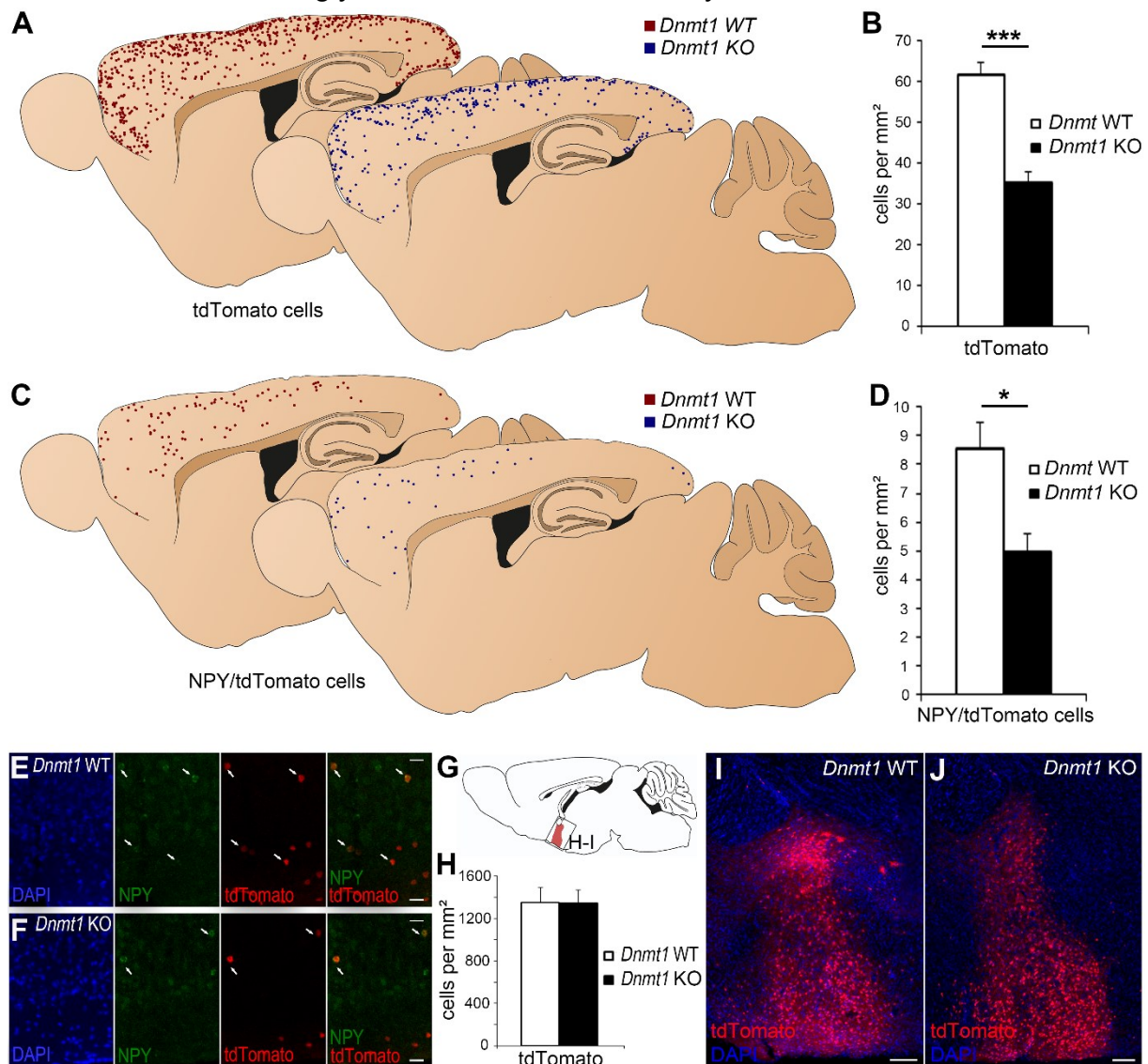


Figure 22 - *Dnmt1* deficiency in post-mitotic POA-derivates reduces cortical interneuron number. (A-D) Schemes depicting the distribution of tdTomato (A) and NPY-expressing tdTomato interneurons (C) in adult *Hmx3-Cre/tdTomato/Dnmt1* wild-type (red) and *Hmx3-Cre/tdTomato/Dnmt1 loxP²* mice (blue) at 6 months of age along the rostral-caudal level of the cerebral cortex (Bregma 1.44-1.68). (B, D) Quantification of the cell density of tdTomato (B; 10 sections for wild-type and 7 sections for knockout mice, of 3 brains per genotype; *** $p < 0.001$, Student's t-test) and NPY-expressing tdTomato interneurons (D; 7 sections of 3 brains per genotype; * $p < 0.05$, Student's t-test) over the whole cortex (Bregma 1.44-1.68). (E, F) Representative examples of NPY immunoreactivity of tdTomato interneurons in the cerebral cortex of *Hmx3-Cre/tdTomato/Dnmt1* wild-type and *Hmx3-Cre/tdTomato/Dnmt1 loxP²* mice (6 months). Filled arrows point to NPY/tdTomato double labeled cells, open arrows depict NPY-negative tdTomato cells. (G) Schematic illustration of the region of the pre optic area (POA; red) in a sagittal brain section adapted from Paxinos (2001) (Bregma 0.12-0.24), the square indicates the area magnified in (I, J). (G) Quantification of *Hmx3-Cre/tdTomato* cell density in the POA of *Dnmt1* wild-type and *Dnmt1 loxP²* mice did not reveal significant differences ($n=9$ sections for wild-type and $n=11$ sections for knockout mice; of 3 brains per genotype; 6 months of age; $p=0.97$, Student's t-test). POA region of wild-type (H) and knockout (I) used for analysis. Scale bars: 20 μm in (E, F), 200 μm in (H, I).

loxP² cells of the cerebral cortex, which in turn was evident in most wild-type cells (Fig. 21E-G).

The analysis of adult *Hmx3-Cre/tdTomato/Dnmt1 loxP²* mice showed a severe reduction of tdTomato positive cells of about 42% compared to *Hmx3-Cre/tdTomato/Dnmt1* wild-type. This loss of cells was detected over the entire anterior-posterior extension of the cerebral cortex (Bregma 1.44-1.68; Fig. 22A, B) including motor, somatosensory and visual cortical areas. As reported by Gelman et al. (2009), a large proportion of cortical fated cells of the *Hmx3*-lineage was identified as functionally homogenous GABAergic interneurons, of which some express NPY (Fig. 22E, F), while the remaining GABA-positive cells were not identified based on common interneuron subtype marker (Gelman et al. 2009). Quantifying the number of NPY-expressing tdTomato cells, a comparable proportional decrease in *Dnmt1* deficient

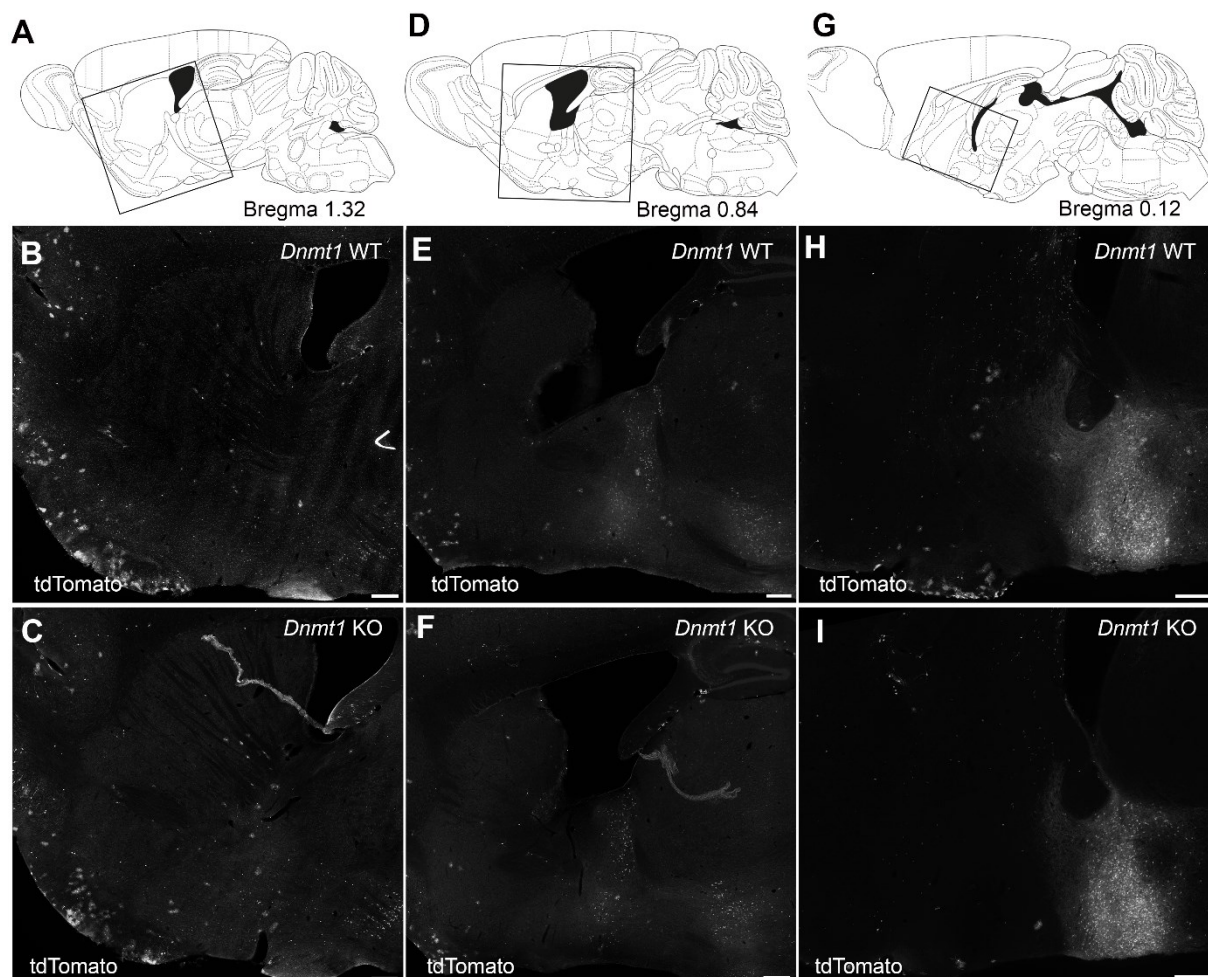


Figure 23 - Illustration of the tdTomato cells in different regions of the adult brains of *Hmx3-Cre/tdTomato/Dnmt1* wild-type and *Hmx3-Cre/tdTomato/Dnmt1 loxP²* mice. In sagittal brain sections of different Bregma no differences in the number of tdTomato cells were observed in the basal telencephalon between *Hmx3-Cre/tdTomato/Dnmt1 loxP²* and *Hmx3-Cre/tdTomato/Dnmt1* wild-type mice (6 months). The basal part of the telencephalon in sagittal sections of different lateral-medial level is depicted in (A-C) (Bregma 1.32), (D-F) (Bregma 0.84) and (G-I) (Bregma 0.12). Grey squares in the schemes shown in (C, F, I), which were modified according to Paxinos (2001), illustrate the location of the presented sections for *Hmx3-Cre/tdTomato/Dnmt1 loxP²* and *Hmx3-Cre/tdTomato/Dnmt1* wild-type mice. Scale bars: 250 μ m.

animals was revealed (Fig. 22C, D), suggesting a subtype independent reduction of cortical interneurons that derived from the *Hmx3*-lineage. In contrast to the cortical fated cells, the number of *Hmx3-Cre/tdTomato* cells populating the mantle zone of the POA was not altered by *Dnmt1* deletion (Bregma 0.12-0.36; Fig. 22G-J). Moreover, different bregmas of sagittal sections were screened to investigate if ectopic located cells were present at adult stages, which could explain the reduction in cortical cell number. But as illustrated exemplarily in Figure 23, no differences were observed between *Dnmt1* deficient and wild-type animals in the basal telencephalon.

Taken together, these data propose that postmitotic *Dnmt1* deletion during embryonic development diminished the number of POA-derived cortical interneurons reaching their target via long range-migration, while the density of residual POA-fated cells remain unchanged in adults. In accordance with the previous data, these results pointed to a role of DNMT1 in regulating aspects of cortical interneuron migration, which represents an important phase of interneuron development.

5.3.5 *Dnmt1*-deficiency led to a reduction of migrating cells during embryonic development

Hmx3 expression in the POA has been described from midgestation to late embryonic stages (Gelman et al. 2009) leading to *Dnmt1* knockdown in immature postmitotic POA-derived interneurons. As *Dnmt1* expression was observed in migrating interneurons, the next set of experiments aimed at investigating if migratory defects account for the decreased cell numbers observed in the adult cortex. For this, we focused our analysis at E16.5, when first cohorts of the *Hmx3/tdTomato* cells have reached the developing cortex and a large fraction of migrating cells could be observed within the basal telencephalon of wild-type animals (Fig. 24A, C, E). Consistent with the reduction of cortical *Dnmt1* deficient *Hmx3/tdTomato* cells at adult stages, the numbers of cells reaching the cortex at E16.5 was diminished from 128.01 ± 8.55 cell/mm² in wild-type animals to 45.67 ± 7.09 cell/mm² in *Dnmt1* knockout animals ($p < 0.001$; $n=10$ for wild-type; $n=8$ for *Dnmt1* knockout; Fig. 24G). This decrease of cells is consistent with already reduced numbers of migrating cells inside the basal telencephalon of E16.5 *Hmx3-Cre/tdTomato/Dnmt1 loxP²* mice compared to wild-type mice (Fig. 24B, D, F). To address this, *Hmx3/tdTomato* cells were analyzed in regard to their relative position to the POA. An accumulation of cells

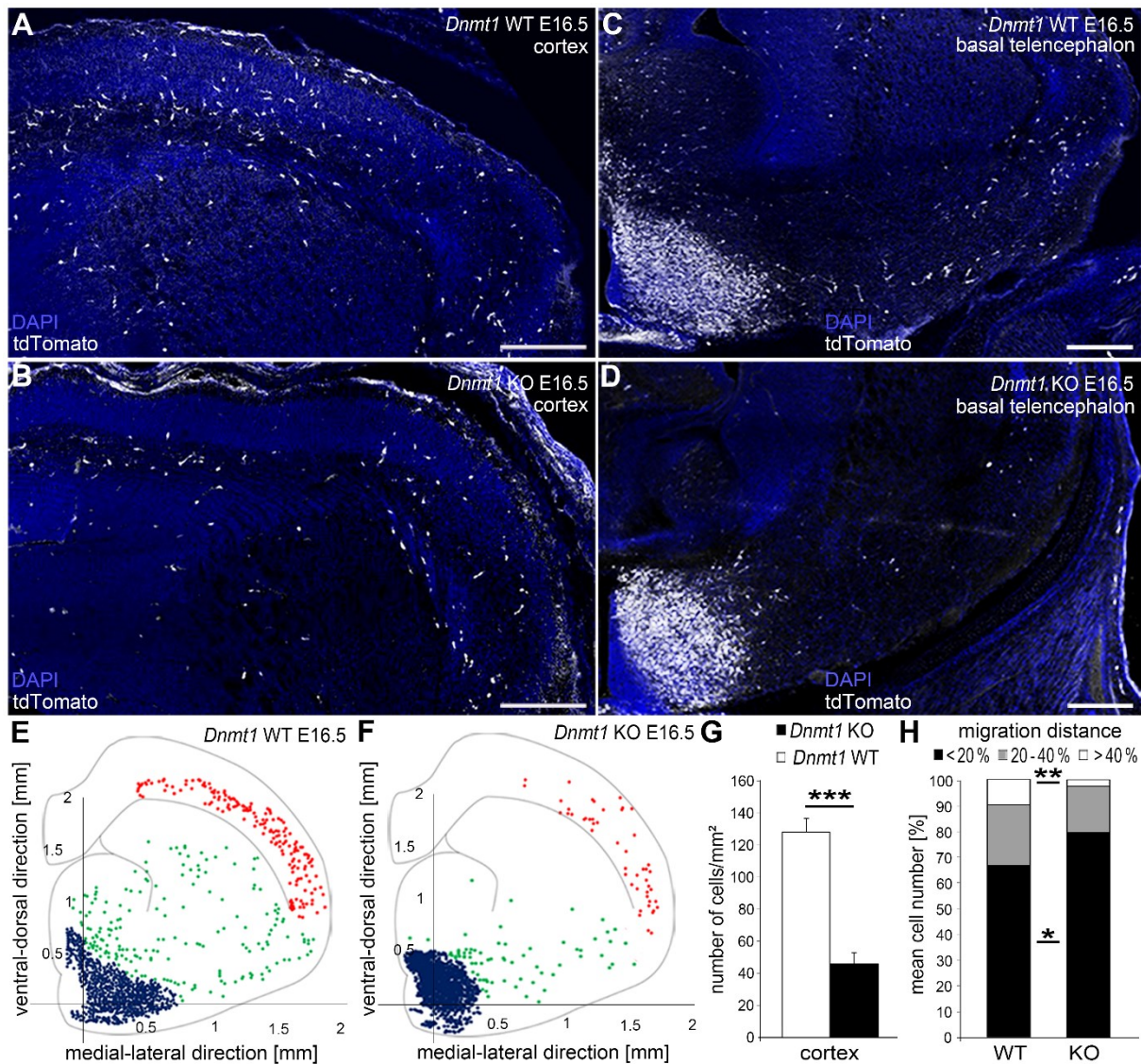


Figure 24 - Postmitotic *Dnmt1* deletion in POA-derived interneurons leads to migratory defects during embryonic development. (A-D) Representative magnified merged sections composed of DAPI (blue channel) and tdTomato (white channel) microphotographs of the cortex (A, B) and the basal telencephalon (C, D) of E16.5 *Hmx3-Cre/tdTomato/Dnmt1* wild-type and *Hmx3-Cre/tdTomato/Dnmt1* loxP2 embryos. (E, F) Location and number of *Dnmt1* wild-type (E) and *Dnmt1* knockout cells (F) are shown color-coded in the different compartments of coronally sectioned brain hemispheres (E16.5). Blue, green and red cells represent cells within the POA, in the basal telencephalon but outside of the POA and in the cortex, respectively. (G) Quantification of the cell density of cells in the cortex (n=10 for wild-type; n=8 for *Dnmt1* knockout). (H) For quantitative analysis of the migratory distances of tdTomato cells in the basal telencephalon, groups were defined as follows: cells with migration of less than 20%, between 20%–40% and more than 40% of the overall distance between the POA and the cortex (n=10 for wild-type; n=8 for *Dnmt1* knockat). "n" refers to the number of sections from three animals per genotype. *p<0.05; **p<0.01; ***p<0.001; Student's t-test. POA, pre optic area; Scale bars: 200 μ m in (A, B); 100 μ m in (C, D).

in close proximity to the POA was detected in E16.5 *Dnmt1* deficient animals compared to wild-type animals (Fig. 24H), indicating an impaired migration upon *Dnmt1* deletion.

Together with the results presented so far, these data, kindly provided by Judit Symmank, suggest that a major fraction of cortical-fated *Hmx3/tdTomato* failed to reach the cortex upon *Dnmt1* deletion, likely due to impaired migratory capabilities.

5.3.6 DNMT1 promotes migration by suppression of post-migratory processes

What could be the underlying mechanism by which DNMT1 promotes the migration of immature cortical interneurons? The results described so far propose a relevance of DNMT1 during cortical interneuron migration. As DNMT1 is involved in regulation of gene expression (Bestor 2000, Feng and Fan 2009, Baets et al. 2015), RNA-sequencing data of FAC-sorted E16.5 *Dnmt1* deficient and wild-type tdTomato cells dissected from E16.5 basal telencephalons were evaluated for differential gene expression followed by GO-enrichment analysis (Fig. 25A, B).

Interestingly, transcripts assigned to GO-terms related to neuronal maturation (like *synapse*, *axon ensheathment*, *regulation of action potential*, *transmission of nerve impulse*), cell adhesion (including *cell junction*, *biological adhesion*, *cell substrate adhesion*, *regulation of cell adhesion*) and cytoskeleton organization (like *actin cytoskeleton organization*, *actin filament-based process*, *morphogenesis of a branching structure*) were up-regulated in *Dnmt1* deficient cells (Fig. 25B). To perform proper migration, it is essential for cells to keep their migratory capabilities, making it necessary to prevent premature differentiation processes like neurite outgrowth and synapse formation. These results suggest a role of DNMT1 in suppression of maturation-associated processes, as DNMT1 regulates gene expression commonly by methylation leading to gene silencing (Feng and Fan 2009). In addition, genes associated to cell-death were also found to be enriched among the genes upregulated in *Dnmt1* knockout (Fig. 25C; *** cluster p-value = 0.0001952968; Fisher's exact test). As the adult phenotypic analysis did not reveal increased cell numbers in the POA or ectopic located cells within the basal telencephalon of *Hmx3-Cre/tdTomato/Dnmt1 loxP²* mice compared to wild-type mice (see chapter 5.3.4), the induction of apoptosis-related genes provided a possible mechanism for the loss of *Dnmt1* deficient cells. In contrast, genes associated with GO-terms referring to motility and neuronal migration were found enriched among the genes upregulated in wild-type cells (Fig. 25D; * cluster p-value = 0.03612473; Fisher's exact test). This is consistent with the fact that a larger fraction of migrating cells was observed in *Hmx3-Cre/tdTomato/Dnmt1 wt²* compared to *loxP²* mice (see chapter 5.3.5).

These sequencing results, analyzed by Anne Hahn, confirmed the phenotypical data showing impaired migration upon *Dnmt1* deletion, as genes relevant for migration are deriched in this population. Instead, expression of genes involved in post-migratory

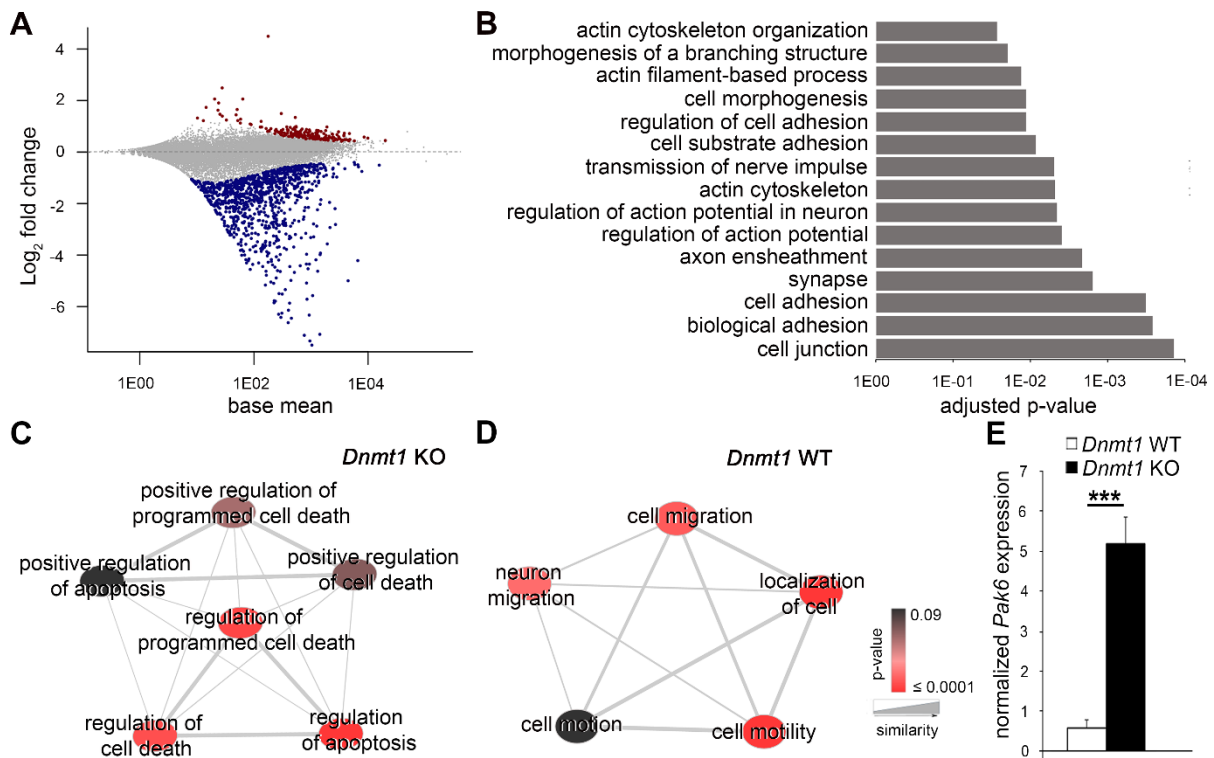


Figure 25 - *Dnmt1*-deficient *Hmx3-Cre/tdTomato* cells exhibit maturation specific gene expression. (A) MA plot illustrating the differentially expressed genes (red dots upregulated in wild-type; blue dots upregulated in *Dnmt1* knockout, adjusted p-value <0.05) obtained by RNA sequencing of FACS-enriched *Hmx3-Cre/tdTomato/Dnmt1* loxP² cells (n=10 brains) compared to *Hmx3-Cre/tdTomato/Dnmt1* wild-type cells (n=12 brains prepared from the basal telencephalon). (B) Gene ontology (GO) analysis of genes upregulated in *Hmx3-Cre/tdTomato/Dnmt1* loxP² samples revealed an enrichment of genes assigned to GO terms related to mature neuronal function, cell adhesion and cytoskeleton organization. Benjamini-Hochberg correction was applied to adjust the p-value. (C, D) GO analysis of transcripts differentially expressed in *Hmx3-Cre/tdTomato/Dnmt1* loxP² cells (adjusted p-value <0.05) revealed an enrichment of genes assigned to GO-terms related to cell death and apoptosis (B, cluster p-value = 0.0001952968). In contrast, differentially expressed genes in wild-type cells (adjusted p-value < 0.05) revealed an enrichment of genes assigned to GO-terms related to migration (A, cluster p-value = 0.03612473). (E) Quantitative RT-PCR of mRNA obtained from FACS-enriched tdTomato cells of E16.5 *Dnmt1* wild-type (n=12 brains) and knockout mice (n=6 brains) revealed a significantly elevated *Pak6* transcript abundance in *Hmx3-Cre/tdTomato/Dnmt1* loxP² samples (normalized to *Rps29* expression).

processes were found to be increased, providing evidence for a model, where DNMT1 suppresses the transcription of maturity associated genes in immature migrating cortical interneurons to preserve the migratory capability.

5.3.7 *Pak6* expression levels are elevated in *Dnmt1* deficient cells

According to the NGS results, genes associated to processes involved in rather later stages of maturation were enriched in *Dnmt1* deficient cells. In addition, genes of various GO-terms associated to cytoskeleton organization are up-regulated upon *Dnmt1* deletion. The morphologic changes during later stages of maturation involving neurite outgrowth, branching and synapse formation require major cytoskeleton reorganization (Boda et al. 2006, Kelsom and Lu 2013, Peyre et al. 2015). A gene already described in neurite formation (Zhao et al. 2011, Furnari et al. 2013) and shown to be important for a subpopulation of the *Hmx3*-lineage by single-cell transcriptomics (see 5.3.1.4) as well as based on siRNA in vitro studies (see 5.3.2) is

Pak6. In support of a direct or indirect regulation of *Pak6* by DNMT1, *Pak6* was found to negatively correlate with *Dnmt1* transcript levels with NanoString (see 5.3.2). To test for a regulatory link between *Pak6* expression and *Dnmt1*, quantitative real-time PCR with *Pak6* sequence-specific primers was performed with RNA prepared from the FACS enriched embryonic *Dnmt1* knockout and wild-type cells. Indeed, a 9-fold increase in *Pak6* expression in *Dnmt1* deficient cells was detected ($p > 0.001$; Student's t-Test; $n = 12$ for WT; $n = 6$ for KO; Fig. 25E), suggesting that Pak6 is suppressed directly or indirectly by *Dnmt1* in wild-type cells.

Altogether, based on the data of the single cell profiling carried out to find regulators of postmitotic determinates for processes like migration and maturation, it was possible to ascertain evidence for a model in which DNMT1 represses gene expression involved in post-migratory processes, thereby facilitating migration. In particular, DNMT1-mediated suppression of *Pak6* seems to be involved in maintaining the immature state and migratory shape of a distinct subtype of postmitotic POA-derived cortical interneurons as a prerequisite for long-range migration to the cerebral cortex. The differential gene expression analysis of purified *Hmx3-Cre/tdTomato/Dnmt1 loxP²* and wild-type cells reveal further genes potentially regulated by DNMT1 creating a comprehensive information resource for future research projects.

6 Discussion

6.1 Advantages and limitations of the single cell analysis strategy

Considering the enormous heterogeneity of excitatory and inhibitory neurons in the central nervous system, the necessity for single cell mRNA analysis to reveal the underlying transcriptional mechanism orchestrating the establishment of their structural and functional identity is obvious. This knowledge may provide valuable insights into the processes of neuronal development and causes of neurodevelopmental diseases. Single-cell analysis seems to be indispensable for a better understanding of cellular diversity, as even in seemingly homogeneous tissue gene expression has been described to be heterogeneous (Jaitin et al. 2014). As cell-fate decisions can be governed by stochastic transcriptome variations (Eldar and Elowitz 2010, Gitig 2010, Janes et al. 2010, Kellogg and Tay 2015), which will be masked when analyzing a pool of cells, single cell resolution is highly favorable. Several high-throughput approaches for global analysis of gene expression in single cells, such as microarray analysis and single cell RNA-sequencing (scRNA-seq) are available nowadays (Kolodziejczyk et al. 2015a, Liu and Trapnell 2016). However, most of the described protocols for single cell transcriptome analysis require exponential amplification to produce sufficient material for analysis, which has the disadvantage to induce shifts in representation or loss of low abundant transcripts, as transcripts of different sizes are amplified with variable efficiencies (Freeman et al. 1999, Baugh et al. 2001). To circumvent this issue, many approaches, including the protocol presented here, use the strategy of limited reverse transcription, to generate cDNAs homogenous in length. Previous studies apply microarray analysis, real time PCR or single cell RNA sequencing (scRNA-seq) as methods for evaluation (Dulac and Axel 1995, Klein et al. 2002, Chiang and Melton 2003, Tietjen et al. 2003, Kurimoto et al. 2006, Haag 2009). Here, the NanoString nCounter technology for quantification of representative amplification of single cell mRNA was used, applying an amplification protocol based on a strategy of Brady and Iscove (1993), which was modified to improve the bias-free amplification and to increase the maximum yield (Haag 2009). The applicability of this protocol was shown for a broad range of RNA concentrations (Fig. 9), which is relevant in regard to the fact that transcript abundances can vary strongly depending on cell volume and transcriptional state (Baserga 2007, Bengtsson et al. 2008, Eldar and Elowitz 2010, Marguerat and Bahler 2012, Padovan-Merhar et al. 2015). For copy numbers as low as ten representative rates of amplification were

obtained. Even low abundant transcript species with theoretical copy numbers down to one were robustly amplified with the applied protocol (Fig. 9C). However, for such transcripts, relatively high deviations between replicates were observed, which is likely caused by dilution errors considering a 1:22000 dilution of the original RNA. Interestingly, comparing transcript counts between scPCR1 and scPCR2 products, no shifts in transcript representation were observed (Fig. 10), suggesting that transcript length dependent changes in amplification efficiencies are rather unlikely to occur in the first round of amplification. Thereby, this comparison represented further indirect proof for the validity of the described amplification protocol, but did not allow conclusions on the mRNA capturing efficiency of the SR-T₂₄-primer used.

6.1.1 The relevance of low abundant transcript detection

The transcript copy numbers for individual mRNA species is dependent on their function and localization. Genes involved in maintenance of cellular processes like metabolism, mostly taking place inside the cell soma, have been shown to be present with copy numbers up to several thousand (Bengtsson et al. 2008, Zhu et al. 2008, White et al. 2011). In contrast, genes relevant for the regulatory machinery like transcription factors localized in the nucleus are often limited to some dozens of transcript copies (Zhong et al. 2008, Zhu et al. 2008). In general, around 85% of all transcripts in human cells are present with less than 100 copies (Bengtsson et al. 2008, Zhu et al. 2008, White et al. 2011). Keeping this in mind and considering the fact, that most of the single cell methods, especially for scRNA-seq, have a low mRNA capturing efficiency (Islam et al. 2014), leading to a transcriptome coverage of only 10-20% (Deng et al. 2014, Islam et al. 2014, Saliba et al. 2014), demonstrate the necessity of a highly sensitive single cell transcriptome analysis protocol capturing also the low abundant genes with high efficiency. In more detail, the protocol applied here outperformed the sensitivity reported for single cell RNA Sequencing (Islam et al. 2014, Liu and Trapnell 2016), detecting only about 50% of the genes with 4-5 copies and the multiplex RNA sequencing as described by Islam et al. (2011), reporting the loss of 61-71% of transcripts in the copy number range of 10. Consequently, in the study of Gerstmann et al. (2015) this enormous sensitivity led to the detection of *EfnA5* transcripts in thalamic fibers *in vitro*, which were not measurable with non-radioactive *in situ* hybridization.

6.1.2 Comparison to other single cell approaches

As NanoString enables quantitative expression analysis of several hundred different transcript species in large numbers of samples with relatively simple bioinformatics analysis (Geiss et al. 2008), it represents a suitable approach in combination with the amplification strategy presented here, to obtain statistically valid expression profiles for single cell analysis. NanoString already provides a commercially available single cell kit (NanoString Inc., U.S.A.), which amplifies up to 800 fragments of particular mRNA species. In contrast to this kit, an analysis of the same single cell library with multiple different NanoString codesets can be performed with the protocol presented here, due to the global mRNA reverse transcription and the high quantities, exceeding the possible overall readout of gene expression in comparison to the NanoString single cell kit. In addition, once distinct cell-types are identified based on NanoString analysis, representative cDNA libraries can be analyzed with scRNA-seq, as the amplification strategy presented here generates material in sufficient quantities. This strategy was applied for several embryonic POA-derived cells to obtain a comprehensive gene expression profile (Fig. 20A-C). As illustrated in Figure 20A-C the cell segregation based on the sequencing data was similar to the NanoString based analysis. This indicates that even limited gene profiles like the used NanoString codeset are suitable to obtain reliable cluster information.

Anyhow, it has to be mentioned, that for any NanoString based analysis the identity of analyzed genes has to be pre-defined, similar to all non-*de novo* approaches like microarray, RNA-FISH or qRT-PCR. For this, RNA sequencing of POA and MGE tissue was performed and based on this information a codeset for the validation experiments as well as for the interneuron profiling was generated. As tissue RNA of both domains and single cell equivalent dilutions as templates for amplification were used for the evaluation of the amplification protocol, the validation codeset includes high abundant expressed gene of both tissues. In addition, by differential gene expression analysis a pool of information for potentially relevant transcripts for interneuron lineage specification in these domains was obtained. Based on these data a profiling codeset was designed and further NanoString codesets can be generated to decode transcriptional programs aiming to address distinct issues like the initial determination of cell fate or the regulation of distinct aspects of migration including cytoskeleton remodeling or the expression profile of a distinct guidance receptor repertoire and their

downstream pathways. Due to the limited reverse transcription procedure, ensuring the highly representative amplification, the mean fragment size of the cDNA libraries is around 500 bp (see chapter 4.5.2.3). In comparison, a full length transcriptome consist of fragments ranching on average from 1.5-10 kb (Okayama and Berg 1982, Wellenreuther et al. 2004). To achieve quantitative results, the probes for the NanoString codeset have to be designed against regions close to the 3' end of the respective mRNA (Pensold 2012).

Yet, NanoString represents a good choice for analysis, as this simple and fast approach combines a sensitivity comparable to real-time PCR (Geiss et al. 2008), but without additional enzymatic reaction, with the possibility to test several mRNA species in parallel. Microarray analysis comes with the shortcoming of limited sensitivity, while for scRNA-seq additional amplification is required, like also for qRT-PCR. Moreover, the sample preparation procedures needed for scRNA-seq and Microarray analysis represent a potential source of additional errors and might lead to alterations in transcript representation. Nevertheless, sequencing approaches enables *de novo* detection of RNA species as well as analysis of differential splicing, but as the amplification protocol led to 3' limited cDNA libraries, this technical advantage is of diminished relevance as both issues require full length RNA for investigation (Shalek et al. 2013, Kolodziejczyk et al. 2015a). Single cell protocols focusing on full length RNA come at the expense of strongly reduced quantitative detection (Boutin et al. , Kolodziejczyk et al. 2015a, Liu and Trapnell 2016). A recent strategy to improve the quantitative nature of scRNA-seq in general, is to use unique molecular identifiers (UMIs) barcoding each individual mRNA molecule within a cell during reverse transcription (Hug and Schuler 2003, Fu et al. 2011). In consequence, sequenced reads arising from PCR-duplicated mRNA fragments will have the same random barcode sequence. The copy number of a particular mRNA species in a given cell lysate is hence equivalent to the number of UMIs associated with all reads that map to a transcript. One important consideration when using UMIs is that the sequencing needs a high saturation of the flow-cell in order to achieve reliable quantification of transcript abundances (Kolodziejczyk et al. 2015a). In addition, for low abundant transcript levels the transcriptome coverage of only 10-20% still limits the quantitative measurement (Kolodziejczyk et al. 2015a, Liu and Trapnell 2016).

6.1.3 Manual isolation – old fashioned or still required?

The presented approach for the extraction of single cell transcriptome includes the manual isolation of cells according to Hempel et al. (2007) including two washing steps prior to cell lysis. Although this procedure is quite labor intensive, it represents optimal conditions for a contamination free isolation and is therefore often the method of choice (Hempel et al. 2007, Tang et al. 2009, Grindberg et al. 2011, Xue et al. 2013, Yan et al. 2013). Several negative controls for potential genomic contamination as well as contamination with other cells or mRNAs of destroyed cellular material were included (see chapter 4.5.2.4). With alternative methods like FAC-sorting and Laser Capture Microdissection contaminations cannot be excluded to this extent (Fink et al. 1998, Mawrin et al. 2003, Hempel et al. 2007, Frumkin et al. 2008). While Laser Capture Microdissection comes with the risk of contamination by the surrounding tissue, isolation of duplets can never be completely excluded with FAC-sorting. Using FACS the number of single cells can be easily scaled up to hundreds of cells, provided the flow cytometrist and FACS instrument are able to consistently and accurately sort cells into the center of the well, thus ensuring that each cell is immersed in the lysis buffer (Kolodziejczyk et al. 2015a).

Another recent possibility is presented by the Fluidigm C1 microfluidic robotic platform, where cells are captured using integrated fluidic circuits, enabling analysis of up to 96 cells per chip (Kolodziejczyk et al. 2015a). An advantage compared to FACS is, that captured cells can subsequently be inspected under a microscope inside the chip prior to the automated cell lysis, reverse transcription and pre-amplification in nanoliter volumes. A major limitation of this method is that it only works for cells relatively homogeneous in size, since the capture sites are tuned to three size ranges (5–10, 10–17, and 17–25 microns in diameter). In general, the here applied amplification protocol should also be applicable to microfluidic platforms, which could drastically reduce the reagents cost and standardize the procedure, while increasing the throughput (Shalek et al. 2014, Trapnell et al. 2014, Treutlein et al. 2014). But the need of an expensive microfluidic robotic platform and the high costs for each chip have to be considered as well as the probable reduction in yield due to the downscaling of reaction volume. The latest innovations regarding single cell analysis, called dropseq, combines a novel strategy for contamination free isolation by collecting individual cells together with a distinct barcode in a lipid vesicle enabling multiplexing sequencing

(Macosko et al. 2015). With this innovative isolation procedure several thousands of cells can be isolated individually in a minimal volume, processed in a short time and subsequently sequenced. Nevertheless, the reduced transcriptome coverage of scRNA-seq is still a limitation of this approach (Kolodziejczyk et al. 2015a, Liu and Trapnell 2016).

In addition, all these high throughput isolation methods are not applicable when it comes to mRNA isolation of distinct cellular compartments like thalamic fibers as performed in this study (Fig. 12E-H). Here, manual isolation under visual control is still required to obtain satisfactory results.

6.2 EFNA5/EPHA4 interaction influence cortical projection neurogenesis

6.2.1 Eph-receptor/Ephrin-ligand interactions are involved in neuronal proliferation and differentiation

The applicability of single cell analysis is manifold. In the study of Gerstmann et al. (2015) the described single cell protocol was applied to reveal the source of *EfnA5* in cortical regions due to the high sensitivity of the method. Based on an *EfnA5* knockout mouse model an influence of this protein on cortical progenitor division has been revealed (Gerstmann et al. 2015). Eph-receptor/ephrin-ligand interactions have already been described to be important for regulation of proliferation and differentiation. (Qiu et al. 2008) showed that, *EFNB1* alters the division mode shifting the proportions to an increase of neurogenic division on the expense of proliferative division. In addition, *EFNB1* and *EFNB2* have been demonstrated to regulate the activity of the Par-protein complex (Lee et al. 2008, Lee and Daar 2009, Nakayama and Berger 2013), which is located at the apical process of the radial glia cells (Gotz and Huttner 2005), enhancing the formation of progenitors in general and especially for SVZ-located intermediate progenitors (Costa et al. 2010). Here, *EFNA5*-FC stimulation in the pair cell assay of mouse cortical progenitors led to an increase in proliferative division (Fig. 11A-D), which is consistent with the *EfnA5* knockout model revealing more postmitotic cells during early development (Gerstmann et al. 2015). In addition, the modified pair cell assay using thalamic explants as ephrin A-ligand source led also to a larger neurogenic output (Fig. 13A-D).

6.2.2 EPHA4 mediates the effect on progenitor division in *EfnA5* knockout mice

Different mechanism can be suggested for the EFNA5 mediated effect on progenitors leading to a cortical layer shift with expanded deep layers at the expense of the upper layers in the knockout mice (Gerstmann et al. 2015). As Eph/ephrin interaction required direct contact (Kania and Klein 2016) paracrine activation seemed first to be reasonable. Paracrine EPHB1-induced reverse signaling on *EfnB1* expressing cortical progenitors has already been reported to maintain their self-renewal (Qiu et al. 2008). Moreover, EPHA4 induced signaling by EFNB1 also stimulates the proliferation leading to an accumulation of neuronal progenitors (North et al. 2009). In the study of Gerstmann et al. (2015), EPHA4 has also been shown to be the interacting receptor for the EFNA5 mediated alterations in the cortical progenitor differentiation. In this context, the *Epha4* knockout mice reveal a similar phenotype regarding the cortical layer shift (Gerstmann 2014, Gerstmann et al. 2015) and consistently, *Epha4* mRNA was shown by single cell analysis in cortical progenitors as defined by *Pax6* and *Tbr1* expression (Fig. 11E, F; Englund et al. 2005). A direct interaction of both proteins had already been described by different groups (Davis et al. 1994, Zimmer et al. 2007, Stocker and Chenn 2009, Zhang et al. 2010, Rousso et al. 2012). In more detail, EFNA5/EPHA4 interaction in cortical neurons affects their motility *in vitro* by alterations of cell adhesion (Zimmer et al. 2007). In turn, cell adhesion is an essential requirement for proper regulation of proliferation and differentiation, as delamination of cells from the neuro epithelium lead to premature neurogenesis (Stocker and Chenn 2009, Zhang et al. 2010, Rousso et al. 2012).

6.2.3 *EfnA5* imported by thalamic fibers into the developing cortex has an impact on cortical progenitor division

A major issue was that cortical *EfnA5* expression could not be detected with different approaches (North et al. 2009, Deschamps et al. 2010, Gerstmann et al. 2015). But as the effects in the knockout mice suggest a function of EFNA5 in cortical development and at least small amounts of mRNA were observed with RT-PCR in cortical tissue (Gerstmann et al. 2015), a more sensitive approach was required. Based on single cell expression study, the hypothesis of a paracrine activation of the EPHA4 receptor by *EfnA5*-expressing cortical progenitors was eliminated, as no *EfnA5* expression was detected in individual cortical progenitors (Fig. 11E, F). As EPHA4 protein is also evident on the radial processes of the basal progenitors reaching from the ventricular

zone, where the cell somas are located up to the meninges, EFNA5 sources outside the proliferation zone have to be considered (Gerstmann et al. 2015). Factors secreted by the meninges have been shown to affect the proliferation and differentiation of radial glia cells (Gerstmann et al. 2015). Further, the neurotrophin NTF3 secreted by postmitotic neurons of the cortical plate is detected by progenitors in the ventricular zone thereby regulating the cell fate of radial glia cells (Seuntjens et al. 2009, Parthasarathy et al. 2014). Other studies have shown, that the apical process of the radial glia cells extended into the ventricle have the capability to perceive growth factors and other proliferative-favorable signals inside the liquor (Lehtinen and Walsh 2011, Tiberi et al. 2012). However, all postmitotic neurons tested were negative for *EfnA5* expression (Fig. 11G).

Interestingly, Gerstmann et al. (2015) provided evidence that the changes in proliferation occur upon EFNA5 stimulation somewhere along the radial processes, as EFNA5-FC coated beads placed inside the cortical plate, lead to a partial rescue of the *EfnA5* knockout phenotype. As neither progenitors nor postmitotic neurons expressed *EfnA5*, but a direct interaction of the membrane bound ligand and receptors are required and RT-PCR data reveal at least some *EfnA5* mRNA in the cortex (Gerstmann et al. 2015), we were taking extra-cortical source into account. Migrating glutamatergic neurons as well as GABAergic interneurons can influence cortical progenitor division (Haydar et al. 2000, Wang and Kriegstein 2009, Teissier et al. 2012). Since *EfnA5* is also expressed in the basal telencephalon and is involved in cell motility of interneurons, this could lead to an altered migration resulting in less interneurons, that reach the cortex. But according to Gerstmann (2014) the interneurons did not enter the dorsolateral cortex as early as E13.5, excluding them as possible *EfnA5* source at least at early stages. Interestingly, *EfnA5* expression is obvious in the thalamus during embryonic development and thalamocortical projections are described to reach the cortex already at E13.5 (Auladell et al. 2000, Gerstmann et al. 2015). Some decades ago, Gong and Shipley (1995) have already postulated that axonal afferences influence the cell cycle kinetics of olfactory bulb precursors. In addition, the thalamus has been reported to modulate the tangential expansion of the cortex in ferrets (Reillo et al. 2011). Also the proper arealisation of the cortex needs thalamic input (O'Leary 1989, Dehay et al. 1996). Gerstmann et al. (2015) have provided evidence that axonal projections of the *EfnA5* expressing thalamus reached the cortex at E13.5. Using the sensitive amplification protocol described here, it was possible to reveal *EfnA5* mRNA

in fibers of E13.5 cultivated thalamic explants (Fig. 12E-F). Together with the EPHA3-FC binding assay demonstrating ephrin A-ligand expression on these explants (Fig. 11A-D), this suggests that *EfnA5* is imported into the cortex by thalamic afferents. At the time point, when first thalamocortical projections reach the cortex, the early neurogenesis of cortical projection neurons populating the deeper layers V-VI takes place (Shatz and Luskin 1986, Auladell et al. 2000, Gerstmann et al. 2015). This timing correlates with the first observed alterations regarding the layer shift in the *EfnA5* knockout mice (Gerstmann et al. 2015). Uziel et al. (2002) showed that EFNA5 is involved in axon guidance of thalamic fibers projecting to limbic cortical areas. Thus, *EfnA5* knockout lead to formation of additional projections of some fibers to somatosensory areas, but did not have an impact on the general formation of thalamocortical projections. In addition, the formation of synapses in the cortical plate occurs during later developmental stages. Therefore, these effects seemed not causative for the here described changes in progenitor division. This is further suggested as Gerstmann et al. (2015) observe no differences in the time course of thalamic fibers reaching the cortex between *EfnA5* knockout and wild-type animals. Interestingly, Dehay et al. (2001) already show that diffusible factors secreted by thalamic fibers regulate cortical progenitor differentiation *in vitro*. To follow the idea that *EfnA5* expressing thalamic fibers regulate cortical progenitor division a pair cell assay with cultured thalamic explants was performed, showing increased proportions of NES/TUBB3 cell pairs, similar to what was observed in the EFNA5-FC stimulated pair cell assay (Fig. 13).

In conclusion, the results shown here propose an influence of invading thalamic axons on the balance of cortical progenitor division, thereby regulating cortical neurogenesis via EFNA5-EPHA4 interactions.

6.3 Exploring interneuron diversity and the factors driving their developmental maturation

GABAergic interneurons are essential for proper function of the cerebral cortex and already minor alterations in interneuron subtype composition or number can lead to severe dysfunctions and neuropsychiatric diseases, which are often developmental in their origin (Corbin and Butt 2011, Marin 2012). For this, revealing the mechanisms involved in interneuron generation, specification, migration and maturation as well as their integration into cortical circuits hold great promise to reveal the causes for

interneuron dysfunction and to develop therapy strategies (Marin 2012, Southwell et al. 2014). As the basal telencephalon is a highly complex tissue during embryonic stages contemporaneously producing various neuronal and non-neuronal cell types (Bulfone et al. 1993, Flames et al. 2007), single cell transcriptome analysis is required. This cellular heterogeneity is further increased as the transcriptome changes during postmitotic development to achieve maturational stage specific functions (Xue et al. 2013, Shalek et al. 2014, Skinner et al. 2016). Newborn cortical interneurons have to adopt a migratory morphology (Martini et al. 2009, Cooper 2013) that enables long-range tangential migration along particular routes through the basal telencephalon to the cortex (Corbin and Butt 2011, Marin 2013). This further complicates the investigation of distinct interneuron subtypes as migrating cells shift their expression profile along their route through to the cortex. Thereby, various membrane-bound and secreted molecules as well as cell type-specific receptor combinations orchestrate the directionality (Antypa et al. 2011, Zimmer et al. 2011, Andrews et al. 2013), while motogenic factors like EPHA4 and hepatocyte growth factor/scatter factor drive the migration of interneuron precursors (Levitt et al. 2004, Steinecke et al. 2014). Consistently, in the single cell profiling data *Epha4* expression was elevated in postmitotic MGE-derived cortical interneurons of cluster III (Fig. 16E). In addition to the well-documented significance of progenitor information (Nery et al. 2002, Valcanis and Tan 2003, Xu et al. 2004, Butt et al. 2005, Cobos et al. 2006, Flames et al. 2007), recent studies have underlined the importance of postmitotic regulatory instances for maturation, which exert control over initiation, motility, directionality and termination of interneuron migration (Cobos et al. 2006, Bortone and Polleux 2009, De Marco Garcia et al. 2011, McKinsey et al. 2013, van den Berghe et al. 2013, Harwell et al. 2015, Mayer et al. 2015). This is supported by clonal analyses, proposing that the migratory mechanisms related to the organization of interneurons within the cortex take place independent of their clonal origin to a large extent (Harwell et al. 2015, Mayer et al. 2015). Even region-specific migration can be altered at postmitotic stages (McKinsey et al. 2013, van den Berghe et al. 2013) and electrical activity influences the migration of cortical interneurons (Bortone and Polleux 2009, De Marco Garcia et al. 2011).

6.3.1 Principal component analysis results in biological reasonable cluster affiliations

Single-cell transcriptome analysis of cellular transitions between developmental states, like in the presented study during development and differentiation, can reveal new insights into regulatory mechanisms. The transitions during development can be binary or gradual, and can involve one or even multiple intermediate stages (Guo et al. 2010, Xue et al. 2013, Treutlein et al. 2014, Kolodziejczyk et al. 2015b, Skinner et al. 2016). Revealing the nature of such processes and intermediate stages can lead to the identification of genes that act as regulators.

Hence, the correct initial clustering of cells into groups on the basis of their gene expression pattern is an important challenge. To reveal distinct cell subtypes of the developing basal telencephalon and their gene expression profile, a combination of PCA followed by hierarchical clustering was used in this study. This state of the art approach has the advantage of an unsupervised clustering without any presuppositions (Lê et al. 2008). In contrast, methods like kmeans-clustering or bi-clustering, require additional information like the expected numbers of cluster or their center position as distinct expression profiles for at least some representative candidate genes of an expected cluster (Abbas 2008, Andreopoulos et al. 2009). Nevertheless, after some fittings of the parameters both methods provide comparable results to the PCA-based analysis in regard to the major cluster formation, but individual cells were shifted to neighboring cluster (data not shown). For density based clustering approaches like DBSCAN or OPTICS the data sets have to be larger to obtain reliable results (Ankerst et al. 1999, Abbas 2008, Andreopoulos et al. 2009). Moreover, a general problem of single cell methods is the high impact of technical noise leading to negative as well as in a smaller extend to positive false detection of transcript species, which complicates differential gene expression analysis (Kharchenko et al. 2014). For scRNA-seq data different analysis strategies have been developed fitting error models to the data, which make the detection of differential gene expression signatures more tolerant to noise (Kharchenko et al. 2014). Such error models require large data sets to work properly, for which they were not suitable to analyze the NanoString data, resulting in quite stringent differential gene expression pattern in this study. For analysis of the data presented here, the PCA-based gene expression clustering approach seemed to represent a valid strategy to discriminate different neuronal subtypes in a correct biological context, as most of the cells were

correctly segregated according to their source of preparation including the differentiation between MGE and POA as well as the integration of cells isolated from the POA-derived postmitotic *Hmx3*-Cre lineage (Fig. 14).

Once subpopulations are segregated by distinct gene expression profiles, they can be further characterized and matched to known cell types by differential expression analysis and correlation analysis. The most common approach is to validate the identity of clusters by examining the expression of known marker genes of a given population (Jaitin et al. 2014, Pollen et al. 2014, Shalek et al. 2014, Treutlein et al. 2014, Zeisel et al. 2015). Here, mostly the MGE-derived cells were used for validation of correct clustering as only limited information is available for POA-derived subpopulations. For the MGE, the mechanisms of interneuron generation and differentiation are already explored to some extent and according to this knowledge, it was possible to discriminate between apical progenitors of the MGE in cluster I, intermediate MGE progenitors in cluster II and postmitotic MGE-derived interneurons in cluster III (Fig. 16). It has to be mentioned, that also POA precursors integrate into cluster I due to the fact, that the codeset was focused on postmitotic gene expression and hence unsuitable to discriminate these precursor fractions in more detail. Interestingly, for these three clusters it is particularly evident that quantitative analysis is highly relevant for cluster formation, as genes like *Tcf4*, *Abrac1* and *Glcc1* reveal cluster specific expression levels. The assignment of these clusters is consistent with the observed *in situ* hybridization pattern showing strongest expression in the SVZ being mainly populated by intermediate progenitors, which are collected in cluster II (Fig. 16; Englund et al. 2005). Lower expression levels were observed in the VZ and IMZ of the MGE, which are represented in cluster I and III as apical progenitors and postmitotic interneurons, respectively (Fig. 16; Englund et al. 2005). These differences in expression levels are suggested to represent intrinsic variations caused by burst-like stochastic activation of transcription (Chubb et al. 2006) and have already been reported for various genes. *ActB* mRNA contents fluctuate more than three orders of magnitude between pancreatic islets cells (Bengtsson et al. 2008). Similar data have been provided for many other transcripts including RNA polymerase II (Raj et al. 2006), human GAPDH (Warren et al. 2006, Lagunavicius et al. 2009), and TBP, B2M, SDHA, and EEF1G mRNAs (Taniguchi et al. 2009). To account for these stochastic gene expression events, which are also evident for commonly used housekeeping genes like *ActB* and *Gapdh* in single cells (Barber et al. 2005, Warren et al. 2006, Muramoto

et al. 2012), the NanoString data were not normalized to expression of individual genes. Indeed, for *Gapdh* quite strong fluctuations were found between the different clusters (data not shown). However, for test purposes data were normalized to *ActB* and/or *Gapdh* resulting in disturbed cluster affiliation according to the origin of cells (data not shown).

With a similar strategy including PCA-based hierarchical clustering, Pollen et al. (2014) have identified mitotic markers of radial glia from neuronal scRNA-seq data, which enable staging of radial glia according to their cell-cycle progression. Moreover, even cellular developmental stages can be studied by separating cell states using PCA followed by hierarchical clustering. Based on the relative proximity of the cluster it is subsequently possible to conclude temporal relationships between them. In this way, Deng et al. (2014) analyzed cells from different stages of embryonic development from zygote to the late blastocyst showing that the transcriptome composition of cells gradually changes along the developmental time course. Heterogeneity in gene expression levels across cells suggest the existence of new underlying subpopulations and provide insights into gene function (Shalek et al. 2014). In a homogeneous cell population, heterogeneity in gene expression will likely arise from stochastic gene expression as well as nonsynchronous cellular processes such as the cell cycle or circadian rhythm (Raj et al. 2006, Zopf et al. 2013, Buettner et al. 2015). Furthermore, it has already been described that these stochastic variations in transcriptomes are relevant for cell-fate decisions (Eldar and Elowitz 2010). Even stochastic single molecule events lead to changes of bacteria phenotype (Choi et al. 2008, Taniguchi et al. 2010). For cortical projection neurons it has already been reported, that expression levels of genes are specific for distinct subtypes (Arlotta et al. 2005).

Interestingly, several studies described a concept of transcriptional burst like expression, resulting in short term boost of transcript levels, which degrade over time (Chubb et al. 2006, Muramoto et al. 2012). According to Muramoto et al. (2012) most genes display their own transcriptional signature, differing in probability of firing and pulse duration, frequency, and intensity. This fits to our observation that despite the fact of different transcript level in distinct cluster, there also exist variability within distinct cluster supporting a model of dynamic gene expression resulting from burst like transcriptional events.

Based on the provided data it was also possible to ascertain distinct cluster for cells isolated from the POA domain. Cluster IV cells are defined as pallial excitatory neurons

invading the pre optic area, whereas postmitotic POA-derived cells including most of the *Hmx3*-lineage form cluster V and cluster VI is composed of striatal-fated neurons generated in the POA. Interestingly, we observed co-expression of *Isl1* and the GABA-synthesizing enzymes *Gad65* and *Gad67*. At adult stages *Isl1* expression is limited to cholinergic striatal interneurons (Elshatory and Gan 2008), but it has been reported that almost all striatal fated non-cholinergic interneurons express *Isl1* during development (Wang and Liu 2001). Thus, even there is no obvious literature describing co-expression of *Isl1* and *Gad65/67* it seems to be reasonable to expect co-expression of both mRNAs, as 90% of all adult striatal neurons consists of GABAergic projection neurons (Wang and Liu 2001).

6.3.2 Epigenetic regulation of cell migration by DNMT1

While miRNA-mediated epigenetic regulation of post-mitotic interneuron development has recently been reported (Tuncdemir et al. 2015), the impact of DNA methylation performed by DNMTs remains unknown. In this context, the here provided single cell data revealed *Dnmt1* expression in a subset of postmitotic POA-derived interneurons, in addition to its expression in progenitors (Fig. 14 and Fig. 19D-F). This was further supported by DNMT1 immunostaining at embryonic stages showing co-expression with calbindin, a marker for migrating cortical interneurons (Fig. 20F-H). DNMT1 has already been reported to promote migration in cancer cells by hypermethylation of tumor metastasis suppressors like BRMS1, the long non-coding RNA ADAMTS9-AS2 or the microRNA miR-124 (Zeng et al. 2012, Yao et al. 2014, Xing et al. 2015). Moreover, Estève et al. (2006) currently showed a DNMT1-dependent regulation of a variety of genes involved in cell migration, mobility, proliferation and focal adhesion in NHI3T3 cells by RNA-seq. Interestingly, the conditional knockout of *Dnmt1* in POA-derived *Hmx3*-Cre expressing cells led to a selective reduction of cortical interneurons, whereas the number of cells remaining in the POA was not altered (Fig. 22). The reduction of cells reaching the cortex was already evident at embryonic stages (Fig. 24), and together with the accumulation of cells at E16.5 in the pre optic area, this suggested a developmental migration defect. The possibility of a change in cell fate could mostly be excluded as no ectopic located cells were observed in other brain regions (Fig. 23). Moreover, staining against parvalbumin, calbindin, calretinin, somatostatin and VIP, which are the most common interneuron markers of distinct

subtypes revealed no colocalisation with tdTomato cells, neither in wild-types nor in the *Dnmt1* knockout strain (data not shown; Gelman et al. 2009).

During migration, immature interneurons display a characteristic bipolar morphology with a highly motile leading process and a rather short trailing process (Martini et al. 2009, Cooper 2013). This typical migratory shape, which is clearly different to the highly branched morphology of differentiating neurons as well as to dividing progenitors (Peyre et al. 2015), has to be sustained until the interneurons reach their final destination. Live-cell imaging experiments performed in our group, had revealed disturbance in the migratory morphology of *Hmx3/tdTomato/Dnmt1 loxP²* animals in comparison to wild-type animals, leading to increased branching frequencies of cells and a significant reduction in movement (data not shown). In agreement with this, loss of function of *Dnmt1* has already been associated with abnormal dendritic arborization and morphology in cortical projection and retinal neurons (Hutnick et al. 2009, Rhee et al. 2012). So far, this information suggests, that DNMT1 is involved in the maintenance of the polarized migratory morphology of POA-derived cortical interneurons, enabling long-range migration to the cerebral cortex. According to the differential gene expression data of FACS-enriched *Dnmt1* deficient and wild-type cells, this seemed to be achieved by suppression of genes involved in late maturation associated processes like *synapse*, *regulation of axon potential* or *morphogenesis of a branching structure*, in addition to the regulation of cytoskeleton-associated gene expression (Fig. 25B).

The loss of cortical interneurons seemed to result from reduced survival of the postmitotic *Dnmt1* deficient cells during their migratory period. Consistent with the increased gene expression associated to apoptosis in the FACS-enriched *Dnmt1* deficient cells (Fig. 25C), we also observed elevated numbers of TUNEL-positive tdTomato cells in the *Hmx3/tdTomato/DNMT1 loxP²* compared to wild-type animals (data not shown), indicating an elimination of the ectopically and precociously matured *Dnmt1* deficient interneurons during the developmental time course. In addition, live cell imaging revealed massive fragmentation of *Dnmt1* knockout cells due to their migrational defects, likely resulting in cell death (data not shown). Similar consequences have been observed in cortical projection and retinal neuron, where *Dnmt1* loss also leads to increase in cell death (Hutnick et al. 2009, Rhee et al. 2012).

6.3.3 DNMT1 regulates gene expression of maturational processes like neurite outgrowth, which is promoted by PAK6

The RNA sequencing data of FACS enriched *Dnmt1* deficient and wild-type cells indicated a role of DNMT1 in regulation of post-migratory maturation processes (Fig. 25B). Interestingly, post-mitotic POA cells of Cluster V were characterized by significant expression of *Pak6* (Fig. 18A, B), which has been shown to promote neurite outgrowth and neurite complexity of cortical projection neurons (Civiero et al. 2015). Further, according to the single cell profiling presented here, *Pak6* and *Dnmt1* are expressed in different neuronal subsets of post-mitotic POA cells (Fig. 19D-F). *Dnmt1* seemed predominantly present in migrating cells, as *Dnmt1* expression correlates with motility associated genes (Fig. 20D), and as *Dnmt1* deletion selectively affects migratory active cortical interneurons (Fig. 22 and 24). PAK6 in turn facilitated neuritogenesis, appearing rather relevant for the maturation of post-migratory cells (Fig. 19A-C). As we selectively prepared cells of the POA domain, the *Pak6*-positive and *Dnmt1*-negative cells revealed by single cell profiling could represent post-migratory residual neurons populating the POA, already enrolled in the process of neuritogenesis. This is consistent with the observation that a large fraction of cells populates the region of the POA at adult stages (Fig. 22G-J).

PAK6 belongs to the family of p21-activated kinases (PAKs), common effector proteins for the Rho GTPases Rac and Cdc42, which play an important role in cytoskeletal organization affecting cell shape, motility and adhesion (Rane and Minden 2014). Thereby, PAKs act primarily through the regulation of polymerized actin structures, and further control microtubule organization. The group B PAKs, which consist of PAK4, PAK5 and PAK6, have a major role in filopodia formation in response to CDC42 (Abo et al. 1998). Activated PAK5 induces filopodia and neurite-like processes in neuroblastoma cells (Dan et al. 2002). Moreover, cultured cortical neurons from *Pak5/Pak6* double knockout mice, which display significant learning and memory deficits, showed a reduction in neurite outgrowth (Nekrasova et al. 2008, Furnari et al. 2013). This supports the presented data, suggesting a role of PAK6 in promoting neurite outgrowth and branching (Fig. 19A-C).

Increased *Pak6* level in *Dnmt1* deficient cells (Fig. 25E) as well as the divergent expression of *Pak6* and *Dnmt1* at single cell level (Fig. 19D-F), pointed to a repression of *Pak6* by DNMT1 in migratory active cortical interneurons of the POA, to prevent

premature maturation and to maintain the migratory shape. This is reminiscent to what was reported by Cobos et al. (2007), showing that *Dlx1,2* facilitates the tangential migration of MGE-derived cortical interneurons through negative regulation of neurite outgrowth by repressing *Pak3*, which in turn promotes neuritogenesis. Interestingly, intrinsic expression level of *Pak3* was found elevated in cortical interneurons once they reached the cortex and start to establish dendritic and axonal arborizations (Cobos et al. 2007). In agreement with Cobos et al. (2007), in this study decreased neurite numbers of POA-derived neurons upon *Pak6* down regulation were identified (Fig. 19A-C). This proposed a comparable role of PAK6 in branch formation and/or maintenance. In support of this, forced expression of *Pak6* in COS-7 cells caused the formation of strongly branched filopodia (Fig. 6).

Overall, based on the single cell data it was possible to characterize distinct neuronal subpopulations and to reveal a DNMT1-dependent regulation of maturational processes in certain subsets of POA-derived postmitotic interneurons, in addition to its known role in dividing progenitors. Further, the results suggested that DNMT1 especially regulates expression of cytoskeleton-associated genes involved in processes like branching of neurites. In support of this, we observed drastic increase in the expression level of *Pak6* in FACS-enriched *Dnmt1* deficient cells, which was shown to promote neurite outgrowth, a process of post-migratory maturational stages. Hence, these data could further be relevant in a disease-related context as DNMT1-dependent alterations have already been proposed to cause cortical interneuron dysfunction in patients with neuropsychiatric diseases (Benes 2015, Dong et al. 2015).

6.4 Conclusion and further perspectives

In this thesis a highly quantitative single cell transcriptome analysis approach was successfully validated in regard to the preservation of original transcript abundancies and the determination of detection limits. Subsequently, this method was applied to investigate two distinct neurodevelopmental issues. In regard to detection limits, the presented method seems to be highly favorable in comparison to most published NGS single cell transcriptome analysis protocols reporting a low mRNA capturing efficiency (Islam et al. 2014), leading to a transcriptome coverage of only 10-20% (Deng et al. 2014, Islam et al. 2014, Saliba et al. 2014). This is especially relevant for investigation of transcription factor expression, which have often far less than 100 transcript copies per cell (Zhong et al. 2008, Zhu et al. 2008). To improve normalization and enable a direct correlation to original transcript copy numbers it would be beneficial to include spike-in RNA's as already proposed by different other protocols (Kolodziejczyk et al. 2015a, Liu and Trapnell 2016). Due to the fact that the NanoString technology used for detection already comprise several spike-in RNA's this was not feasible in the scope of this project, but should be addressed in future. Also a parallelization of the whole amplification procedure should be anticipated to increase the throughput of the method. For this, it would be possible to automate the process by using pipetting robots including PCR capabilities or to transfer the protocol to a microfluidic chip-based platform (Zhong et al. 2008, White et al. 2011). Beside the economy of time this would also improve the accuracy of the method by reducing pipetting errors and minimizing handling time, which are highly relevant.

In the issue of *EfnA5* function during cortical projection neuron development the method was used to qualitatively detect *EfnA5* transcripts in thalamic axons and the expression of the corresponding *EphA4* receptor in cortical progenitors. With this high resolution gene expression data, it was possible to gradually narrow down the source of *EfnA5* inside the cortex, which was not possible with standard detection methods (Gerstmann et al. 2015). As the source of *EfnA5* and the consequences of knockdown for cortical progenitors are now described, it would be interesting to study the molecular mechanisms leading to the observed phenotype in *EfnA5* deficient animals. Several downstream components of Eph-receptor signaling have already been described (Kullander and Klein 2002, Pitulescu and Adams 2010). In this context, the downstream signaling pathways of *EPHA4* could be examined using a NanoString

codeset to reveal the molecular mechanisms behind the observed changes in progenitor division mode. Further the presented data (Fig. 11E-G) suggest a maturational stage and subtype specific expression pattern, as all radial glia cells show expression of *EphA4*, but only about half of the tested intermediate progenitors and postmitotic neurons do. Hence, in parallel it would be interesting to investigate the expression level of *EphA4* in combination with subtype specific markers in a quantitative manner, to check for distinct expression levels in the different populations. During postmitotic development *EPHA4* function is different from progenitors, as it was already shown that the Eph-receptor/ephrin-ligand system is involved in axonal pathfinding and dendritic organization (Egea and Klein 2007, Guellmar et al. 2009). Thus, applying a comprehensive signaling codeset also to *EphA4* expressing postmitotic neurons could reveal maturational stage specific differences in *EphA4* downstream signaling.

In the second field of application, the single cell transcriptomics embody the basis information to reveal maturation specific function of DNMT1 in controlling the expression of late maturation specific gene expression. In this context, the expression of *Pak6*, a gene which is highly expressed in the residual fraction of the POA-derived *Hmx3*-lineage seems to be regulated by DNMT1. But if DNMT1 affects *Pak6* expression directly or indirectly, and if DNMT1 additionally positively acts on targets that promote the migratory state of cortical interneurons is beyond the scope of this study and will be addressed in ongoing experiments. The ways of action of DNMTs are manifold and require detailed and comprehensive analysis. First, DNA-methylation is not restricted to promotor regions, but also occurs at intragenic sites (Sharma et al. 2016). While DNA-methylation was traditionally associated with transcriptional repression, proximal promotor methylation also occurs in transcribed genes during neurogenesis (Wu et al. 2010). Moreover, DNMTs regulate gene expression independent of their methyltransferase activity by recruiting adaptor complexes, which in turn silence or activate transcription, further increasing the spectrum of effects (Hung et al. 1999, Robertson et al. 2000, Robertson 2002). More recently, DNMT1 function was also associated to histone modification, which were described to potentially activate or inactivate gene expression dependent on the side of modification (Hashimoto et al. 2010, Noguchi et al. 2016). To address distinct DNMT1 function on gene expression cell culture experiments with inhibitors for particular DNMT1 abilities are conceivable (Asgatay et al. 2014).

7 References

- Abbas OA. 2008. Comparisons Between Data Clustering Algorithms. *Int Arab J Inf Technol*, 5 (3):320-325.
- Abo A, Qu J, Cammarano MS, Dan C, Fritsch A, Baud V, Belisle B, Minden A. 1998. PAK4, a novel effector for Cdc42Hs, is implicated in the reorganization of the actin cytoskeleton and in the formation of filopodia. *Embo j*, 17 (22):6527-6540.
- Aboitiz F, Montiel J, Garcia RR. 2005. Ancestry of the mammalian preplate and its derivatives: evolutionary relicts or embryonic adaptations? *Rev Neurosci*, 16 (4):359-376.
- Adefuin AM, Kimura A, Noguchi H, Nakashima K, Namihira M. 2014. Epigenetic mechanisms regulating differentiation of neural stem/precursor cells. *Epigenomics*, 6 (6):637-649.
- Alifragis P, Liapi A, Parnavelas JG. 2004. Lhx6 regulates the migration of cortical interneurons from the ventral telencephalon but does not specify their GABA phenotype. *J Neurosci*, 24 (24):5643-5648.
- Anders S, Pyl PT, Huber W. 2015. HTSeq--a Python framework to work with high-throughput sequencing data. *Bioinformatics*, 31 (2):166-169.
- Anderson RB, Walz A, Holt CE, Key B. 1998. Chondroitin sulfates modulate axon guidance in embryonic *Xenopus* brain. *Dev Biol*, 202 (2):235-243.
- Anderson SA, Marin O, Horn C, Jennings K, Rubenstein JL. 2001. Distinct cortical migrations from the medial and lateral ganglionic eminences. *Development*, 128 (3):353-363.
- Andreopoulos B, An A, Wang X, Schroeder M. 2009. A roadmap of clustering algorithms: finding a match for a biomedical application. *Brief Bioinform*, 10 (3):297-314.
- Andrews WD, Zito A, Memi F, Jones G, Tamamaki N, Parnavelas JG. 2013. Limk2 mediates semaphorin signalling in cortical interneurons migrating through the subpallium. *Biol Open*, 2 (3):277-282.
- Angevine JB, Jr., Sidman RL. 1961. Autoradiographic study of cell migration during histogenesis of cerebral cortex in the mouse. *Nature*, 192:766-768.
- Hrsg. 1999. OPTICS: ordering points to identify the clustering structure. *ACM Sigmod Record*. ACM.
- Antypa M, Faux C, Eichele G, Parnavelas JG, Andrews WD. 2011. Differential gene expression in migratory streams of cortical interneurons. *Eur J Neurosci*, 34 (10):1584-1594.
- Arlotta P, Molyneaux BJ, Chen J, Inoue J, Kominami R, Macklis JD. 2005. Neuronal subtype-specific genes that control corticospinal motor neuron development in vivo. *Neuron*, 45 (2):207-221.
- Arshad A, Vose LR, Vinukonda G, Hu F, Yoshikawa K, Csiszar A, Brumberg JC, Ballabh P. 2016. Extended Production of Cortical Interneurons into the Third Trimester of Human Gestation. *Cereb Cortex*, 26 (5):2242-2256.
- Asgatay S, Champion C, Marloie G, Drujon T, Senamaud-Beaufort C, Ceccaldi A, Erdmann A, Rajavelu A, Schambel P, Jeltsch A, Lequin O, Karoyan P, Arimondo PB, Guianvarc'h D. 2014. Synthesis and evaluation of analogues of N-phthaloyl-L-tryptophan (RG108) as inhibitors of DNA methyltransferase 1. *J Med Chem*, 57 (2):421-434.
- Auladell C, Perez-Sust P, Super H, Soriano E. 2000. The early development of thalamocortical and corticothalamic projections in the mouse. *Anat Embryol (Berl)*, 201 (3):169-179.
- Azim E, Jabaudon D, Fame RM, Macklis JD. 2009. SOX6 controls dorsal progenitor identity and interneuron diversity during neocortical development. *Nat Neurosci*, 12 (10):1238-1247.
- Azuara V, Perry P, Sauer S, Spivakov M, Jorgensen HF, John RM, Gouti M, Casanova M, Warnes G, Merkenschlager M, Fisher AG. 2006. Chromatin signatures of pluripotent cell lines. *Nat Cell Biol*, 8 (5):532-538.
- Baets J, Duan X, Wu Y, Smith G, Seeley WW, Mademan I, McGrath NM, Beadell NC, Khoury J, Botuyan MV, Mer G, Worrell GA, Hojo K, DeLeon J, Laura M, Liu YT, Senderek J, Weis J, Van den Bergh P, Merrill SL, Reilly MM, Houlden H, Grossman M, Scherer SS, De Jonghe P, Dyck PJ, Klein CJ. 2015. Defects of mutant DNMT1 are linked to a spectrum of neurological disorders. *Brain*, 138 (Pt 4):845-861.
- Barber RD, Harmer DW, Coleman RA, Clark BJ. 2005. GAPDH as a housekeeping gene: analysis of GAPDH mRNA expression in a panel of 72 human tissues. *Physiol Genomics*, 21 (3):389-395.

- Baserga R. 2007. Is cell size important? *Cell Cycle*, 6 (7):814-816.
- Batista-Brito R, Rossignol E, Hjerling-Leffler J, Denaxa M, Wegner M, Lefebvre V, Pachnis V, Fishell G. 2009. The cell-intrinsic requirement of Sox6 for cortical interneuron development. *Neuron*, 63 (4):466-481.
- Baugh LR, Hill AA, Brown EL, Hunter CP. 2001. Quantitative analysis of mRNA amplification by in vitro transcription. *Nucleic Acids Res*, 29 (5):E29.
- Benes FM. 2015. The GABA system in schizophrenia: cells, molecules and microcircuitry. *Schizophr Res*, 167 (1-3):1-3.
- Benes FM, Berretta S. 2001. GABAergic interneurons: implications for understanding schizophrenia and bipolar disorder. *Neuropsychopharmacology*, 25 (1):1-27.
- Bengtsson M, Hemberg M, Rorsman P, Stahlberg A. 2008. Quantification of mRNA in single cells and modelling of RT-qPCR induced noise. *Bmc Molecular Biology*, 9.
- Bernstein BE, Mikkelsen TS, Xie X, Kamal M, Huebert DJ, Cuff J, Fry B, Meissner A, Wernig M, Plath K, Jaenisch R, Wagschal A, Feil R, Schreiber SL, Lander ES. 2006. A bivalent chromatin structure marks key developmental genes in embryonic stem cells. *Cell*, 125 (2):315-326.
- Bestor TH. 2000. The DNA methyltransferases of mammals. *Hum Mol Genet*, 9 (16):2395-2402.
- Boda B, Nikonenko I, Alberi S, Muller D. 2006. Central nervous system functions of PAK protein family: from spine morphogenesis to mental retardation. *Mol Neurobiol*, 34 (1):67-80.
- Boda B, Alberi S, Nikonenko I, Node-Langlois R, Jourdain P, Moosmayer M, Parisi-Jourdain L, Muller D. 2004. The mental retardation protein PAK3 contributes to synapse formation and plasticity in hippocampus. *J Neurosci*, 24 (48):10816-10825.
- Bohlen, Halbach. 2007. Immunohistological markers for staging neurogenesis in adult hippocampus. *Cell and tissue research*, 329 (3):409-420.
- Boitard M, Bocchi R, Egervari K, Petrenko V, Viale B, Gremaud S, Zraggen E, Salmon P, Kiss JZ. 2015. Wnt signaling regulates multipolar-to-bipolar transition of migrating neurons in the cerebral cortex. *Cell Rep*, 10 (8):1349-1361.
- Bokoch GM. 2003. Biology of the p21-activated kinases. *Annu Rev Biochem*, 72:743-781.
- Bolz J, Castellani V. 1997. How do wiring molecules specify cortical connections? *Cell Tissue Res*, 290 (2):307-314.
- Bolz J, Uziel D, Muhlfriedel S, Gullmar A, Peuckert C, Zarbalis K, Wurst W, Torii M, Levitt P. 2004. Multiple roles of ephrins during the formation of thalamocortical projections: maps and more. *J Neurobiol*, 59 (1):82-94.
- Book KJ, Morest DK. 1990. Migration of neuroblasts by perikaryal translocation: role of cellular elongation and axonal outgrowth in the acoustic nuclei of the chick embryo medulla. *J Comp Neurol*, 297 (1):55-76.
- Bortone D, Polleux F. 2009. KCC2 expression promotes the termination of cortical interneuron migration in a voltage-sensitive calcium-dependent manner. *Neuron*, 62 (1):53-71.
- Boutin C, Hardt O, de Chevigny A, Core N, Goebbels S, Seidenfaden R, Bosio A, Cremer H. NeuroD1 induces terminal neuronal differentiation in olfactory neurogenesis. *Proc Natl Acad Sci U S A*, 107 (3):1201-1206.
- Brady G, Iscove NN. 1993. Construction of cDNA libraries from single cells. *Methods Enzymol*, 225:611-623.
- Brady G, Barbara M, Iscove NN. 1990. Representative in vitro cDNA amplification from individual hemopoietic cells and colonies. *Methods Molec Cell Biol*, 2:17-25.
- Bruckner K, Pasquale EB, Klein R. 1997. Tyrosine phosphorylation of transmembrane ligands for Eph receptors. *Science*, 275 (5306):1640-1643.
- Brunstrom JE, Gray-Swain MR, Osborne PA, Pearlman AL. 1997. Neuronal heterotopias in the developing cerebral cortex produced by neurotrophin-4. *Neuron*, 18 (3):505-517.
- Buettner F, Natarajan KN, Casale FP, Proserpio V, Scialdone A, Theis FJ. 2015. Computational analysis of cell-to-cell heterogeneity in single-cell RNA-sequencing data reveals hidden subpopulations of cells. *33 (2):155-160*.

- Bulfone A, Puelles L, Porteus MH, Frohman MA, Martin GR, Rubenstein JL. 1993. Spatially restricted expression of Dlx-1, Dlx-2 (Tes-1), Gbx-2, and Wnt-3 in the embryonic day 12.5 mouse forebrain defines potential transverse and longitudinal segmental boundaries. *J Neurosci*, 13 (7):3155-3172.
- Bupesh M, Legaz I, Abellan A, Medina L. 2011. Multiple telencephalic and extratelencephalic embryonic domains contribute neurons to the medial extended amygdala. *J Comp Neurol*, 519 (8):1505-1525.
- Butt SJ, Fuccillo M, Nery S, Noctor S, Kriegstein A, Corbin JG, Fishell G. 2005. The temporal and spatial origins of cortical interneurons predict their physiological subtype. *Neuron*, 48 (4):591-604.
- Butt SJ, Sousa VH, Fuccillo MV, Hjerling-Leffler J, Miyoshi G, Kimura S, Fishell G. 2008. The requirement of Nkx2-1 in the temporal specification of cortical interneuron subtypes. *Neuron*, 59 (5):722-732.
- Campbell K. 2005. Cortical neuron specification: it has its time and place. *Neuron*, 46 (3):373-376.
- Casanova MF, Trippe J, 2nd. 2006. Regulatory mechanisms of cortical laminar development. *Brain Res Rev*, 51 (1):72-84.
- Casarosa S, Fode C, Guillemot F. 1999. Mash1 regulates neurogenesis in the ventral telencephalon. *Development*, 126 (3):525-534.
- Castellani V, Bolz J. 1996. Developmental strategies underlying the elaboration of cortical circuits. *Rev Bras Biol*, 56 Su 1 Pt 1:21-31.
- Cauli B, Porter JT, Tsuzuki K, Lambolez B, Rossier J, Quenet B, Audinat E. 2000. Classification of fusiform neocortical interneurons based on unsupervised clustering. *Proc Natl Acad Sci U S A*, 97 (11):6144-6149.
- Chiang MK, Melton DA. 2003. Single-cell transcript analysis of pancreas development. *Dev Cell*, 4 (3):383-393.
- Choi PJ, Cai L, Frieda K, Xie XS. 2008. A stochastic single-molecule event triggers phenotype switching of a bacterial cell. *Science*, 322 (5900):442-446.
- Chubb JR, Trcek T, Shenoy SM, Singer RH. 2006. Transcriptional pulsing of a developmental gene. *Curr Biol*, 16 (10):1018-1025.
- Ciceri G, Dehorter N, Sols I, Huang ZJ, Maravall M, Marin O. 2013. Lineage-specific laminar organization of cortical GABAergic interneurons. *Nat Neurosci*, 16 (9):1199-1210.
- Civiero L, Cirnaru MD, Beilina A, Rodella U, Russo I, Belluzzi E, Lobbstaël E, Reyniers L, Hondhamuni G, Lewis PA, Van den Haute C, Baekelandt V, Bandopadhyay R, Bubacco L, Piccoli G, Cookson MR, Taymans JM, Greggio E. 2015. Leucine-rich repeat kinase 2 interacts with p21-activated kinase 6 to control neurite complexity in mammalian brain. *J Neurochem*, 135 (6):1242-1256.
- Clowry GJ. 2015. An enhanced role and expanded developmental origins for gamma-aminobutyric acidergic interneurons in the human cerebral cortex. *J Anat*, 227 (4):384-393.
- Cobos I, Borello U, Rubenstein JL. 2007. Dlx transcription factors promote migration through repression of axon and dendrite growth. *Neuron*, 54 (6):873-888.
- Cobos I, Long JE, Thwin MT, Rubenstein JL. 2006. Cellular patterns of transcription factor expression in developing cortical interneurons. *Cereb Cortex*, 16 Suppl 1:i82-88.
- Cooper JA. 2013. Cell biology in neuroscience: mechanisms of cell migration in the nervous system. *J Cell Biol*, 202 (5):725-734.
- Cooper MA, Son AI, Komlos D, Sun Y, Kleiman NJ, Zhou R. 2008. Loss of ephrin-A5 function disrupts lens fiber cell packing and leads to cataract. *Proceedings of the National Academy of Sciences of the United States of America*, 105 (43):16620-16625.
- Corbin JG, Butt SJ. 2011. Developmental mechanisms for the generation of telencephalic interneurons. *Dev Neurobiol*.
- Costa MR, Hedin-Pereira C. 2010. Does cell lineage in the developing cerebral cortex contribute to its columnar organization? *Front Neuroanat*, 4:26.
- Costa MR, Gotz M, Berninger B. 2010. What determines neurogenic competence in glia? *Brain Res Rev*, 63 (1-2):47-59.

- Dalva MB, Takasu MA, Lin MZ, Shamah SM, Hu L, Gale NW, Greenberg ME. 2000. EphB receptors interact with NMDA receptors and regulate excitatory synapse formation. *Cell*, 103 (6):945-956.
- Dan C, Nath N, Liberto M, Minden A. 2002. PAK5, a new brain-specific kinase, promotes neurite outgrowth in N1E-115 cells. *Mol Cell Biol*, 22 (2):567-577.
- Dani VS, Chang Q, Maffei A, Turrigiano GG, Jaenisch R, Nelson SB. 2005. Reduced cortical activity due to a shift in the balance between excitation and inhibition in a mouse model of Rett syndrome. *Proc Natl Acad Sci U S A*, 102 (35):12560-12565.
- Daniels RH, Hall PS, Bokoch GM. 1998. Membrane targeting of p21-activated kinase 1 (PAK1) induces neurite outgrowth from PC12 cells. *Embo j*, 17 (3):754-764.
- Davis S, Gale NW, Aldrich TH, Maisonpierre PC, Lhotak V, Pawson T, Goldfarb M, Yancopoulos GD. 1994. Ligands for EPH-related receptor tyrosine kinases that require membrane attachment or clustering for activity. *Science*, 266 (5186):816-819.
- Davy A, Gale NW, Murray EW, Klinghoffer RA, Soriano P, Feuerstein C, Robbins SM. 1999. Compartmentalized signaling by GPI-anchored ephrin-A5 requires the Fyn tyrosine kinase to regulate cellular adhesion. *Genes Dev*, 13 (23):3125-3135.
- de Carlos JA, Lopez-Mascaraque L, Valverde F. 1996. Dynamics of cell migration from the lateral ganglionic eminence in the rat. *J Neurosci*, 16 (19):6146-6156.
- De Marco Garcia NV, Karayannis T, Fishell G. 2011. Neuronal activity is required for the development of specific cortical interneuron subtypes. *Nature*, 472 (7343):351-355.
- Dehay C, Kennedy H. 2007. Cell-cycle control and cortical development. *Nat Rev Neurosci*, 8 (6):438-450.
- Dehay C, Savatier P, Cortay V, Kennedy H, Hrsg. 2001. Cell-cycle kinetics of neocortical precursors are influenced by embryonic thalamic axons. United States.
- Dehay C, Giroud P, Berland M, Killackey H, Kennedy H. 1996. Contribution of thalamic input to the specification of cytoarchitectonic cortical fields in the primate: effects of bilateral enucleation in the fetal monkey on the boundaries, dimensions, and gyrification of striate and extrastriate cortex. *J Comp Neurol*, 367 (1):70-89.
- Deng Q, Ramsköld D, Reinius B, Sandberg R. 2014. Single-cell RNA-seq reveals dynamic, random monoallelic gene expression in mammalian cells. *Science*, 343 (6167):193-196.
- Deschamps C, Morel M, Janet T, Page G, Jaber M, Gaillard A, Prestoz L, Hrsg. 2010. EphrinA5 protein distribution in the developing mouse brain.
- Dessaud E, McMahon AP, Briscoe J. 2008. Pattern formation in the vertebrate neural tube: a sonic hedgehog morphogen-regulated transcriptional network. *Development*, 135 (15):2489-2503.
- Dong E, Ruzicka WB, Grayson DR, Guidotti A. 2015. DNA-methyltransferase1 (DNMT1) binding to CpG rich GABAergic and BDNF promoters is increased in the brain of schizophrenia and bipolar disorder patients. *Schizophr Res*, 167 (1-3):35-41.
- Druga R. 2009. Neocortical inhibitory system. *Folia Biol (Praha)*, 55 (6):201-217.
- Du T, Xu Q, Ocbina PJ, Anderson SA. 2008. NKX2.1 specifies cortical interneuron fate by activating Lhx6. *Development*, 135 (8):1559-1567.
- Dulac C, Axel R. 1995. A novel family of genes encoding putative pheromone receptors in mammals. *Cell*, 83 (2):195-206.
- Eberwine J, Yeh H, Miyashiro K, Cao Y, Nair S, Finnell R, Zettel M, Coleman P. 1992. Analysis of gene expression in single live neurons. *Proc Natl Acad Sci U S A*, 89 (7):3010-3014.
- Egea J, Klein R. 2007. Bidirectional Eph-ephrin signaling during axon guidance. *Trends Cell Biol*, 17 (5):230-238.
- Eldar A, Elowitz MB. 2010. Functional roles for noise in genetic circuits. *Nature*, 467 (7312):167-173.
- Elshatory Y, Gan L. 2008. The LIM-homeobox gene *Islet-1* is required for the development of restricted forebrain cholinergic neurons. *J Neurosci*, 28 (13):3291-3297.
- Englund C, Fink A, Lau C, Pham D, Daza RA, Bulfone A, Kowalczyk T, Hevner RF, Hrsg. 2005. Pax6, Tbr2, and Tbr1 are expressed sequentially by radial glia, intermediate progenitor cells, and postmitotic neurons in developing neocortex. United States.

- Erlander MG, Tillakaratne NJ, Feldblum S, Patel N, Tobin AJ. 1991. Two genes encode distinct glutamate decarboxylases. *Neuron*, 7 (1):91-100.
- Estève P-O, Chin HG, Smallwood A, Feehery GR, Gangisetty O, Karpf AR, Carey MF, Pradhan S. 2006. Direct interaction between DNMT1 and G9a coordinates DNA and histone methylation during replication. *Genes & Development*, 20 (22):3089-3103.
- Fan X, Labrador JP, Hing H, Bashaw GJ. 2003. Slit stimulation recruits Dock and Pak to the roundabout receptor and increases Rac activity to regulate axon repulsion at the CNS midline. *Neuron*, 40 (1):113-127.
- Faro A, Boj SF, Ambrosio R, van den Broek O, Korving J, Clevers H. 2009. T-cell factor 4 (tcf7l2) is the main effector of Wnt signaling during zebrafish intestine organogenesis. *Zebrafish*, 6 (1):59-68.
- Felsenfeld DP, Schwartzberg PL, Venegas A, Tse R, Sheetz MP. 1999. Selective regulation of integrin--cytoskeleton interactions by the tyrosine kinase Src. *Nat Cell Biol*, 1 (4):200-206.
- Feng J, Fan G. 2009. The role of DNA methylation in the central nervous system and neuropsychiatric disorders. *Int Rev Neurobiol*, 89:67-84.
- Feng J, Zhou Y, Campbell SL, Le T, Li E, Sweatt JD, Silva AJ, Fan G. 2010. Dnmt1 and Dnmt3a maintain DNA methylation and regulate synaptic function in adult forebrain neurons. *Nat Neurosci*, 13 (4):423-430.
- Fink L, Seeger W, Ermert L, Hanze J, Stahl U, Grimminger F, Kummer W, Bohle RM. 1998. Real-time quantitative RT-PCR after laser-assisted cell picking. *Nat Med*, 4 (11):1329-1333.
- Fishell G, Kriegstein AR. 2003. Neurons from radial glia: the consequences of asymmetric inheritance. *Curr Opin Neurobiol*, 13 (1):34-41.
- Flames N, Marin O. 2005. Developmental mechanisms underlying the generation of cortical interneuron diversity. *Neuron*, 46 (3):377-381.
- Flames N, Pla R, Gelman DM, Rubenstein JL, Puelles L, Marin O. 2007. Delineation of multiple subpallial progenitor domains by the combinatorial expression of transcriptional codes. *J Neurosci*, 27 (36):9682-9695.
- Flames N, Long JE, Garratt AN, Fischer TM, Gassmann M, Birchmeier C, Lai C, Rubenstein JL, Marin O. 2004. Short- and long-range attraction of cortical GABAergic interneurons by neuregulin-1. *Neuron*, 44 (2):251-261.
- Flanagan JG, Vanderhaeghen P. 1998. The ephrins and Eph receptors in neural development. *Annu Rev Neurosci*, 21:309-345.
- Fogarty M, Grist M, Gelman D, Marin O, Pachnis V, Kessaris N. 2007. Spatial genetic patterning of the embryonic neuroepithelium generates GABAergic interneuron diversity in the adult cortex. *J Neurosci*, 27 (41):10935-10946.
- Freeman TC, Lee K, Richardson PJ. 1999. Analysis of gene expression in single cells. *Curr Opin Biotechnol*, 10 (6):579-582.
- Frumkin D, Wasserstrom A, Itzkovitz S, Harmelin A, Rechavi G, Shapiro E. 2008. Amplification of multiple genomic loci from single cells isolated by laser micro-dissection of tissues. *BMC Biotechnol*, 8:17.
- Fu GK, Hu J, Wang PH, Fodor SP. 2011. Counting individual DNA molecules by the stochastic attachment of diverse labels. *Proc Natl Acad Sci U S A*, 108 (22):9026-9031.
- Fujino T, Wu Z, Lin WC, Phillips MA, Nedivi E. 2008. cpg15 and cpg15-2 constitute a family of activity-regulated ligands expressed differentially in the nervous system to promote neurite growth and neuronal survival. *J Comp Neurol*, 507 (5):1831-1845.
- Fujiwara Y, Kasashima K, Saito K, Fukuda M, Fukao A, Sasano Y, Inoue K, Fujiwara T, Sakamoto H. 2011. Microtubule association of a neuronal RNA-binding protein HuD through its binding to the light chain of MAP1B. *Biochimie*, 93 (5):817-822.
- Fuks F, Burgers WA, Brehm A, Hughes-Davies L, Kouzarides T. 2000. DNA methyltransferase Dnmt1 associates with histone deacetylase activity. *Nat Genet*, 24 (1):88-91.
- Furnari MA, Jobes ML, Nekrasova T, Minden A, Wagner GC. 2013. Functional deficits in PAK5, PAK6 and PAK5/PAK6 knockout mice. *PLoS One*, 8 (4):e61321.

- Gale NW, Holland SJ, Valenzuela DM, Flenniken A, Pan L, Ryan TE, Henkemeyer M, Strebhardt K, Hirai H, Wilkinson DG, Pawson T, Davis S, Yancopoulos GD. 1996. Eph receptors and ligands comprise two major specificity subclasses and are reciprocally compartmentalized during embryogenesis. *Neuron*, 17 (1):9-19.
- Garcia-Lopez M, Abellan A, Legaz I, Rubenstein JL, Puellas L, Medina L. 2008. Histogenetic compartments of the mouse centromedial and extended amygdala based on gene expression patterns during development. *J Comp Neurol*, 506 (1):46-74.
- Gauthier-Fisher A, Lin DC, Greeve M, Kaplan DR, Rottapel R, Miller FD. 2009. Lfc and Tctex-1 regulate the genesis of neurons from cortical precursor cells. *Nature neuroscience*, 12 (6):735-744.
- Geiss GK, Bumgarner RE, Birditt B, Dahl T, Dowidar N, Dunaway DL, Fell HP, Ferree S, George RD, Grogan T, James JJ, Maysuria M, Mitton JD, Oliveri P, Osborn JL, Peng T, Ratcliffe AL, Webster PJ, Davidson EH, Hood L, Dimitrov K. 2008. Direct multiplexed measurement of gene expression with color-coded probe pairs. *Nat Biotechnol*, 26 (3):317-325.
- Gelman D, Griveau A, Dehorter N, Teissier A, Varela C, Pla R, Pierani A, Marin O. 2011. A wide diversity of cortical GABAergic interneurons derives from the embryonic preoptic area. *J Neurosci*, 31 (46):16570-16580.
- Gelman DM, Marin O. 2010. Generation of interneuron diversity in the mouse cerebral cortex. *Eur J Neurosci*, 31 (12):2136-2141.
- Gelman DM, Marin, Rubenstein JLR. 2012. The Generation of Cortical Interneurons. In: Noebels JL, Avoli M, Rogawski MA, Olsen RW, Delgado-Escueta AV, Hrsg. *Jasper's Basic Mechanisms of the Epilepsies*. 4th Aufl. Bethesda (MD).
- Gelman DM, Martini FJ, Nobrega-Pereira S, Pierani A, Kessar N, Marin O. 2009. The embryonic preoptic area is a novel source of cortical GABAergic interneurons. *J Neurosci*, 29 (29):9380-9389.
- Gerstmann K. 2014. Der Einfluss von EphrinA5 auf die Proliferation und Identität kortikaler Vorläuferzellen während der embryonalen Neurogenese [PhD Thesis]. Friedrich-Schiller-Universität Jena.
- Gerstmann K, Pensold D, Symmank J, Khundadze M, Hubner CA, Bolz J, Zimmer G. 2015. Thalamic afferents influence cortical progenitors via ephrin A5-EphA4 interactions. *Development*, 142 (1):140-150.
- Gitig D. 2010. Transcriptomics: individuality in the cellular world. *Biotechniques*, 48 (6):439-443.
- Gong Q, Shipley MT. 1995. Evidence that pioneer olfactory axons regulate telencephalon cell cycle kinetics to induce the formation of the olfactory bulb. *Neuron*, 14 (1):91-101.
- Gotz M, Bolz J. 1992. Formation and preservation of cortical layers in slice cultures. *J Neurobiol*, 23 (7):783-802.
- Gotz M, Huttner WB. 2005. The cell biology of neurogenesis. *Nat Rev Mol Cell Biol*, 6 (10):777-788.
- Gotz M, Stoykova A, Gruss P. 1998. Pax6 controls radial glia differentiation in the cerebral cortex. *Neuron*, 21 (5):1031-1044.
- Govek EE, Newey SE, Van Aelst L. 2005. The role of the Rho GTPases in neuronal development. *Genes Dev*, 19 (1):1-49.
- Grindberg RV, Ishoey T, Brinza D, Esquenazi E, Coates RC, Liu WT, Gerwick L, Dorrestein PC, Pevzner P, Lasken R, Gerwick WH. 2011. Single cell genome amplification accelerates identification of the apratoxin biosynthetic pathway from a complex microbial assemblage. *PLoS One*, 6 (4):e18565.
- Guellmar A, Rudolph J, Bolz J. 2009. Structural alterations of spiny stellate cells in the somatosensory cortex in ephrin-A5-deficient mice. *J Comp Neurol*, 517 (5):645-654.
- Guillemot F. 2007. Cortical interneurons refuse to follow the PAK. *Neuron*, 54 (6):845-847.
- Guo G, Huss M, Tong GQ, Wang C, Li Sun L, Clarke ND, Robson P. 2010. Resolution of cell fate decisions revealed by single-cell gene expression analysis from zygote to blastocyst. *Dev Cell*, 18 (4):675-685.
- Haag N. 2009. Differenzielle Einzelzell-Transkriptomanalyse zur Identifizierung geruchsrezeptorassoziierter Differenzierungsmoleküle während der Entwicklung des

- olfaktorischen Systems der Maus [Dissertation]. Thüringer Universitäts- und Landesbibliothek Jena: Friedrich-Schiller-Universität Jena.
- Hao L, Zhou X, Liu S, Sun M, Song Y, Du S, Sun B, Guo C, Gong L, Hu J, Guan H, Shao S. 2015. Elevated GAPDH expression is associated with the proliferation and invasion of lung and esophageal squamous cell carcinomas. *Proteomics*, 15 (17):3087-3100.
- Harwell CC, Fuentealba LC, Gonzalez-Cerrillo A, Parker PR, Gertz CC, Mazzola E, Garcia MT, Alvarez-Buylla A, Cepko CL, Kriegstein AR. 2015. Wide Dispersion and Diversity of Clonally Related Inhibitory Interneurons. *Neuron*, 87 (5):999-1007.
- Hashimoto H, Vertino PM, Cheng X. 2010. Molecular coupling of DNA methylation and histone methylation. *Epigenomics*, 2 (5):657-669.
- Hashimshony T, Wagner F, Sher N, Yanai I. 2012. CEL-Seq: Single-Cell RNA-Seq by Multiplexed Linear Amplification. *Cell Rep*, 2 (3):666-673.
- Haubensak W, Attardo A, Denk W, Huttner WB. 2004. Neurons arise in the basal neuroepithelium of the early mammalian telencephalon: a major site of neurogenesis. *Proc Natl Acad Sci U S A*, 101 (9):3196-3201.
- Haydar TF, Wang F, Schwartz ML, Rakic P. 2000. Differential modulation of proliferation in the neocortical ventricular and subventricular zones. *J Neurosci*, 20 (15):5764-5774.
- Hempel CM, Sugino K, Nelson SB. 2007. A manual method for the purification of fluorescently labeled neurons from the mammalian brain. *Nat Protoc*, 2 (11):2924-2929.
- Higuchi R, Fockler C, Dollinger G, Watson R. 1993. Kinetic PCR analysis: real-time monitoring of DNA amplification reactions. *Biotechnology (N Y)*, 11 (9):1026-1030.
- Hing H, Xiao J, Harden N, Lim L, Zipursky SL. 1999. Pak functions downstream of Dock to regulate photoreceptor axon guidance in *Drosophila*. *Cell*, 97 (7):853-863.
- Hirabayashi Y, Gotoh Y. 2010. Epigenetic control of neural precursor cell fate during development. *Nat Rev Neurosci*, 11 (6):377-388.
- Hofmann C, Shepelev M, Chernoff J. 2004. The genetics of Pak. *J Cell Sci*, 117 (Pt 19):4343-4354.
- Holland SJ, Gale NW, Mbamalu G, Yancopoulos GD, Henkemeyer M, Pawson T. 1996. Bidirectional signalling through the EPH-family receptor Nuk and its transmembrane ligands. *Nature*, 383 (6602):722-725.
- Holmberg J, Clarke DL, Frisen J. 2000. Regulation of repulsion versus adhesion by different splice forms of an Eph receptor. *Nature*, 408 (6809):203-206.
- Hsieh J, Eisch AJ. 2010. Epigenetics, hippocampal neurogenesis, and neuropsychiatric disorders: unraveling the genome to understand the mind. *Neurobiol Dis*, 39 (1):73-84.
- Huang C, Ni Y, Wang T, Gao Y, Haudenschild CC, Zhan X. 1997. Down-regulation of the filamentous actin cross-linking activity of cortactin by Src-mediated tyrosine phosphorylation. *J Biol Chem*, 272 (21):13911-13915.
- Hubel DH, Wiesel TN. 1962. Receptive fields, binocular interaction and functional architecture in the cat's visual cortex. *J Physiol*, 160:106-154.
- Huber W, Gentleman R. 2006. *estrogen: 2x2 factorial design exercise for the Bioconductor short course R package version 1.18.0*.
- Hug H, Schuler R. 2003. Measurement of the number of molecules of a single mRNA species in a complex mRNA preparation. *J Theor Biol*, 221 (4):615-624.
- Hung MS, Karthikeyan N, Huang B, Koo HC, Kiger J, Shen CJ. 1999. *Drosophila* proteins related to vertebrate DNA (5-cytosine) methyltransferases. *Proc Natl Acad Sci U S A*, 96 (21):11940-11945.
- Hutnick LK, Golshani P, Namihira M, Xue Z, Matynia A, Yang XW, Silva AJ, Schweizer FE, Fan G. 2009. DNA hypomethylation restricted to the murine forebrain induces cortical degeneration and impairs postnatal neuronal maturation. *Hum Mol Genet*, 18 (15):2875-2888.
- Inano K, Suetake I, Ueda T, Miyake Y, Nakamura M, Okada M, Tajima S. 2000. Maintenance-type DNA methyltransferase is highly expressed in post-mitotic neurons and localized in the cytoplasmic compartment. *J Biochem*, 128 (2):315-321.

- Iscove NN, Barbara M, Gu M, Gibson M, Modi C, Winegarden N. 2002. Representation is faithfully preserved in global cDNA amplified exponentially from sub-picogram quantities of mRNA. *Nat Biotechnol*, 20 (9):940-943.
- Islam S, Kjallquist U, Moliner A, Zajac P, Fan JB, Lonnerberg P, Linnarsson S. 2011. Characterization of the single-cell transcriptional landscape by highly multiplex RNA-seq. *Genome Res*, 21 (7):1160-1167.
- Islam S, Zeisel A, Joost S, La Manno G, Zajac P, Kasper M, Lönnerberg P, Linnarsson S. 2014. Quantitative single-cell RNA-seq with unique molecular identifiers. *Nature methods*, 11 (2):163-166.
- Jackson-Grusby L, Beard C, Possemato R, Tudor M, Fambrough D, Csankovszki G, Dausman J, Lee P, Wilson C, Lander E, Jaenisch R. 2001. Loss of genomic methylation causes p53-dependent apoptosis and epigenetic deregulation. *Nat Genet*, 27 (1):31-39.
- Jaitin DA, Kenigsberg E, Keren-Shaul H, Elefant N, Paul F, Zaretsky I, Mildner A, Cohen N, Jung S, Tanay A, Amit I. 2014. Massively parallel single-cell RNA-seq for marker-free decomposition of tissues into cell types. *Science*, 343 (6172):776-779.
- Janes KA, Wang CC, Holmberg KJ, Cabral K, Brugge JS. 2010. Identifying single-cell molecular programs by stochastic profiling. *Nat Methods*, 7 (4):311-317.
- Jessell TM. 2000. Neuronal specification in the spinal cord: inductive signals and transcriptional codes. *Nat Rev Genet*, 1 (1):20-29.
- Jetty PV, Charney DS, Goddard AW. 2001. Neurobiology of generalized anxiety disorder. *Psychiatr Clin North Am*, 24 (1):75-97.
- Jiang Y, Langley B, Lubin FD, Renthal W, Wood MA, Yasui DH, Kumar A, Nestler EJ, Akbarian S, Beckel-Mitchener AC. 2008. Epigenetics in the nervous system. *J Neurosci*, 28 (46):11753-11759.
- Jobe EM, McQuate AL, Zhao X. 2012. Crosstalk among Epigenetic Pathways Regulates Neurogenesis. *Front Neurosci*, 6:59.
- Jung H, Yoon BC, Holt CE. 2012. Axonal mRNA localization and local protein synthesis in nervous system assembly, maintenance and repair. *Nat Rev Neurosci*, 13 (5):308-324.
- Kamme F, Salunga R, Yu J, Tran DT, Zhu J, Luo L, Bittner A, Guo HQ, Miller N, Wan J, Erlander M. 2003. Single-cell microarray analysis in hippocampus CA1: demonstration and validation of cellular heterogeneity. *J Neurosci*, 23 (9):3607-3615.
- Kania A, Klein R. 2016. Mechanisms of ephrin-Eph signalling in development, physiology and disease. *Nat Rev Mol Cell Biol*, 17 (4):240-256.
- Karnak D, Lee S, Margolis B. 2002. Identification of multiple binding partners for the amino-terminal domain of synapse-associated protein 97. *Journal of Biological Chemistry*, 277 (48):46730-46735.
- Kawaguchi A, Ikawa T, Kasukawa T, Ueda HR, Kurimoto K, Saitou M, Matsuzaki F. 2008. Single-cell gene profiling defines differential progenitor subclasses in mammalian neurogenesis. *Development*, 135 (18):3113-3124.
- Keitt T. 2012. colorRamps: Builds color tables. R package version 2.3.
- Kellogg RA, Tay S. 2015. Noise facilitates transcriptional control under dynamic inputs. *Cell*, 160 (3):381-392.
- Kelsom C, Lu W. 2013. Development and specification of GABAergic cortical interneurons. *Cell Biosci*, 3 (1):19.
- Kepecs A, Fishell G. 2014. Interneuron cell types are fit to function. *Nature*, 505 (7483):318-326.
- Kharchenko PV, Silberstein L, Scadden DT. 2014. Bayesian approach to single-cell differential expression analysis. *Nat Methods*, 11 (7):740-742.
- Klein CA, Seidl S, Petat-Dutter K, Offner S, Geigl JB, Schmidt-Kittler O, Wendler N, Passlick B, Huber RM, Schlimok G, Baeuerle PA, Riethmuller G. 2002. Combined transcriptome and genome analysis of single micrometastatic cells. *Nat Biotechnol*, 20 (4):387-392.
- Klinghoffer RA, Sachsenmaier C, Cooper JA, Soriano P. 1999. Src family kinases are required for integrin but not PDGFR signal transduction. *Embo J*, 18 (9):2459-2471.
- Knoll B, Drescher U, Hrsg. 2002. Ephrin-As as receptors in topographic projections. England.

- Kolodziejczyk Aleksandra A, Kim JK, Svensson V, Marioni John C, Teichmann Sarah A. 2015a. The Technology and Biology of Single-Cell RNA Sequencing. *Molecular Cell*, 58 (4):610-620.
- Kolodziejczyk AA, Kim JK, Tsang JC, Ilicic T, Henriksson J, Natarajan KN, Tuck AC, Gao X, Buhler M, Liu P, Marioni JC, Teichmann SA. 2015b. Single Cell RNA-Sequencing of Pluripotent States Unlocks Modular Transcriptional Variation. *Cell Stem Cell*, 17 (4):471-485.
- Kowalczyk T, Pontious A, Englund C, Daza RA, Bedogni F, Hodge R, Attardo A, Bell C, Huttner WB, Hevner RF. 2009. Intermediate neuronal progenitors (basal progenitors) produce pyramidal-projection neurons for all layers of cerebral cortex. *Cereb Cortex*, 19 (10):2439-2450.
- Kriegstein AR, Gotz M. 2003. Radial glia diversity: a matter of cell fate. *Glia*, 43 (1):37-43.
- Kullander K, Klein R. 2002. Mechanisms and functions of Eph and ephrin signalling. *Nat Rev Mol Cell Biol*, 3 (7):475-486.
- Kumar RN, Ha JH, Radhakrishnan R, Dhanasekaran DN. 2006. Transactivation of platelet-derived growth factor receptor alpha by the GTPase-deficient activated mutant of Galpha12. *Mol Cell Biol*, 26 (1):50-62.
- Kurimoto K, Yabuta Y, Ohinata Y, Ono Y, Uno KD, Yamada RG, Ueda HR, Saitou M. 2006. An improved single-cell cDNA amplification method for efficient high-density oligonucleotide microarray analysis. *Nucleic Acids Res*, 34 (5):e42.
- Labrador JP, Brambilla R, Klein R. 1997. The N-terminal globular domain of Eph receptors is sufficient for ligand binding and receptor signaling. *Embo J*, 16 (13):3889-3897.
- Lackmann M, Oates AC, Dottori M, Smith FM, Do C, Power M, Kravets L, Boyd AW. 1998. Distinct subdomains of the EphA3 receptor mediate ligand binding and receptor dimerization. *J Biol Chem*, 273 (32):20228-20237.
- Lagunavicius A, Merkiene E, Kiveryte Z, Savaneviciute A, Zimbaite-Ruskulienė V, Radzvilavicius T, Janulaitis A. 2009. Novel application of Phi29 DNA polymerase: RNA detection and analysis in vitro and in situ by target RNA-primed RCA. *RNA*, 15 (5):765-771.
- Langmead B, Salzberg SL. 2012. Fast gapped-read alignment with Bowtie 2. *Nat Methods*, 9 (4):357-359.
- Lao KQ, Tang F, Barbacioru C, Wang Y, Nordman E, Lee C, Xu N, Wang X, Tuch B, Bodeau J, Siddiqui A, Surani MA. 2009. mRNA-sequencing whole transcriptome analysis of a single cell on the SOLiD system. *J Biomol Tech*, 20 (5):266-271.
- Lavdas AA, Grigoriou M, Pachnis V, Parnavelas JG. 1999. The medial ganglionic eminence gives rise to a population of early neurons in the developing cerebral cortex. *J Neurosci*, 19 (18):7881-7888.
- Lê S, Josse J, Husson F. 2008. FactoMineR: An R Package for Multivariate Analysis. 2008, 25 (1):18.
- Lee HS, Daar IO. 2009. EphrinB reverse signaling in cell-cell adhesion: is it just par for the course? *Cell Adh Migr*, 3 (3):250-255.
- Lee HS, Nishanian TG, Mood K, Bong YS, Daar IO. 2008. EphrinB1 controls cell-cell junctions through the Par polarity complex. *Nat Cell Biol*, 10 (8):979-986.
- Lee SK, Pfaff SL. 2001. Transcriptional networks regulating neuronal identity in the developing spinal cord. *Nat Neurosci*, 4 Suppl:1183-1191.
- Lehtinen MK, Walsh CA. 2011. Neurogenesis at the brain-cerebrospinal fluid interface. *Annu Rev Cell Dev Biol*, 27:653-679.
- Levitt P. 2005. Disruption of interneuron development. *Epilepsia*, 46 Suppl 7:22-28.
- Levitt P, Eagleson KL, Powell EM. 2004. Regulation of neocortical interneuron development and the implications for neurodevelopmental disorders. *Trends Neurosci*, 27 (7):400-406.
- Lewis DA. 2000. GABAergic local circuit neurons and prefrontal cortical dysfunction in schizophrenia. *Brain Res Brain Res Rev*, 31 (2-3):270-276.
- Lewis DA, Hashimoto T, Volk DW. 2005. Cortical inhibitory neurons and schizophrenia. *Nat Rev Neurosci*, 6 (4):312-324.
- Li G, Adesnik H, Li J, Long J, Nicoll RA, Rubenstein JL, Pleasure SJ. 2008. Regional distribution of cortical interneurons and development of inhibitory tone are regulated by Cxcl12/Cxcr4 signaling. *J Neurosci*, 28 (5):1085-1098.

- Li H. 2014. Toward better understanding of artifacts in variant calling from high-coverage samples. *Bioinformatics*, 30 (20):2843-2851.
- Liebl DJ, Morris CJ, Henkemeyer M, Parada LF. 2003. mRNA expression of ephrins and Eph receptor tyrosine kinases in the neonatal and adult mouse central nervous system. *J Neurosci Res*, 71 (1):7-22.
- Liodis P, Denaxa M, Grigoriou M, Akufo-Addo C, Yanagawa Y, Pachnis V. 2007. Lhx6 activity is required for the normal migration and specification of cortical interneuron subtypes. *J Neurosci*, 27 (12):3078-3089.
- Liu S, Trapnell C. 2016. Single-cell transcriptome sequencing: recent advances and remaining challenges. *F1000Res*, 5.
- Livak KJ, Schmittgen TD. 2001. Analysis of relative gene expression data using real-time quantitative PCR and the 2^{-Delta Delta C(T)} Method. *Methods*, 25 (4):402-408.
- Livnat I, Finkelshtein D, Ghosh I, Arai H, Reiner O. 2010. PAF-AH Catalytic Subunits Modulate the Wnt Pathway in Developing GABAergic Neurons. *Front Cell Neurosci*, 4.
- Lodato S, Arlotta P. 2015. Generating neuronal diversity in the mammalian cerebral cortex. *Annu Rev Cell Dev Biol*, 31:699-720.
- Lodato S, Rouaux C, Quast KB, Jantrachotechatchawan C, Studer M, Hensch TK, Arlotta P. 2011. Excitatory projection neuron subtypes control the distribution of local inhibitory interneurons in the cerebral cortex. *Neuron*, 69 (4):763-779.
- Lopez-Bendito G, Chan CH, Mallamaci A, Parnavelas J, Molnar Z. 2002. Role of Emx2 in the development of the reciprocal connectivity between cortex and thalamus. *J Comp Neurol*, 451 (2):153-169.
- Lopez-Bendito G, Lujan R, Shigemoto R, Ganter P, Paulsen O, Molnar Z. 2003. Blockade of GABA(B) receptors alters the tangential migration of cortical neurons. *Cereb Cortex*, 13 (9):932-942.
- Lopez-Bendito G, Sturgess K, Erdelyi F, Szabo G, Molnar Z, Paulsen O. 2004. Preferential origin and layer destination of GAD65-GFP cortical interneurons. *Cereb Cortex*, 14 (10):1122-1133.
- Lund RD, Mustari MJ. 1977. Development of the geniculocortical pathway in rats. *J Comp Neurol*, 173 (2):289-306.
- Luo L. 2000. Rho GTPases in neuronal morphogenesis. *Nat Rev Neurosci*, 1 (3):173-180.
- Macosko EZ, Basu A, Satija R, Nemes J, Shekhar K, Goldman M, Tirosh I, Bialas AR, Kamitaki N, Martersteck EM, Trombetta JJ, Weitz DA, Sanes JR, Shalek AK, Regev A, McCarroll SA. 2015. Highly Parallel Genome-wide Expression Profiling of Individual Cells Using Nanoliter Droplets. *Cell*, 161 (5):1202-1214.
- Madisen L, Zwingman TA, Sunkin SM, Oh SW, Zariwala HA, Gu H, Ng LL, Palmiter RD, Hawrylycz MJ, Jones AR, Lein ES, Zeng H. 2010. A robust and high-throughput Cre reporting and characterization system for the whole mouse brain. *Nat Neurosci*, 13 (1):133-140.
- Marguerat S, Bahler J. 2012. Coordinating genome expression with cell size. *Trends Genet*, 28 (11):560-565.
- Marin-Padilla M. 1971. Early prenatal ontogenesis of the cerebral cortex (neocortex) of the cat (*Felis domestica*). A Golgi study. I. The primordial neocortical organization. *Z Anat Entwicklungsgesch*, 134 (2):117-145.
- Marin O. 2012. Interneuron dysfunction in psychiatric disorders. *Nat Rev Neurosci*, 13 (2):107-120.
- Marin O. 2013. Cellular and molecular mechanisms controlling the migration of neocortical interneurons. *Eur J Neurosci*, 38 (1):2019-2029.
- Marin O, Rubenstein JL. 2001. A long, remarkable journey: tangential migration in the telencephalon. *Nat Rev Neurosci*, 2 (11):780-790.
- Marin O, Muller U. 2014. Lineage origins of GABAergic versus glutamatergic neurons in the neocortex. *Curr Opin Neurobiol*, 26:132-141.
- Marin O, Anderson SA, Rubenstein JL. 2000. Origin and molecular specification of striatal interneurons. *J Neurosci*, 20 (16):6063-6076.
- Marin O, Yaron A, Bagri A, Tessier-Lavigne M, Rubenstein JL. 2001. Sorting of striatal and cortical interneurons regulated by semaphorin-neuropilin interactions. *Science*, 293 (5531):872-875.

- Marin O, Plump AS, Flames N, Sanchez-Camacho C, Tessier-Lavigne M, Rubenstein JL. 2003. Directional guidance of interneuron migration to the cerebral cortex relies on subcortical Slit1/2-independent repulsion and cortical attraction. *Development*, 130 (9):1889-1901.
- Martin M. 2011. Cutadapt removes adapter sequences from high-throughput sequencing reads. 2011, 17 (1).
- Martinez A, Soriano E. 2005. Functions of ephrin/Eph interactions in the development of the nervous system: emphasis on the hippocampal system. *Brain Res Brain Res Rev*, 49 (2):211-226.
- Martini FJ, Valiente M, Lopez Bendito G, Szabo G, Moya F, Valdeolmillos M, Marin O. 2009. Biased selection of leading process branches mediates chemotaxis during tangential neuronal migration. *Development*, 136 (1):41-50.
- Matrisciano F, Tueting P, Dalal I, Kadriu B, Grayson DR, Davis JM, Nicoletti F, Guidotti A. 2013. Epigenetic modifications of GABAergic interneurons are associated with the schizophrenia-like phenotype induced by prenatal stress in mice. *Neuropharmacology*, 68:184-194.
- Mawrin C, Kirches E, Dietzmann K. 2003. Single-cell analysis of mtDNA in amyotrophic lateral sclerosis: towards the characterization of individual neurons in neurodegenerative disorders. *Pathol Res Pract*, 199 (6):415-418.
- Mayer C, Jaglin XH, Cobbs LV, Bandler RC, Streicher C, Cepko CL, Hippenmeyer S, Fishell G. 2015. Clonally Related Forebrain Interneurons Disperse Broadly across Both Functional Areas and Structural Boundaries. *Neuron*, 87 (5):989-998.
- McConnell SK. 1989. The determination of neuronal fate in the cerebral cortex. *Trends Neurosci*, 12 (9):342-349.
- McConnell SK. 1995. Constructing the cerebral cortex: neurogenesis and fate determination. *Neuron*, 15 (4):761-768.
- McKinsey GL, Lindtner S, Trzcinski B, Visel A, Pennacchio LA, Huylebroeck D, Higashi Y, Rubenstein JL. 2013. Dlx1&2-Dependent Expression of Zfhx1b (Sip1, Zeb2) Regulates the Fate Switch between Cortical and Striatal Interneurons. *Neuron*, 77 (1):83-98.
- Meng J, Meng Y, Hanna A, Janus C, Jia Z. 2005. Abnormal long-lasting synaptic plasticity and cognition in mice lacking the mental retardation gene Pak3. *J Neurosci*, 25 (28):6641-6650.
- Merico D, Isserlin R, Stueker O, Emili A, Bader GD. 2010. Enrichment map: a network-based method for gene-set enrichment visualization and interpretation. *PLoS One*, 5 (11):e13984.
- Merot Y, Retaux S, Heng JI. 2009. Molecular mechanisms of projection neuron production and maturation in the developing cerebral cortex. *Semin Cell Dev Biol*, 20 (6):726-734.
- Meyer-Siegler K, Rahman-Mansur N, Wurzer JC, Sirover MA. 1992. Proliferative dependent regulation of the glyceraldehyde-3-phosphate dehydrogenase/uracil DNA glycosylase gene in human cells. *Carcinogenesis*, 13 (11):2127-2132.
- Michalczyk K, Ziman M. 2005. Nestin structure and predicted function in cellular cytoskeletal organisation. *Histol Histopathol*, 20 (2):665-671.
- Mikkelsen TS, Ku M, Jaffe DB, Issac B, Lieberman E, Giannoukos G, Alvarez P, Brockman W, Kim TK, Koche RP, Lee W, Mendenhall E, O'Donovan A, Presser A, Russ C, Xie X, Meissner A, Wernig M, Jaenisch R, Nusbaum C, Lander ES, Bernstein BE. 2007. Genome-wide maps of chromatin state in pluripotent and lineage-committed cells. *Nature*, 448 (7153):553-560.
- Misawa H, Kawasaki Y, Mellor J, Sweeney N, Jo K, Nicoll RA, Bredt DS. 2001. Contrasting localizations of MALS/LIN-7 PDZ proteins in brain and molecular compensation in knockout mice. *Journal of Biological Chemistry*, 276 (12):9264-9272.
- Miyata T, Kawaguchi A, Okano H, Ogawa M. 2001. Asymmetric inheritance of radial glial fibers by cortical neurons. *Neuron*, 31 (5):727-741.
- Miyata T, Kawaguchi A, Saito K, Kawano M, Muto T, Ogawa M. 2004. Asymmetric production of surface-dividing and non-surface-dividing cortical progenitor cells. *Development*, 131 (13):3133-3145.
- Miyoshi G, Fishell G. 2011. GABAergic interneuron lineages selectively sort into specific cortical layers during early postnatal development. *Cereb Cortex*, 21 (4):845-852.

- Miyoshi G, Butt SJ, Takebayashi H, Fishell G. 2007. Physiologically distinct temporal cohorts of cortical interneurons arise from telencephalic Olig2-expressing precursors. *J Neurosci*, 27 (29):7786-7798.
- Miyoshi G, Hjerling-Leffler J, Karayannis T, Sousa VH, Butt SJ, Battiste J, Johnson JE, Machold RP, Fishell G. 2010. Genetic fate mapping reveals that the caudal ganglionic eminence produces a large and diverse population of superficial cortical interneurons. *J Neurosci*, 30 (5):1582-1594.
- Mohn F, Weber M, Rebhan M, Roloff TC, Richter J, Stadler MB, Bibel M, Schubeler D. 2008. Lineage-specific polycomb targets and de novo DNA methylation define restriction and potential of neuronal progenitors. *Mol Cell*, 30 (6):755-766.
- Molnar Z, Adams R, Blakemore C. 1998. Mechanisms underlying the early establishment of thalamocortical connections in the rat. *J Neurosci*, 18 (15):5723-5745.
- Monschau B, Kremoser C, Ohta K, Tanaka H, Kaneko T, Yamada T, Handwerker C, Hornberger MR, Loschinger J, Pasquale EB, Siever DA, Verderame MF, Muller BK, Bonhoeffer F, Drescher U. 1997. Shared and distinct functions of RAGS and ELF-1 in guiding retinal axons. *Embo J*, 16 (6):1258-1267.
- Monyer H, Lambolez B. 1995. Molecular biology and physiology at the single-cell level. *Curr Opin Neurobiol*, 5 (3):382-387.
- Morris SM, Albrecht U, Reiner O, Eichele G, Yu-Lee LY. 1998. The lissencephaly gene product Lis1, a protein involved in neuronal migration, interacts with a nuclear movement protein, NudC. *Curr Biol*, 8 (10):603-606.
- Mountcastle VB. 1997. The columnar organization of the neocortex. *Brain*, 120 (Pt 4):701-722.
- Murai KK, Pasquale EB. 2003. 'Eph'ective signaling: forward, reverse and crosstalk. *J Cell Sci*, 116 (Pt 14):2823-2832.
- Muramoto T, Cannon D, Gierlinski M, Corrigan A, Barton GJ, Chubb JR. 2012. Live imaging of nascent RNA dynamics reveals distinct types of transcriptional pulse regulation. *Proc Natl Acad Sci U S A*, 109 (19):7350-7355.
- Nadarajah B, Parnavelas JG. 2002. Modes of neuronal migration in the developing cerebral cortex. *Nat Rev Neurosci*, 3 (6):423-432.
- Nadarajah B, Brunstrom JE, Grutzendler J, Wong RO, Pearlman AL. 2001. Two modes of radial migration in early development of the cerebral cortex. *Nat Neurosci*, 4 (2):143-150.
- Nakayama M, Berger P. 2013. Coordination of VEGF receptor trafficking and signaling by coreceptors. *Exp Cell Res*, 319 (9):1340-1347.
- Nekrasova T, Jobes ML, Ting JH, Wagner GC, Minden A. 2008. Targeted disruption of the Pak5 and Pak6 genes in mice leads to deficits in learning and locomotion. *Dev Biol*, 322 (1):95-108.
- Nelson SB, Hempel C, Sugino K. 2006. Probing the transcriptome of neuronal cell types. *Curr Opin Neurobiol*, 16 (5):571-576.
- Nery S, Fishell G, Corbin JG. 2002. The caudal ganglionic eminence is a source of distinct cortical and subcortical cell populations. *Nat Neurosci*, 5 (12):1279-1287.
- Neves G, Shah MM, Liodis P, Achimastou A, Denaxa M, Roalfe G, Sesay A, Walker MC, Pachnis V. 2013. The LIM homeodomain protein Lhx6 regulates maturation of interneurons and network excitability in the mammalian cortex. *Cereb Cortex*, 23 (8):1811-1823.
- Nobrega-Pereira S, Kessar N, Du T, Kimura S, Anderson SA, Marin O. 2008. Postmitotic Nkx2-1 controls the migration of telencephalic interneurons by direct repression of guidance receptors. *Neuron*, 59 (5):733-745.
- Noctor SC, Martinez-Cerdeno V, Ivic L, Kriegstein AR. 2004. Cortical neurons arise in symmetric and asymmetric division zones and migrate through specific phases. *Nat Neurosci*, 7 (2):136-144.
- Noguchi H, Murao N, Kimura A, Matsuda T, Namihira M. 2016. DNA Methyltransferase 1 Is Indispensable for Development of the Hippocampal Dentate Gyrus. *36 (22):6050-6068*.
- North HA, Zhao X, Kolk SM, Clifford MA, Ziskind DM, Donoghue MJ. 2009. Promotion of proliferation in the developing cerebral cortex by EphA4 forward signaling. *Development*, 136 (14):2467-2476.
- O'Leary DD. 1989. Do cortical areas emerge from a protocortex? *Trends Neurosci*, 12 (10):400-406.

- Okayama H, Berg P. 1982. High-efficiency cloning of full-length cDNA. *Mol Cell Biol*, 2 (2):161-170.
- Olivier C, Cobos I, Perez Villegas EM, Spassky N, Zalc B, Martinez S, Thomas JL. 2001. Monofocal origin of telencephalic oligodendrocytes in the anterior entopeduncular area of the chick embryo. *Development*, 128 (10):1757-1769.
- Pacal M, Bremner R. 2012. Mapping differentiation kinetics in the mouse retina reveals an extensive period of cell cycle protein expression in post-mitotic newborn neurons. *Dev Dyn*, 241 (10):1525-1544.
- Padovan-Merhar O, Nair GP, Biaesch AG, Mayer A, Scarfone S, Foley SW, Wu AR, Churchman LS, Singh A, Raj A. 2015. Single mammalian cells compensate for differences in cellular volume and DNA copy number through independent global transcriptional mechanisms. *Mol Cell*, 58 (2):339-352.
- Parthasarathy S, Srivatsa S, Nityanandam A, Tarabykin V. 2014. Ntf3 acts downstream of Sip1 in cortical postmitotic neurons to control progenitor cell fate through feedback signaling. *Development*, 141 (17):3324-3330.
- Paxinos G. 2001. *The mouse brain in stereotaxic coordinates* / George Paxinos, Keith B.J. Franklin. San Diego, Calif. ; London: Academic.
- Pensold D. 2012. *ETABLIERUNG DER TRANSKRIPTOM-ANALYSE VON EMBRYONALEN INTERNEURON-SUBTYPEN AUF EINZELZELLEBENE [Diploma Thesis]*. ThULB Jena: Friedrich-Schiller-Universität Jena.
- Petalidis L, Bhattacharyya S, Morris GA, Collins VP, Freeman TC, Lyons PA. 2003. Global amplification of mRNA by template-switching PCR: linearity and application to microarray analysis. *Nucleic Acids Res*, 31 (22):e142.
- Petros TJ, Bultje RS, Ross ME, Fishell G, Anderson SA. 2015. Apical versus Basal Neurogenesis Directs Cortical Interneuron Subclass Fate. *Cell Rep*, 13 (6):1090-1095.
- Peyre E, Silva CG, Nguyen L. 2015. Crosstalk between intracellular and extracellular signals regulating interneuron production, migration and integration into the cortex. *Front Cell Neurosci*, 9:129.
- Phillips JK, Lipski J. 2000. Single-cell RT-PCR as a tool to study gene expression in central and peripheral autonomic neurones. *Auton Neurosci*, 86 (1-2):1-12.
- Pilz GA, Shitamukai A, Reillo I, Pacary E, Schwausch J, Stahl R, Ninkovic J, Snippert HJ, Clevers H, Godinho L, Guillemot F, Borrell V, Matsuzaki F, Gotz M. 2013. Amplification of progenitors in the mammalian telencephalon includes a new radial glial cell type. *Nat Commun*, 4:2125.
- Pitulescu ME, Adams RH. 2010. Eph/ephrin molecules--a hub for signaling and endocytosis. *Genes Dev*, 24 (22):2480-2492.
- Pla R, Borrell V, Flames N, Marin O. 2006. Layer acquisition by cortical GABAergic interneurons is independent of Reelin signaling. *J Neurosci*, 26 (26):6924-6934.
- Pollen AA, Nowakowski TJ, Shuga J, Wang X, Leyrat AA, Lui JH, Li N, Szpankowski L, Fowler B, Chen P, Ramalingam N, Sun G, Thu M, Norris M, Lebofsky R, Toppani D, Kemp DW, 2nd, Wong M, Clerkson B, Jones BN, Wu S, Knutsson L, Alvarado B, Wang J, Weaver LS, May AP, Jones RC, Unger MA, Kriegstein AR, West JA. 2014. Low-coverage single-cell mRNA sequencing reveals cellular heterogeneity and activated signaling pathways in developing cerebral cortex. *Nat Biotechnol*, 32 (10):1053-1058.
- Polleux F, Dehay C, Kennedy H. 1997. The timetable of laminar neurogenesis contributes to the specification of cortical areas in mouse isocortex. *J Comp Neurol*, 385 (1):95-116.
- Porteus MH, Bulfone A, Liu JK, Puellas L, Lo LC, Rubenstein JL. 1994. DLX-2, MASH-1, and MAP-2 expression and bromodeoxyuridine incorporation define molecularly distinct cell populations in the embryonic mouse forebrain. *J Neurosci*, 14 (11 Pt 1):6370-6383.
- Powell EM, Mars WM, Levitt P. 2001. Hepatocyte growth factor/scatter factor is a motogen for interneurons migrating from the ventral to dorsal telencephalon. *Neuron*, 30 (1):79-89.
- Pratt T, Quinn JC, Simpson TI, West JD, Mason JO, Price DJ. 2002. Disruption of early events in thalamocortical tract formation in mice lacking the transcription factors Pax6 or Foxg1. *J Neurosci*, 22 (19):8523-8531.

- Price DJ, Kennedy H, Dehay C, Zhou L, Mercier M, Jossin Y, Goffinet AM, Tissir F, Blakey D, Molnar Z. 2006. The development of cortical connections. *Eur J Neurosci*, 23 (4):910-920.
- Puelles L, Kuwana E, Puelles E, Bulfone A, Shimamura K, Keleher J, Smiga S, Rubenstein JL. 2000. Pallial and subpallial derivatives in the embryonic chick and mouse telencephalon, traced by the expression of the genes *Dlx-2*, *Emx-1*, *Nkx-2.1*, *Pax-6*, and *Tbr-1*. *J Comp Neurol*, 424 (3):409-438.
- Qi Y, Stapp D, Qiu M. 2002. Origin and molecular specification of oligodendrocytes in the telencephalon. *Trends Neurosci*, 25 (5):223-225.
- Qiu R, Wang X, Davy A, Wu C, Murai K, Zhang H, Flanagan JG, Soriano P, Lu Q, Hrsg. 2008. Regulation of neural progenitor cell state by ephrin-B. United States.
- Raj A, Peskin CS, Tranchina D, Vargas DY, Tyagi S. 2006. Stochastic mRNA synthesis in mammalian cells. *PLoS Biol*, 4 (10):e309.
- Rakic P. 1988. Specification of cerebral cortical areas. *Science*, 241 (4862):170-176.
- Rakic P. 1995. A small step for the cell, a giant leap for mankind: a hypothesis of neocortical expansion during evolution. *Trends Neurosci*, 18 (9):383-388.
- Rakic P. 2009. Evolution of the neocortex: a perspective from developmental biology. *Nat Rev Neurosci*, 10 (10):724-735.
- Rane CK, Minden A. 2014. P21 activated kinases: structure, regulation, and functions. *Small GTPases*, 5.
- Rashid T, Banerjee M, Nikolic M. 2001. Phosphorylation of Pak1 by the p35/Cdk5 kinase affects neuronal morphology. *J Biol Chem*, 276 (52):49043-49052.
- Razin A, Shemer R. 1995. DNA methylation in early development. *Hum Mol Genet*, 4 Spec No:1751-1755.
- Reid CB, Liang I, Walsh C. 1995. Systematic widespread clonal organization in cerebral cortex. *Neuron*, 15 (2):299-310.
- Reillo I, de Juan Romero C, Garcia-Cabezas MA, Borrell V. 2011. A role for intermediate radial glia in the tangential expansion of the mammalian cerebral cortex. *Cereb Cortex*, 21 (7):1674-1694.
- Remedios R, Huilgol D, Saha B, Hari P, Bhatnagar L, Kowalczyk T, Hevner RF, Suda Y, Aizawa S, Ohshima T, Stoykova A, Tole S. 2007. A stream of cells migrating from the caudal telencephalon reveals a link between the amygdala and neocortex. *Nat Neurosci*, 10 (9):1141-1150.
- Rhee KD, Yu J, Zhao CY, Fan G, Yang XJ. 2012. Dnmt1-dependent DNA methylation is essential for photoreceptor terminal differentiation and retinal neuron survival. *Cell Death Dis*, 3:e427.
- Rickmann M, Chronwall BM, Wolff JR. 1977. On the development of non-pyramidal neurons and axons outside the cortical plate: the early marginal zone as a pallial anlage. *Anat Embryol (Berl)*, 151 (3):285-307.
- Robertson KD. 2002. DNA methylation and chromatin - unraveling the tangled web. *Oncogene*, 21 (35):5361-5379.
- Robertson KD, Ait-Si-Ali S, Yokochi T, Wade PA, Jones PL, Wolffe AP. 2000. DNMT1 forms a complex with Rb, E2F1 and HDAC1 and represses transcription from E2F-responsive promoters. *Nat Genet*, 25 (3):338-342.
- Robinson MD, McCarthy DJ, Smyth GK. 2010. edgeR: a Bioconductor package for differential expression analysis of digital gene expression data. *Bioinformatics*, 26 (1):139-140.
- Roidl D, Hacker C. 2014. Histone methylation during neural development. *Cell Tissue Res*, 356 (3):539-552.
- Rossman KL, Der CJ, Sondek J. 2005. GEF means go: turning on RHO GTPases with guanine nucleotide-exchange factors. *Nat Rev Mol Cell Biol*, 6 (2):167-180.
- Rousso DL, Pearson CA, Gaber ZB, Miquelajauregui A, Li S, Portera-Cailliau C, Morrisey EE, Novitch BG. 2012. Foxp-mediated suppression of N-cadherin regulates neuroepithelial character and progenitor maintenance in the CNS. *Neuron*, 74 (2):314-330.
- Rubenstein JL, Merzenich MM. 2003. Model of autism: increased ratio of excitation/inhibition in key neural systems. *Genes Brain Behav*, 2 (5):255-267.

- Rudolph J, Zimmer G, Steinecke A, Barchmann S, Bolz J. 2010. Ephrins guide migrating cortical interneurons in the basal telencephalon. *Cell Adh Migr*, 4 (3):400-408.
- Rudolph J, Gerstmann K, Zimmer G, Steinecke A, Doding A, Bolz J. 2014. A dual role of EphB1/ephrin-B3 reverse signaling on migrating striatal and cortical neurons originating in the preoptic area: should I stay or go away? *Front Cell Neurosci*, 8:185.
- Ruediger T, Zimmer G, Barchmann S, Castellani V, Bagnard D, Bolz J. 2013. Integration of opposing semaphorin guidance cues in cortical axons. *Cereb Cortex*, 23 (3):604-614.
- Rymar VV, Sadikot AF. 2007. Laminar fate of cortical GABAergic interneurons is dependent on both birthdate and phenotype. *J Comp Neurol*, 501 (3):369-380.
- Saliba A-E, Westermann AJ, Gorski SA, Vogel J. 2014. Single-cell RNA-seq: advances and future challenges. *Nucleic acids research*, 42 (14):8845-8860.
- Samuels BA, Hsueh YP, Shu T, Liang H, Tseng HC, Hong CJ, Su SC, Volker J, Neve RL, Yue DT, Tsai LH. 2007. Cdk5 promotes synaptogenesis by regulating the subcellular distribution of the MAGUK family member CASK. *Neuron*, 56 (5):823-837.
- Sarkar D. 2008. *Lattice : multivariate data visualization with R*. New York: Springer.
- Seuntjens E, Nityanandam A, Miquelajauregui A, Debruyne J, Stryjewska A, Goebbels S, Nave KA, Huybreck D, Tarabykin V. 2009. Sip1 regulates sequential fate decisions by feedback signaling from postmitotic neurons to progenitors. *Nat Neurosci*, 12 (11):1373-1380.
- Shalek AK, Satija R, Adiconis X, Gertner RS, Gaublomme JT, Raychowdhury R, Schwartz S, Yosef N, Malboeuf C, Lu D, Trombetta JJ, Gennert D, Gnirke A, Goren A, Hacohen N, Levin JZ, Park H, Regev A. 2013. Single-cell transcriptomics reveals bimodality in expression and splicing in immune cells. *Nature*, 498 (7453):236-240.
- Shalek AK, Satija R, Shuga J, Trombetta JJ, Gennert D, Lu D, Chen P, Gertner RS, Gaublomme JT, Yosef N, Schwartz S, Fowler B, Weaver S, Wang J, Wang X, Ding R, Raychowdhury R, Friedman N, Hacohen N, Park H, May AP, Regev A. 2014. Single-cell RNA-seq reveals dynamic paracrine control of cellular variation. *Nature*, 510 (7505):363-369.
- Sharma A, Klein SS, Barboza L, Lohdi N, Toth M. 2016. Principles Governing DNA Methylation during Neuronal Lineage and Subtype Specification. *J Neurosci*, 36 (5):1711-1722.
- Shatz CJ, Luskin MB. 1986. The relationship between the geniculocortical afferents and their cortical target cells during development of the cat's primary visual cortex. *The Journal of neuroscience : the official journal of the Society for Neuroscience*, 6 (12):3655-3668.
- Skinner SO, Xu H, Nagarkar-Jaiswal S, Freire PR, Zwaka TP, Golding I. 2016. Single-cell analysis of transcription kinetics across the cell cycle. *Elife*, 5:e12175.
- Song J, Vranken W, Xu P, Gingras R, Noyce RS, Yu Z, Shen SH, Ni F. 2002. Solution structure and backbone dynamics of the functional cytoplasmic subdomain of human ephrin B2, a cell-surface ligand with bidirectional signaling properties. *Biochemistry*, 41 (36):10942-10949.
- Southwell DG, Nicholas CR, Basbaum AI, Stryker MP, Kriegstein AR, Rubenstein JL, Alvarez-Buylla A. 2014. Interneurons from embryonic development to cell-based therapy. *Science*, 344 (6180):1240622.
- Steinecke A, Gampe C, Zimmer G, Rudolph J, Bolz J. 2014. EphA/ephrin A reverse signaling promotes the migration of cortical interneurons from the medial ganglionic eminence. *Development*, 141 (2):460-471.
- Stocker AM, Chenn A. 2009. Focal reduction of alphaE-catenin causes premature differentiation and reduction of beta-catenin signaling during cortical development. *Dev Biol*, 328 (1):66-77.
- Stuhmer T, Anderson SA, Ekker M, Rubenstein JL. 2002. Ectopic expression of the *Dlx* genes induces glutamic acid decarboxylase and *Dlx* expression. *Development*, 129 (1):245-252.
- Takahashi T, Nowakowski RS, Caviness VS, Jr. 1996. The leaving or Q fraction of the murine cerebral proliferative epithelium: a general model of neocortical neuronogenesis. *J Neurosci*, 16 (19):6183-6196.
- Tang F, Barbacioru C, Wang Y, Nordman E, Lee C, Xu N, Wang X, Bodeau J, Tuch BB, Siddiqui A, Lao K, Surani MA. 2009. mRNA-Seq whole-transcriptome analysis of a single cell. *Nat Methods*, 6 (5):377-382.

- Taniguchi K, Kajiyama T, Kambara H. 2009. Quantitative analysis of gene expression in a single cell by qPCR. *Nat Methods*, 6 (7):503-506.
- Taniguchi Y, Choi PJ, Li GW, Chen H, Babu M, Hearn J, Emili A, Xie XS. 2010. Quantifying E. coli proteome and transcriptome with single-molecule sensitivity in single cells. *Science*, 329 (5991):533-538.
- Teissier A, Waclaw RR, Griveau A, Campbell K, Pierani A. 2012. Tangentially migrating transient glutamatergic neurons control neurogenesis and maintenance of cerebral cortical progenitor pools. *Cereb Cortex*, 22 (2):403-416.
- Tiberi L, Vanderhaeghen P, van den Aemele J. 2012. Cortical neurogenesis and morphogens: diversity of cues, sources and functions. *Curr Opin Cell Biol*, 24 (2):269-276.
- Tietjen I, Rihel JM, Cao Y, Koentges G, Zakhary L, Dulac C. 2003. Single-cell transcriptional analysis of neuronal progenitors. *Neuron*, 38 (2):161-175.
- Tiveron MC, Rossel M, Moepps B, Zhang YL, Seidenfaden R, Favor J, Konig N, Cremer H. 2006. Molecular interaction between projection neuron precursors and invading interneurons via stromal-derived factor 1 (CXCL12)/CXCR4 signaling in the cortical subventricular zone/intermediate zone. *J Neurosci*, 26 (51):13273-13278.
- Tokunaga A, Kohyama J, Yoshida T, Nakao K, Sawamoto K, Okano H. 2004. Mapping spatio-temporal activation of Notch signaling during neurogenesis and gliogenesis in the developing mouse brain. *Journal of neurochemistry*, 90 (1):142-154.
- Toma K, Kumamoto T, Hanashima C. 2014. The timing of upper-layer neurogenesis is conferred by sequential derepression and negative feedback from deep-layer neurons. *J Neurosci*, 34 (39):13259-13276.
- Torii M, Hashimoto-Torii K, Levitt P, Rakic P. 2009. Integration of neuronal clones in the radial cortical columns by EphA and ephrin-A signalling. *Nature*, 461 (7263):524-528.
- Torres R, Firestein BL, Dong H, Staudinger J, Olson EN, Hagan RL, Bredt DS, Gale NW, Yancopoulos GD. 1998. PDZ proteins bind, cluster, and synaptically colocalize with Eph receptors and their ephrin ligands. *Neuron*, 21 (6):1453-1463.
- Trapnell C, Cacchiarelli D, Grimsby J, Pokharel P, Li S, Morse M, Lennon NJ, Livak KJ, Mikkelsen TS. 2014. The dynamics and regulators of cell fate decisions are revealed by pseudotemporal ordering of single cells. *32 (4):381-386*.
- Treutlein B, Brownfield DG, Wu AR, Neff NF, Mantalas GL, Espinoza FH, Desai TJ, Krasnow MA, Quake SR. 2014. Reconstructing lineage hierarchies of the distal lung epithelium using single-cell RNA-seq. *Nature*, 509 (7500):371-375.
- Tuncdemir SN, Fishell G, Batista-Brito R. 2015. miRNAs are Essential for the Survival and Maturation of Cortical Interneurons. *Cereb Cortex*, 25 (7):1842-1857.
- Uziel D, Muhlfriedel S, Bolz J. 2008. Ephrin-A5 promotes the formation of terminal thalamocortical arbors. *Neuroreport*, 19 (8):877-881.
- Uziel D, Muhlfriedel S, Zarbalis K, Wurst W, Levitt P, Bolz J. 2002. Miswiring of limbic thalamocortical projections in the absence of ephrin-A5. *J Neurosci*, 22 (21):9352-9357.
- Valcanis H, Tan SS. 2003. Layer specification of transplanted interneurons in developing mouse neocortex. *J Neurosci*, 23 (12):5113-5122.
- van den Berghe V, Stappers E, Vandesande B, Dimidschstein J, Kroes R, Francis A, Conidi A, Lesage F, Dries R, Cazzola S, Berx G, Kessaris N, Vanderhaeghen P, van Ijcken W, Grosveld FG, Goossens S, Haigh JJ, Fishell G, Goffinet A, Aerts S, Huylebroeck D, Seuntjens E. 2013. Directed migration of cortical interneurons depends on the cell-autonomous action of sip1. *Neuron*, 77 (1):70-82.
- Vasistha NA, Garcia-Moreno F, Arora S, Cheung AF, Arnold SJ, Robertson EJ, Molnar Z. 2014. Cortical and Clonal Contribution of Tbr2 Expressing Progenitors in the Developing Mouse Brain. *Cereb Cortex*.
- Wagatsuma A, Sadamoto H, Kitahashi T, Lukowiak K, Urano A, Ito E. 2005. Determination of the exact copy numbers of particular mRNAs in a single cell by quantitative real-time RT-PCR. *Journal of Experimental Biology*, 208 (12):2389-2398.

- Waggott D, Chu K, Yin S, Wouters BG, Liu FF, Boutros PC. 2012. NanoStringNorm: an extensible R package for the pre-processing of NanoString mRNA and miRNA data. *Bioinformatics*, 28 (11):1546-1548.
- Wang DD, Kriegstein AR. 2009. Defining the role of GABA in cortical development. *J Physiol*, 587 (Pt 9):1873-1879.
- Wang HF, Liu FC. 2001. Developmental restriction of the LIM homeodomain transcription factor Islet-1 expression to cholinergic neurons in the rat striatum. *Neuroscience*, 103 (4):999-1016.
- Warren L, Bryder D, Weissman IL, Quake SR. 2006. Transcription factor profiling in individual hematopoietic progenitors by digital RT-PCR. *Proc Natl Acad Sci U S A*, 103 (47):17807-17812.
- Wei T, Wei MT. 2016. Package 'corrplot'. *Statistician*, 56:316-324.
- Wellenreuther R, Schupp I, Poustka A, Wiemann S, German c DNAC. 2004. SMART amplification combined with cDNA size fractionation in order to obtain large full-length clones. *BMC Genomics*, 5 (1):36.
- White AK, VanInsberghe M, Petriv OI, Hamidi M, Sikorski D, Marra MA, Piret J, Aparicio S, Hansen CL. 2011. High-throughput microfluidic single-cell RT-qPCR. *Proc Natl Acad Sci U S A*, 108 (34):13999-14004.
- Wichterle H, Alvarez-Dolado M, Erskine L, Alvarez-Buylla A. 2003. Permissive corridor and diffusible gradients direct medial ganglionic eminence cell migration to the neocortex. *Proc Natl Acad Sci U S A*, 100 (2):727-732.
- Wichterle H, Turnbull DH, Nery S, Fishell G, Alvarez-Buylla A. 2001. In utero fate mapping reveals distinct migratory pathways and fates of neurons born in the mammalian basal forebrain. *Development*, 128 (19):3759-3771.
- Wickham H. 2009. *ggplot2: elegant graphics for data analysis*. Springer Science & Business Media.
- Wilkinson DG. 2001. Multiple roles of EPH receptors and ephrins in neural development. *Nat Rev Neurosci*, 2 (3):155-164.
- Wonders CP, Anderson SA. 2006. The origin and specification of cortical interneurons. *Nat Rev Neurosci*, 7 (9):687-696.
- Wu H, Coskun V, Tao J, Xie W, Ge W, Yoshikawa K, Li E, Zhang Y, Sun YE. 2010. Dnmt3a-dependent nonpromoter DNA methylation facilitates transcription of neurogenic genes. *Science*, 329 (5990):444-448.
- Xing WJ, Liao XH, Wang N, Zhao DW, Zheng L, Zheng DL, Dong J, Zhang TC. 2015. MRTF-A and STAT3 promote MDA-MB-231 cell migration via hypermethylating BRSM1. *IUBMB Life*, 67 (3):202-217.
- Xu Q, Cobos I, De La Cruz E, Rubenstein JL, Anderson SA. 2004. Origins of cortical interneuron subtypes. *J Neurosci*, 24 (11):2612-2622.
- Xue Z, Huang K, Cai C, Cai L, Jiang CY, Feng Y, Liu Z, Zeng Q, Cheng L, Sun YE, Liu JY, Horvath S, Fan G. 2013. Genetic programs in human and mouse early embryos revealed by single-cell RNA sequencing. *Nature*, 500 (7464):593-597.
- Yan L, Yang M, Guo H, Yang L, Wu J, Li R, Liu P, Lian Y, Zheng X, Yan J, Huang J, Li M, Wu X, Wen L, Lao K, Li R, Qiao J, Tang F. 2013. Single-cell RNA-Seq profiling of human preimplantation embryos and embryonic stem cells. *Nat Struct Mol Biol*, 20 (9):1131-1139.
- Yao J, Zhou B, Zhang J, Geng P, Liu K, Zhu Y, Zhu W. 2014. A new tumor suppressor lncRNA ADAMTS9-AS2 is regulated by DNMT1 and inhibits migration of glioma cells. *Tumour Biol*, 35 (8):7935-7944.
- Yau HJ, Wang HF, Lai C, Liu FC. 2003. Neural development of the neuregulin receptor ErbB4 in the cerebral cortex and the hippocampus: preferential expression by interneurons tangentially migrating from the ganglionic eminences. *Cereb Cortex*, 13 (3):252-264.
- Yun ME, Johnson RR, Antic A, Donoghue MJ. 2003. EphA family gene expression in the developing mouse neocortex: regional patterns reveal intrinsic programs and extrinsic influence. *J Comp Neurol*, 456 (3):203-216.
- Zeisel A, Munoz-Manchado AB, Codeluppi S, Lonnerberg P, La Manno G, Jureus A, Marques S, Munguba H, He L, Betsholtz C, Rolny C, Castelo-Branco G, Hjerling-Leffler J, Linnarsson S. 2015. Brain

- structure. Cell types in the mouse cortex and hippocampus revealed by single-cell RNA-seq. *Science*, 347 (6226):1138-1142.
- Zeng B, Li Z, Chen R, Guo N, Zhou J, Zhou Q, Lin Q, Cheng D, Liao Q, Zheng L, Gong Y. 2012. Epigenetic regulation of miR-124 by hepatitis C virus core protein promotes migration and invasion of intrahepatic cholangiocarcinoma cells by targeting SMYD3. *FEBS Lett*, 586 (19):3271-3278.
- Zhang H, Webb DJ, Asmussen H, Niu S, Horwitz AF. 2005. A GIT1/PIX/Rac/PAK signaling module regulates spine morphogenesis and synapse formation through MLC. *J Neurosci*, 25 (13):3379-3388.
- Zhang J, Woodhead GJ, Swaminathan SK, Noles SR, McQuinn ER, Pisarek AJ, Stocker AM, Mutch CA, Funatsu N, Chenn A. 2010. Cortical neural precursors inhibit their own differentiation via N-cadherin maintenance of beta-catenin signaling. *Dev Cell*, 18 (3):472-479.
- Zhao W, Yang J, Shi W, Wu X, Shao B, Wu Q, Chen J, Ni L. 2011. Upregulation of p21-activated Kinase 6 in rat brain cortex after traumatic brain injury. *J Mol Histol*, 42 (3):195-203.
- Zhao Y, Flandin P, Long JE, Cuesta MD, Westphal H, Rubenstein JL. 2008. Distinct molecular pathways for development of telencephalic interneuron subtypes revealed through analysis of Lhx6 mutants. *J Comp Neurol*, 510 (1):79-99.
- Zhong JF, Chen Y, Marcus JS, Scherer A, Quake SR, Taylor CR, Weiner LP. 2008. A microfluidic processor for gene expression profiling of single human embryonic stem cells. *Lab on a Chip*, 8 (1):68-74.
- Zhou VW, Goren A, Bernstein BE. 2011. Charting histone modifications and the functional organization of mammalian genomes. *Nat Rev Genet*, 12 (1):7-18.
- Zhu J, He F, Wang J, Yu J. 2008. Modeling transcriptome based on transcript-sampling data. *PLoS One*, 3 (2):e1659.
- Zimmer G, Kastner B, Weth F, Bolz J. 2007. Multiple effects of ephrin-A5 on cortical neurons are mediated by SRC family kinases. *J Neurosci*, 27 (21):5643-5653.
- Zimmer G, Garcez P, Rudolph J, Niehage R, Weth F, Lent R, Bolz J. 2008. Ephrin-A5 acts as a repulsive cue for migrating cortical interneurons. *Eur J Neurosci*, 28 (1):62-73.
- Zimmer G, Schanuel SM, Burger S, Weth F, Steinecke A, Bolz J, Lent R. 2010. Chondroitin Sulfate Acts in Concert with Semaphorin 3A to Guide Tangential Migration of Cortical Interneurons in the Ventral Telencephalon. *Cereb Cortex*.
- Zimmer G, Rudolph J, Landmann J, Gerstmann K, Steinecke A, Gampe C, Bolz J. 2011. Bidirectional ephrinB3/EphA4 signaling mediates the segregation of medial ganglionic eminence- and preoptic area-derived interneurons in the deep and superficial migratory stream. *J Neurosci*, 31 (50):18364-18380.
- Zito A, Cartelli D, Cappelletti G, Cariboni A, Andrews W, Parnavelas J, Poletti A, Galbiati M. 2014. Neuritin 1 promotes neuronal migration. *Brain Struct Funct*, 219 (1):105-118.
- Zopf CJ, Quinn K, Zeidman J, Maheshri N. 2013. Cell-cycle dependence of transcription dominates noise in gene expression. *PLoS Comput Biol*, 9 (7):e1003161.

8 Appendix

8.1 Appendix Tables

NanoString codeset No1 – technical validation of triplicates and scPCR1 vs scPCR2								
No	Gene	Accession	Targ Region	Tm_CP	Tm_RP	PN (CP:RP)	NSID	Distance From 3' end
1	<i>Tubb3</i>	ENSMUST00000071134.1	845-945	85	85	368770;268770	ENSMUST00000071134.1:845	923
2	<i>Dbx1</i>	ENSMUST00000032717.1	1550-1650	80	82	368751;268751	ENSMUST00000032717.1:1550	441
3	<i>EfnA5</i>	ENSMUST00000076840.1	3483-3583	76	76	368744;268744	ENSMUST00000076840.1:3483	449
4	<i>Mki67</i>	ENSMUST00000033310.1	9447-9547	84	85	368761;268761	ENSMUST00000033310.1:9447	528
5	<i>Gad2</i>	ENSMUST00000028123.1	5372-5472	85	84	368745;268745	ENSMUST00000028123.1:5372	272
6	<i>Gad1</i>	ENSMUST00000094934.1	3178-3278	79	80	368763;268763	ENSMUST00000094934.1:3178	77
7	<i>Dnmt1</i>	NM_001199431.1	4481-4581	85	86	368759;268759	NM_001199431.1:4481	789
8	<i>Hmx3</i>	ENSMUST00000046093.1	1082-1182	85	85	368758;268758	ENSMUST00000046093.1:1082	275
9	<i>Cobl</i>	NM_172496.3	5073-5173	85	85	368766;268766	NM_172496.3:5073	460
10	<i>Nkx2-1</i>	ENSMUST0000001536.1	2379-2479	79	83	368755;268755	ENSMUST0000001536.1:2379	353
11	<i>Lhx6</i>	ENSMUST00000112966.1	2871-2971	83	85	368749;268749	ENSMUST00000112966.1:2871	220
12	<i>Actb</i>	ENSMUST00000100497.1	1197-1297	84	78	368769;268769	ENSMUST00000100497.1:1197	623
13	<i>Nrp2</i>	ENSMUST00000114157.1	5859-5959	83	83	368748;268748	ENSMUST00000114157.1:5859	398
14	<i>Epha4</i>	ENSMUST00000027451.1	5750-5850	79	79	368762;268762	ENSMUST00000027451.1:5750	478
15	<i>Isl1</i>	ENSMUST00000036060.1	2074-2174	75	79	368767;268767	ENSMUST00000036060.1:2074	341
16	<i>Efnb3</i>	ENSMUST00000004036.1	2707-2807	86	85	368760;268760	ENSMUST00000004036.1:2707	376
17	<i>Pax6</i>	NM_013627.4	1726-1826	85	85	368772;268772	NM_013627.4:1726	724
18	<i>Gapdh</i>	ENSMUST00000118875.1	1052-1152	85	85	368768;268768	ENSMUST00000118875.1:1052	268
19	<i>Pcdh1</i>	ENSMUST00000057185.1	3040-3140	86	85	368764;268764	ENSMUST00000057185.1:3040	762
20	<i>Pcdh10</i>	ENSMUST00000051181.1	3694-3794	86	85	368750;268750	ENSMUST00000051181.1:3694	173
21	<i>Pcdh10</i>	ENSMUST00000170695.1	7978-8078	79	82	368752;268752	ENSMUST00000170695.1:7978	185
22	<i>Pcdh17</i>	ENSMUST00000071370.1	8934-9034	77	81	368743;268743	ENSMUST00000071370.1:8934	475
23	<i>Pcdh9</i>	ENSMUST00000068992.1	3383-3483	82	83	368771;268771	ENSMUST00000068992.1:3383	231
24	<i>Cdh4</i>	ENSMUST00000000314.1	5858-5958	86	86	368741;268741	ENSMUST00000000314.1:5858	430
25	<i>Btg2</i>	NM_007570.2	2418-2518	83	77	368899;268899	NM_007570.2:2418	665
26	<i>Nes</i>	ENSMUST00000090973.1	5598-5698	85	85	368747;268747	ENSMUST00000090973.1:5598	428
27	<i>Eomes</i>	ENSMUST00000035020.1	2667-2767	78	83	368765;268765	ENSMUST00000035020.1:2667	793
28	<i>Nrp1</i>	ENSMUST00000026917.1	5352-5452	78	81	368746;268746	ENSMUST00000026917.1:5352	455
29	<i>Calb1</i>	ENSMUST00000029876.1	3788-3888	83	80	368742;268742	ENSMUST00000029876.1:3788	334
30	<i>Cdh8</i>	NM_007667.2	2861-2961	86	85	368756;268756	NM_007667.2:2861	197
31	<i>Cdh8</i>	NM_001039154.1	3356-3456	79	78	368754;268754	NM_001039154.1:3356	352
32	<i>Calb1</i>	NM_009788.4	2370-2470	83	77	368898;268898	NM_009788.4:2370	497

Appendix Table 1 - Summary of the NanoString Codeset No1. providing information on gene names, accession numbers, target region and the distance from the 3' end for the probes included. Hybridization temperature for capture probe (Tm_CP) and reporter probe (Tm_RP).

NanoString codeset No2 – validation of representative amplification and scPCR1 vs scPCR2								
No	Gene	Accession	Targ Region	Tm_CP	Tm_RP	PN (CP:RP)	NSID	Distance From 3' end
1	<i>Agrn</i>	NM_021604.3	7155-7255	82	81	367356;267356	NM_021604.3:7155	224
2	<i>Atp5a1</i>	NM_007505.2	1854-1954	82	81	384125;284125	NM_007505.2:1854	589
3	<i>Crrmp1</i>	NM_007765.3	2360-2460	86	86	384120;284120	NM_007765.3:2360	567
4	<i>Dbn1</i>	NM_019813.4	2570-2670	85	80	384110;284110	NM_019813.4:2570	336
5	<i>Dcx</i>	NM_010025.2	8575-8675	77	81	384122;284122	NM_010025.2:8575	407
6	<i>Ddx17</i>	NM_199080.2	4485-4585	79	83	337035;237035	NM_199080.2:4485	287
7	<i>Eef2</i>	NM_007907.2	2855-2955	85	77	384106;284106	NM_007907.2:2855	271
8	<i>Gnas</i>	NM_201616.1	1513-1613	79	82	384116;284116	NM_201616.1:1513	249
9	<i>Gnb1</i>	NM_008142.4	2891-2991	82	85	384121;284121	NM_008142.4:2891	252
10	<i>Hspa8</i>	NM_031165.4	1668-1768	85	83	384124;284124	NM_031165.4:1668	436
11	<i>Lars2</i>	NM_153168.2	3523-3623	84	79	384119;284119	NM_153168.2:3523	358
12	<i>Maged1</i>	NM_019791.2	2496-2596	80	80	384127;284127	NM_019791.2:2496	256
13	<i>Malat1</i>	NR_002847.2	6781-6881	81	79	384115;284115	NR_002847.2:6781	201
14	<i>Map4k4</i>	NM_008696.2	5254-5354	86	85	384117;284117	NM_008696.2:5254	366
15	<i>Marcks</i>	NM_008538.2	3666-3766	82	78	384112;284112	NM_008538.2:3666	520
16	<i>Mtap1b</i>	NM_008634.2	11370-11470	81	85	384107;284107	NM_008634.2:11370	482
17	<i>Mtap2</i>	NM_008632.2	5243-5343	78	77	384123;284123	NM_008632.2:5243	202
18	<i>Nedd4</i>	NM_010890.3	5107-5207	79	78	384108;284108	NM_010890.3:5107	387
19	<i>Nisch</i>	NM_022656.2	5338-5438	83	85	384128;284128	NM_022656.2:5338	268
20	<i>Nnat</i>	NM_010923.2	684-784	84	86	384114;284114	NM_010923.2:684	539
21	<i>Ptma</i>	NM_008972.2	833-933	79	76	384105;284105	NM_008972.2:833	359
22	<i>Ptprs</i>	NM_011218.2	6356-6456	81	82	384126;284126	NM_011218.2:6356	518
23	<i>Scd2</i>	NM_009128.2	5187-5287	79	80	384103;284103	NM_009128.2:5187	266
24	<i>Smarca4</i>	NM_011417.3	6204-6304	86	81	384111;284111	NM_011417.3:6204	163
25	<i>Sox11</i>	NM_009234.6	8177-8277	84	83	384109;284109	NM_009234.6:8177	274

No	Gene	Accession	Targ Region	Tm_CP	Tm_RP	PN (CP:RP)	NSID	Distance From 3' end
26	<i>Spna2</i>	NM_001177667.1	7553-7653	86	82	384118;284118	NM_001177667.1:7553	486
27	<i>Srrm2</i>	NM_175229.3	8361-8461	82	78	384113;284113	NM_175229.3:8361	252
28	<i>Tmsb4x</i>	NM_021278.2	347-447	80	86	384104;284104	NM_021278.2:347	323
29	<i>Tuba1b</i>	NM_011654.2	1426-1526	83	71	384102;284102	NM_011654.2:1426	321
30	<i>Tuba1c</i>	NM_009448.4	1812-1912	87	80	384101;284101	NM_009448.4:1812	165
31	<i>Tubb2b</i>	NM_023716.2	1438-1538	88	89	329645;229645	NM_023716.2:1438	484
32	<i>Tubb5</i>	NM_011655.4	2260-2360	79	82	309903;209903	NM_011655.4:2260	314

Appendix Table 2 - Summary of the NanoString Codeset No2. List of gene names, accession numbers, selected target regions and the distance from the 3' end for the probes included. Hybridization temperature for capture probe (Tm_CP) and reporter probe (Tm_RP).

NanoString codeset No3 – Interneuron profiling and scPCR1 vs scPCR2								
No	Gene	Accession	Targ Region	Tm_CP	Tm_RP	PN (CP:RP)	NSID	Distance From 3' end
1	<i>Trp73</i>	ENSMUST00000133533.1	4469-4569	86	81	376988;276988	ENSMUST00000133533.1:4469	283
2	<i>Lhx5</i>	ENSMUST00000031591.1	2345-2445	86	86	377021;277021	ENSMUST00000031591.1:2345	505
3	<i>Nhlh2</i>	ENSMUST00000066187.1	3166-3266	83	76	376973;276973	ENSMUST00000066187.1:3166	187
4	<i>Tbr1</i>	ENSMUST00000048934.1	3380-3480	75	75	377143;277143	ENSMUST00000048934.1:3380	597
5	<i>Onecut3</i>	ENSMUST00000051773.1	4344-4444	75	89	377148;277148	ENSMUST00000051773.1:4344	432
6	<i>Otp</i>	ENSMUST00000022195.1	586-686	86	86	377152;277152	ENSMUST00000022195.1:586	596
7	<i>Lhx1</i>	ENSMUST00000018842.1	4196-4296	77	82	377026;277026	ENSMUST00000018842.1:4196	437
8	<i>Onecut1</i>	ENSMUST00000056006.1	3191-3291	85	77	377018;277018	ENSMUST00000056006.1:3191	460
9	<i>Insm2</i>	ENSMUST00000051857.1	2847-2947	80	80	377012;277012	ENSMUST00000051857.1:2847	255
10	<i>Lhx9</i>	ENSMUST00000019374.1	4579-4679	84	76	376976;276976	ENSMUST00000019374.1:4579	358
11	<i>Zic4</i>	ENSMUST00000066384.1	3550-3650	76	76	376965;276965	ENSMUST00000066384.1:3550	341
12	<i>Zic5</i>	ENSMUST00000039118.1	4312-4412	75	75	377155;277155	ENSMUST00000039118.1:4312	455
13	<i>Zic2</i>	ENSMUST00000075888.1	2207-2307	76	79	376982;276982	ENSMUST00000075888.1:2207	233
14	<i>Hmx3</i>	ENSMUST00000046093.1	1088-1188	85	86	376993;276993	ENSMUST00000046093.1:1088	369
15	<i>Barhl2</i>	ENSMUST00000086795.1	2126-2226	92	90	377142;277142	ENSMUST00000086795.1:2126	471
16	<i>Dbx1</i>	ENSMUST00000032717.1	1826-1926	76	78	376966;276966	ENSMUST00000032717.1:1826	265
17	<i>Hmx2</i>	ENSMUST00000051997.1	1276-1376	79	83	377016;277016	ENSMUST00000051997.1:1276	393
18	<i>Neurog2</i>	ENSMUST00000029587.1	1988-2088	76	82	376995;276995	ENSMUST00000029587.1:1988	238
19	<i>Zfp804a</i>	ENSMUST00000047527.1	4071-4171	78	80	376951;276951	ENSMUST00000047527.1:4071	549
20	<i>Fezf1</i>	ENSMUST00000031709.1	1762-1862	80	76	376981;276981	ENSMUST00000031709.1:1762	546
21	<i>Ebf3</i>	ENSMUST00000106118.1	4521-4621	79	86	377019;277019	ENSMUST00000106118.1:4521	500
22	<i>Zic3</i>	ENSMUST00000088627.1	3750-3850	76	77	377028;277028	ENSMUST00000088627.1:3750	199
23	<i>Onecut2</i>	ENSMUST00000115145.1	13140-13240	85	76	376975;276975	ENSMUST00000115145.1:13140	249
24	<i>Rasgrp1</i>	ENSMUST00000102534.1	4971-5071	81	83	377161;277161	ENSMUST00000102534.1:4971	258
25	<i>Ppp2r2c</i>	ENSMUST00000031003.1	3896-3996	85	76	376952;276952	ENSMUST00000031003.1:3896	192
26	<i>Reln</i>	ENSMUST00000161356.1	11133-11233	74	76	377140;277140	ENSMUST00000161356.1:11133	566
27	<i>Dlg2</i>	ENSMUST00000107196.1	4956-5056	78	77	376989;276989	ENSMUST00000107196.1:4956	290
28	<i>Lin7a</i>	ENSMUST00000020057.1	5617-5717	78	77	377006;277006	ENSMUST00000020057.1:5617	258
29	<i>Radil</i>	ENSMUST00000063635.1	3288-3388	82	85	376949;276949	ENSMUST00000063635.1:3288	412
30	<i>Pak6</i>	ENSMUST00000099557.1	4203-4303	76	77	377005;277005	ENSMUST00000099557.1:4203	208
31	<i>Rcan2</i>	ENSMUST00000044895.1	3052-3152	80	86	376999;276999	ENSMUST00000044895.1:3052	311
32	<i>Spry1</i>	ENSMUST00000108109.1	2031-2131	79	83	377007;277007	ENSMUST00000108109.1:2031	420
33	<i>Ppp2r2b</i>	ENSMUST00000117687.1	1690-1790	79	76	376958;276958	ENSMUST00000117687.1:1690	581
34	<i>Samd3</i>	ENSMUST00000060716.1	1572-1672	81	78	376977;276977	ENSMUST00000060716.1:1572	302
35	<i>Nxph4</i>	ENSMUST00000095266.1	1409-1509	85	81	376950;276950	ENSMUST00000095266.1:1409	266
36	<i>Shisa6</i>	ENSMUST00000123454.1	6767-6867	84	76	377154;277154	ENSMUST00000123454.1:6767	485
37	<i>Rmst</i>	ENSMUST00000137229.1	2280-2380	83	76	377156;277156	ENSMUST00000137229.1:2280	407
38	<i>Trank1</i>	ENSMUST00000078626.1	10064-10164	85	86	376968;276968	ENSMUST00000078626.1:10064	455
39	<i>Fam70a</i>	ENSMUST00000089056.1	1119-1219	80	80	377160;277160	ENSMUST00000089056.1:1119	626
40	<i>3110035E14Rik</i>	ENSMUST00000088666.1	2943-3043	78	78	376964;276964	ENSMUST00000088666.1:2943	313
41	<i>Wdr52</i>	ENSMUST00000099742.1	6030-6130	83	83	377011;277011	ENSMUST00000099742.1:6030	553
42	<i>Ccdc184</i>	ENSMUST00000031914.1	2144-2244	85	84	376990;276990	ENSMUST00000031914.1:2144	185
43	<i>Nrn1</i>	ENSMUST00000037623.1	1280-1380	85	77	376998;276998	ENSMUST00000037623.1:1280	339
44	<i>Chl1</i>	ENSMUST00000066905.1	7254-7354	77	76	377001;277001	ENSMUST00000066905.1:7254	497
45	<i>Ntng1</i>	ENSMUST00000156177.1	2619-2719	81	76	377000;277000	ENSMUST00000156177.1:2619	253
46	<i>Lingo1</i>	ENSMUST00000053568.1	3123-3223	86	85	376972;276972	ENSMUST00000053568.1:3123	172
47	<i>Dscam</i>	ENSMUST00000056102.1	7215-7315	85	84	376984;276984	ENSMUST00000056102.1:7215	283
48	<i>Lrrc4c</i>	ENSMUST00000135431.1	3460-3560	80	76	376986;276986	ENSMUST00000135431.1:3460	186
49	<i>Ptprt</i>	ENSMUST00000109443.1	11741-11841	85	76	376985;276985	ENSMUST00000109443.1:11741	371
50	<i>Tmem150c</i>	ENSMUST00000063192.1	2768-2868	76	78	376962;276962	ENSMUST00000063192.1:2768	316
51	<i>Igsf21</i>	ENSMUST00000039331.1	1687-1787	84	85	376969;276969	ENSMUST00000039331.1:1687	292
52	<i>Ret</i>	ENSMUST00000032201.1	5682-5782	85	81	377013;277013	ENSMUST00000032201.1:5682	382
53	<i>Camk2b</i>	ENSMUST00000109813.1	3673-3773	84	76	377004;277004	ENSMUST00000109813.1:3673	350
54	<i>Cacna1d</i>	ENSMUST00000112250.1	8414-8514	85	80	377158;277158	ENSMUST00000112250.1:8414	266
55	<i>Fgf17</i>	ENSMUST00000022697.1	1283-1383	85	85	377008;277008	ENSMUST00000022697.1:1283	404
56	<i>Nefl</i>	ENSMUST00000022639.1	3197-3297	79	77	376997;276997	ENSMUST00000022639.1:3197	183

No	Gene	Accession	Targ Region	Tm_CP	Tm_RP	PN (CP:RP)	NSID	Distance From 3' end
57	<i>Snhg11</i>	ENSMUST00000109488.1	5487-5587	79	79	377017;277017	ENSMUST00000109488.1:5487	377
58	<i>Tnfrsf6</i>	ENSMUST00000065927.1	1152-1252	86	79	377151;277151	ENSMUST00000065927.1:1152	558
59	<i>Bmper</i>	ENSMUST00000071982.1	3524-3624	81	76	376970;276970	ENSMUST00000071982.1:3524	269
60	<i>Rgcc</i>	ENSMUST00000022595.1	363-463	85	84	376957;276957	ENSMUST00000022595.1:363	555
61	<i>Wis</i>	ENSMUST00000068952.1	2784-2884	85	78	376996;276996	ENSMUST00000068952.1:2784	520
62	<i>Peli2</i>	ENSMUST00000073150.1	5666-5766	84	77	377002;277002	ENSMUST00000073150.1:5666	183
63	<i>Maf</i>	ENSMUST00000069009.1	3001-3101	77	76	377022;277022	ENSMUST00000069009.1:3001	222
64	<i>Sp9</i>	ENSMUST00000090813.1	4319-4419	86	85	376971;276971	ENSMUST00000090813.1:4319	195
65	<i>Tcf4</i>	ENSMUST00000078486.1	6890-6990	70	73	377141;277141	ENSMUST00000078486.1:6890	257
66	<i>Zeb2</i>	ENSMUST00000068415.1	8690-8790	77	79	376963;276963	ENSMUST00000068415.1:8690	423
67	<i>Lmo1</i>	ENSMUST00000036992.1	614-714	85	77	376991;276991	ENSMUST00000036992.1:614	457
68	<i>Zfp704</i>	ENSMUST00000041124.1	13647-13747	85	76	376948;276948	ENSMUST00000041124.1:13647	196
69	<i>Dleu7</i>	ENSMUST00000063169.1	734-834	76	76	377020;277020	ENSMUST00000063169.1:734	596
71	<i>Abrac1</i>	ENSMUST00000020002.1	378-478	76	77	377153;277153	ENSMUST00000020002.1:378	429
72	<i>Glicc1</i>	ENSMUST00000064285.1	5620-5720	89	89	377149;277149	ENSMUST00000064285.1:5620	580
73	<i>Sh3rf3</i>	ENSMUST00000153031.1	5437-5537	85	85	377009;277009	ENSMUST00000153031.1:5437	245
74	<i>Pcdh19</i>	ENSMUST00000167944.1	9554-9654	77	86	377023;277023	ENSMUST00000167944.1:9554	594
76	<i>Rbfox3</i>	ENSMUST00000117731.1	2917-3017	86	83	376960;276960	ENSMUST00000117731.1:2917	167
77	<i>Tubb3</i>	ENSMUST00000071134.1	1477-1577	88	88	377147;277147	ENSMUST00000071134.1:1477	391
78	<i>Cdh8 (Iso1)</i>	NM_001039154.1	3215-3315	72	71	377166;277166	NM_001039154.1:3215	593
79	<i>Cdh8 (Iso2)</i>	NM_007667.2	2861-2961	86	85	368756;268756	NM_007667.2:2861	297
80	<i>Cdh4</i>	ENSMUST00000000314.1	5858-5958	86	86	368741;268741	ENSMUST00000000314.1:5858	530
81	<i>Cobl</i>	NM_172496.3	5073-5173	85	85	368766;268766	NM_172496.3:5073	560
82	<i>Dnmt1 (B)</i>	ENSMUST00000004202.1	4949-5049	85	85	377010;277010	ENSMUST00000004202.1:4949	421
83	<i>Epha4</i>	ENSMUST00000027451.1	5750-5850	79	79	368762;268762	ENSMUST00000027451.1:5750	578
84	<i>Gapdh</i>	ENSMUST00000118875.1	1052-1152	85	85	368768;268768	ENSMUST00000118875.1:1052	368
85	<i>Gad2</i>	ENSMUST00000028123.1	5372-5472	85	84	368745;268745	ENSMUST00000028123.1:5372	372
86	<i>Gad1</i>	ENSMUST00000094934.1	3178-3278	79	80	368763;268763	ENSMUST00000094934.1:3178	177
87	<i>Isl1</i>	ENSMUST00000036060.1	2074-2174	75	79	368767;268767	ENSMUST00000036060.1:2074	441
88	<i>Mki67</i>	ENSMUST00000033310.1	9447-9547	84	85	368761;268761	ENSMUST00000033310.1:9447	628
89	<i>Lhx6</i>	ENSMUST00000112966.1	2871-2971	83	85	368749;268749	ENSMUST00000112966.1:2871	320
90	<i>Nes</i>	ENSMUST00000090973.1	5598-5698	85	85	368747;268747	ENSMUST00000090973.1:5598	528
91	<i>Nkx2-1</i>	ENSMUST00000001536.1	2379-2479	79	83	368755;268755	ENSMUST00000001536.1:2379	453
92	<i>Nrp1</i>	ENSMUST00000026917.1	5379-5479	79	77	377164;277164	ENSMUST00000026917.1:5379	528
93	<i>Nrp2</i>	ENSMUST00000114157.1	5859-5959	83	83	368748;268748	ENSMUST00000114157.1:5859	498
94	<i>Pcdh10 (Iso1)</i>	ENSMUST00000051181.1	3694-3794	86	85	368750;268750	ENSMUST00000051181.1:3694	273
95	<i>Pcdh10 (Iso3)</i>	ENSMUST00000170695.1	7978-8078	79	82	368752;268752	ENSMUST00000170695.1:7978	285
96	<i>Pcdh9</i>	ENSMUST00000068992.1	3254-3354	85	84	377015;277015	ENSMUST00000068992.1:3254	460
97	<i>Actb</i>	ENSMUST00000100497.1	1616-1716	88	75	377145;277145	ENSMUST00000100497.1:1616	304
98	<i>Efnb3</i>	ENSMUST00000004036.1	2707-2807	86	85	368760;268760	ENSMUST00000004036.1:2707	476

Appendix Table 3 - Summary of the NanoString Codeset No3. providing information on gene names, accession numbers, target region and the distance from the 3' end for the probes included. Hybridization temperature for capture probe (Tm_CP) and reporter probe (Tm_RP).

number	Gene	mean counts in RNA	theoretical transcript counts per dilution		
			5pg	50pg	300pg
1	<i>Lars2</i>	393	0.8	7.9	39.3
2	<i>Malat1</i>	644	1.3	12.9	64.5
3	<i>Tuba1c</i>	766	1.5	15.3	76.7
4	<i>Nisch</i>	1404	2.8	28.1	140.5
5	<i>Dbn1</i>	1708	3.4	34.2	170.9
6	<i>Map4k4</i>	2342	4.7	46.9	234.4
7	<i>Sox11</i>	2945	5.9	59.0	294.8
8	<i>Srrm2</i>	2957	5.9	59.2	296.0
9	<i>Gnb1</i>	5004	10.0	100.2	500.9
10	<i>Tubb5</i>	5382	10.8	107.7	538.7
11	<i>Agrn</i>	5506	11.0	110.2	551.2
12	<i>Spna2</i>	6604	13.2	132.2	661.1
13	<i>Ddx17</i>	10564	21.1	211.5	1057.4
14	<i>Mtap1b</i>	12776	25.6	255.8	1278.9
15	<i>Maged1</i>	14282	28.6	285.9	1429.6
16	<i>Scd2</i>	14642	29.3	293.1	1465.6
17	<i>Mtap2</i>	14867	29.8	297.6	1488.2
18	<i>Gnas</i>	15487	31.0	310.1	1550.3
19	<i>Dcx</i>	16144	32.3	323.2	1616.0
20	<i>Nedd4</i>	18094	36.2	362.2	1811.2
21	<i>Tuba1b</i>	20066	40.2	401.7	2008.6
22	<i>Hspa8</i>	22642	45.3	453.3	2266.5
23	<i>Tubb2b</i>	26048	52.1	521.5	2607.4
24	<i>Eef2</i>	35367	70.8	708.0	3540.2
25	<i>Tmsb4x</i>	67125	134.4	1343.8	6719.2
26	<i>Ptma</i>	73275	146.7	1467.0	7334.9

Appendix Table 4 - Theoretical transcript copy numbers for genes in the diluted RNA samples serving as template for amplification that were used for the validation of the representative amplification. Theoretical gene copy number calculations were based on actual counts detected in the original tissue RNA (mean counts in RNA) with the validation codeset (**Appendix Tab. 2**), considering the dilution factor and the observation that about 1% of the transcript species are detected by NanoString (Geiss et al. 2008). Transcript copy numbers < 10, < 100 and < 1000 are highlighted in red, green and blue, respectively. Gene copy numbers > 1000 are in black.

8.2 Index of Figures

Figure 1 - Cortical projection neuron development.	6
Figure 2 - Multiple dimensions of interneuron diversity.	9
Figure 3 - Interneuron subtypes are generated from discrete proliferative regions within the subpallium.	10
Figure 4 - General features and binding abilities of Eph receptors and ephrines.	17
Figure 5 - Overview of NanoString nCounter gene expression system.	20
Figure 6 - Validation of <i>Pak6</i> siRNA knockdown efficiency in COS-7 cells.	27
Figure 7 - NanoString reproducibility for non-purified single cell cDNAs.	36
Figure 8 - Schematic workflow of the experimental design.	42
Figure 9 - NanoString-based validation of transcript abundance relationships in amplified cDNA libraries from single-cell RNA equivalents.	43
Figure 10 - Validation of second round amplification.	45
Figure 11 - <i>EfnA5</i> effects on cortical cells and expression pattern at single cell level.	47
Figure 12 - Evidence for <i>EfnA5</i> expression in thalamic axons.	50
Figure 13 - Ephrin A-ligand expressing thalamic fibers regulate progenitor proliferation.	51
Figure 14 - Gene expression profiles of MGE- and POA-derived cells revealed by NanoString-based single-cell transcriptomics.	54
Figure 15 - The contribution of different principal components to the segregation of distinct cellular subsets.	55
Figure 16 - Differential gene expression analysis of Cluster I to III reveal different maturational stages of MGE-derived cells.	57
Figure 17 - Cluster IV represents pallial derived excitatory neurons settle into the POA.	59
Figure 18 - POA-derived interneurons are enriched in Cluster V and VI.	60
Figure 19 - <i>Pak6</i> expression alters morphology and is negatively correlated with <i>Dnmt1</i> expression.	62
Figure 20 - <i>Dnmt1</i> expression in single cells correlated with cell motion associated genes and was detected in migrating POA-derived GABAergic interneurons.	64
Figure 21 - Validation of <i>Dnmt1</i> deletion in <i>Hmx3-Cre/tdTomato/Dnmt1 loxP²</i> mice.	65
Figure 22 - <i>Dnmt1</i> deficiency in post-mitotic POA-derivates reduces cortical interneuron number.	66
Figure 23 - Illustration of the tdTomato cells in different regions of the adult brains of <i>Hmx3-Cre/tdTomato/Dnmt1 wild-type</i> and <i>Hmx3-Cre/tdTomato/Dnmt1 loxP²</i> mice.	67
Figure 24 - Postmitotic <i>Dnmt1</i> deletion in POA-derived interneurons leads to migratory defects during embryonic development.	69
Figure 25 - <i>Dnmt1</i> -deficient <i>Hmx3-Cre/tdTomato</i> cells exhibit maturation specific gene expression.	71

8.3 Index of Table

Table 1 - PCR conditions for genotyping	29
Table 2 - Primer sequences, used temperature and resulting fragment size for qRT-PCR.	29
Table 3 - Primer sequences, used temperature and resulting fragment size for 3'limited cDNA libraries.	32
Table 4 - Primer sequences used to create in situ probes.	39
Table 5 - Summary of fold-changes.	44
Appendix Table 1 - Summary of the NanoString Codeset No1.	XX
Appendix Table 2 - Summary of the NanoString Codeset No2.	XXI
Appendix Table 3 - Summary of the NanoString Codeset No3.	XXII
Appendix Table 4 - Theoretical transcript copy numbers.	XXIII

8.4 Ehrenwörtliche Erklärung

Hiermit erkläre ich, dass mir die Promotionsordnung der Medizinischen Fakultät der Friedrich-Schiller-Universität bekannt ist, ich die Dissertation selbst angefertigt habe und alle von mir benutzten Hilfsmittel, persönlichen Mitteilungen und Quellen in meiner Arbeit angegeben sind, mich folgende Personen bei der Auswahl und Auswertung des Materials sowie bei der Herstellung des Manuskripts unterstützt haben:

Dr. G. Zimmer, J. Symmank, A. Hahn,

die Hilfe eines Promotionsberaters nicht in Anspruch genommen wurde und dass Dritte weder unmittelbar noch mittelbar geldwerte Leistungen von mir für Arbeiten erhalten haben, die im Zusammenhang mit dem Inhalt der vorgelegten Dissertation stehen, dass ich die Dissertation noch nicht als Prüfungsarbeit für eine staatliche oder andere wissenschaftliche Prüfung eingereicht habe und dass ich die gleiche, eine in wesentlichen Teilen ähnliche oder eine andere Abhandlung nicht bei einer anderen Hochschule als Dissertation eingereicht habe.

Ort, Datum

Unterschrift des Verfassers

8.5 Danksagung

An dieser Stelle möchte ich mich bei all denen bedanken, die mich während meiner akademischen Laufbahn beruflich und privat unterstützt haben. Zunächst möchte mich ganz herzlich bei Dr. Geraldine Zimmer bedanken, die mir die Möglichkeit gab, in Ihrer Arbeitsgruppe eine hochinteressante und anspruchsvolle Dissertation anzufertigen. In diesem Zusammenhang möchte ich mich auch für ihre fachliche Betreuung, die konstruktiven Vorschläge und interessanten Diskussionen, welche den Projekten stets neue Impulse gegeben haben, bedanken.

Herrn Prof. Dr. A. Baniahmad möchte ich für die Begutachtung der Dissertation sowie für seine Funktion als Zweitbetreuer meinen Dank aussprechen. Ebenfalls bedanke ich mich bei meinem 3. Gutachter für seine Zeit und Bemühungen.

Mein besonderer Dank gilt auch Prof. Dr. C.A. Hübner für die Möglichkeit die Promotion an seinem Institut durchzuführen und den Arbeitsgruppen funktionelle Genetik I und II für die freundliche Zusammenarbeit und die Hilfsbereitschaft bei jeglichen wissenschaftlichen und technischen Fragestellungen. Insbesondere gilt mein Dank dabei meinen Labor-Genossin Judit Symmank, Katrin Gerstmann sowie Anne Hahn, mit denen die tägliche Arbeit nicht nur produktiv, sondern stets auch erheiternd und motivierend war. In diesem Rahmen möchte ich mich auch für Ihre Beteiligung an den in dieser Arbeit vorgestellten Projekten bedanken. Außerdem möchte ich auch allen übrigen Mitarbeitern des Instituts für die freundliche Zusammenarbeit und das angenehme Arbeitsklima danken.

Des Weiteren möchte ich mich bei Prof. Dr. Tomas Pieler, Dr. Gabriela Salinas-Riester und dem Team des Transkriptom-Analyselabors Göttingen bedanken, die uns die Erhebung der NanoString- und Sequencing-Daten durch Ihre technischen Möglichkeiten und Kompetenzen im Rahmen einer Kooperation erst ermöglicht haben. Dabei möchte ich auch Ihre stete Bereitschaft uns bei der Analyse zu unterstützen und die kompetenten und kritischen Diskussionen würdigen.

Mein Dank gilt ebenfalls Dr. N. Andreas und Katrin Schubert vom FLI Jena für Ihre Unterstützung bei den FACS-Experimenten.

Von ganzem Herzen danke ich abschließend meiner Familie, insbesondere meinen Eltern und Andreas sowie meinen Freunden, insbesondere Anne und Frank, für ihre unendliche Geduld und Unterstützung.